Università degli Studi di Ferrara

DOTTORATO DI RICERCA IN
"SCIENZE BIOMEDICHE E BIOTECNOLOGICHE"

CICLO XXIX

COORDINATORE Prof. Paolo Pinton

Regulation of cell death and differentiation: new roles for ATP synthase, PML and mitochondria metabolites

PhD student

Dott.ssa Claudia Morganti

Supervisor

Dott.ssa Carlotta Giorgi

Co-supervisors
Prof. Paolo Pinton
Prof.ssa Agnieszka Karkucinska-Wieckowska

Anni 2014/2016

Table of Contents

Aims

This thesis is the result of my PhD in "Biomedical and Biotechnological Science" attended in "Signal Trasduction Lab" leaded by Prof. Paolo Pinton.

Our lab is aimed in studying of signal transduction, the process by which a cell receives and responds to stimuli, which lies at the heart of many interesting and important processes, including cell growth, cell death, immune function and differentiation process.

I focused my studies on cell death and differentiation.

The first work (chapter 1) presented is aimed to understand the molecular identity of the "permeability transition pore complex" (PTPC), the supramolecular entity that triggers mitochondrial permeability transition (MPT). MPT drives cell death and provides an etiological contribution to several human disorders characterized by the acute loss of post-mitotic cells, including cardiac and cerebral ischemia. Nevertheless, the precise molecular determinants of MPT remain elusive, which considerably hampers the development of clinically implementable cardio- or neuroprotective strategies targeting this process. We proposed to investigate the precise contribution of the mitochondrial F_1F_O ATP synthase in this process. Moreover we set up and published (attachment A) a comprehensive analysis of mitochondrial permeability transition pore activity in living cells using fluorescence-imaging-based techniques.

The second work (chapter 2) is focus on a new role of promyelocytic leukemia protein (PML), a well-known oncosuppressor directly involved in human tumor development. Indeed, an unexpected and critical role of PML in stem cell biology and in metabolism regulation has recently emerged. On the base of these recent evidences, we decided to study PML as a possible regulator of stem cell adipogenic differentiation. The aim of the project is improve knowledge about the molecular mechanism of adipogenic process in order to suggest novel therapeutic strategies for metabolic and obesity-related disorders.

Finally, in the third work (chapter 3) we investigated the possible involvement of a direct communication between mitochondria and nucleus during stem cell differentiation. Stem cells differentiation process was largely investigated from the transcriptional factors point of view, whereas little is known concerning how metabolism could regulate this complex process. However, understanding exactly how metabolism is linked to pluripotency and differentiation process has becoming a research topic of considerable recent interest.

Chapter 1. Mitochondrial permeability transition involves dissociation of F_1F_O ATP synthase dimers and C-ring conformation

Abstract

The impact of the mitochondrial permeability transition (MPT), a sudden increase in the permeability of the inner mitochondrial membrane to small solutes, on cellular physiology is well characterized. In contrast, the composition and mode of action of the so-called "permeability transition pore complex" (PTPC), the supramolecular entity that triggers MPT, remain to be fully elucidated. In particular, the precise contributions of the mitochondrial F_1F_O ATP synthase or subunit thereof to the MPT are a matter of debate. By using biochemical and imaging approaches, we demonstrate here that F_1F_O ATP synthase dimers dissociate as the PTPC opens in response to classical MPT inducers. Accordingly, stabilizing F_1F_O ATP synthase dimers by various genetic approaches inhibited PTPC opening and MPT. Specific mutations in the F_1F_O ATP synthase c subunit that alter the conformation of the C-ring sensitized cells to MPT induction, and this could be reverted by stabilizing F_1F_O ATP synthase dimers. Conversely, rendering F_1F_O ATP synthase dimers more unstable, by genetic approaches failed to trigger PTPC opening in the presence of c subunit mutants that inhibit MPT. Overall, our findings indicate that PTPC opening is a multistep process that involves the dissociation of F_1F_O ATP synthase dimers followed by the formation of a poorly selective pore involving the C-ring.

Introduction

1. Mitochondrial permeability transition

The term "mitochondrial permeability transition" (MPT) refers to a sudden and irreversible increase in the permeability of the inner mitochondrial membrane (IMM) to small solutes (<1.5 kDa), leading to the instantaneous dissipation of the mitochondrial membrane potential (Δψm). This not only arrests all Δψm-driven mitochondrial functions including ATP synthesis, but also allows for the unregulated entry of water into the mitochondrial matrix, resulting in the osmotic breakdown of the organelle (Kroemer, Galluzzi et al. 2007; Galluzzi, Vitale et al. 2012) (Figure 1).

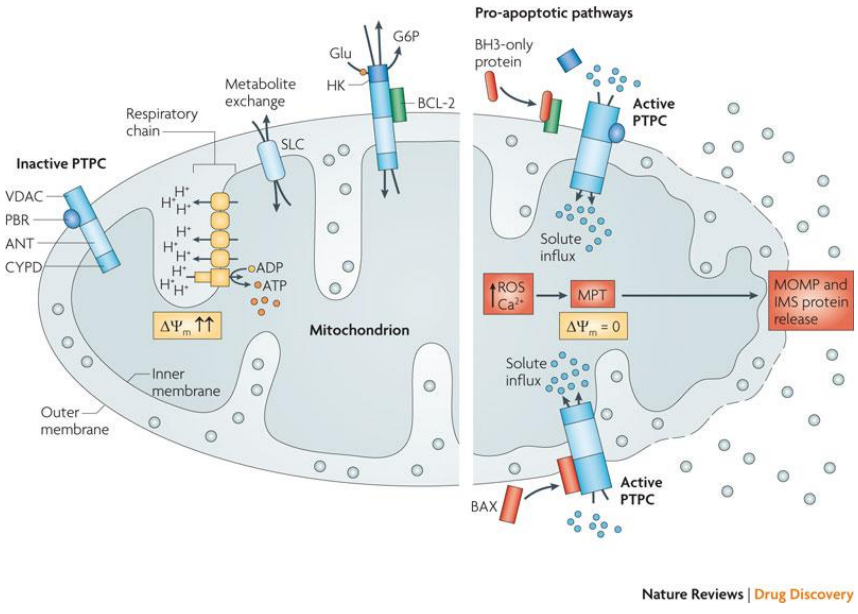

Figure 1. The so-called permeability transition pore complex (PTPC) is a highly dynamic supramolecular entity that can be constituted by the voltage-dependent anion channel (VDAC; embedded in the mitochondrial outer membrane), the adenine nucleotide translocase (ANT; residing in the mitochondrial inner membrane) and cyclophilin D (CYPD; a peptidyl-prolyl cis-trans isomerase of the mitochondrial matrix). In physiological conditions, mitochondria exhibit a high mitochondrial membrane potential (Δψm), which is generated by the respiratory chain and exploited for ATP generation. It has been proposed that in these conditions the PTPC would exist in a low-conductance state (which would be favored by its interaction with anti-apoptotic proteins from the B-cell lymphoma protein 2 (BCL-2) family), thereby contributing to the exchange of small metabolites between the cytosol and the mitochondrial matrix, a process that is predominantly mediated by mitochondrial solute carriers (SLCs). The PTPC has also been suggested to interact with the peripheral benzodiazepine receptor (PBR) and with hexokinase (HK), which uses mitochondrial ATP for catalysing the rate-limiting step of glycolysis; that is, the conversion of glucose (Glu) into glucose-6-phosphate (G6P). In response to some pro-apoptotic signals including the accumulation of reactive oxygen species (ROS) and Ca^{2+} overload, the PTPC assumes a high-conductance conformation that allows the deregulated entry of small solutes into the mitochondrial matrix driven by electrochemical forces. MPT can be favored by pro-apoptotic proteins of the BCL-2 family such as BCL-2-associated X protein (BAX), which directly interact with the PTPC, as well as by BH3-only proteins, which may displace the PTPC from inhibitory interactions with BCL-2. MPT results in the immediate dissipation of the Δψm and in the osmotic swelling of the mitochondrial matrix, which eventually leads to mitochondrial outer membrane permeabilization (MOMP) — as the surface of the inner membrane largely exceeds that of the outer membrane — and to the release into the cytosol of cytotoxic proteins normally confined within the mitochondrial intermembrane space (IMS). Such cytotoxic proteins include caspase activators such as cytochrome c and DIABLO, as well as caspase-independent cell death effectors like apoptosis-inducing factor and endonuclease G.From "Targeting mitochondria for cancer therapy" Simone Fulda, Lorenzo Galluzzi& Guido Kroemer. Nature Reviews Drug Discovery 9, 447-464 (June 2010)

The first description of MPT dates back to 1979, when this phenomenon was shown to stem from the accumulationof Ca^{2+} ions in the mitochondrial matrix and to be responsive to Mg^{2+} ions as well as ADP (Hunter and Haworth 1979). However, the interest in MPT

dropped immediately thereafter, as the process could not be given any pathophysiological relevance. It was only in the mid-1990s when it became evident that mitochondria have a central role in the regulation of cell death elicited by several stimuli (Zamzami, Marchetti et al. 1995; Zamzami, Marchetti et al. 1995). Indeed, while MPT affecting a limited fraction of mitochondria can be managed by their autophagic removal (Green, Galluzzi et al. 2011), widespread MPT commits the cell to death via regulated necrosis or apoptosis.

MPT-driven regulated necrosis mainly, but not only, reflects the bioenergetics outcomes of MPT, that is, the immediate dissipation of the mitochondrial membrane potential ($\Delta\psi m$) and the consequent arrest in all $\Delta\psi m$-dependent mitochondrial activities, including ATP synthesis (Vandenabeele, Galluzzi et al. 2010). Conversely, MPT-driven apoptosis is mainly executed by mitochondrial intermembrane proteins that are released into the cytoplasm upon MPT, including cytochrome c, apoptosis-inducing factor, mitochondrion-associated, 1 (AIFM1, best known as AIF) and diablo, IAP-binding mitochondrial protein (DIABLO, also known as Smac) (Galluzzi, Kepp et al. 2012; Tait and Green 2010). As the apoptotic phenotype requires the activation of caspases (Kroemer, Galluzzi et al. 2009), a family of cysteine proteases that operate in an ATP-dependent manner, MPT may drive apoptosis or regulated necrosis depending on the intracellular availability of ATP (Leist, Single et al. 1997).

According to current models, MPT would be mediated by the so-called permeability transition pore complex (PTPC), a supramolecular entity assembled at the interface between the inner and the outer mitochondrial membranes (Kroemer, Galluzzi et al. 2007; Galluzzi, Vitale et al. 2012).

2. Architecture of the PTPC

Core components

In the early 1990s, electrophysiological studies based on purified mitoplasts (that is, mitochondria stripped of the outer membrane) demonstrated that MPT corresponds to an significant increase in the conductance of the inner mitochondrial membrane (Szabo and Zoratti 1992), pointing to the existence of a pore that would be responsible for this transition. Such a 'mitochondrial megachannel' was rapidly found to share several features with MPT, including its sensitivity to Ca^{2+} ions (which operate as activators) as well as to CsA and various divalent cations, including Mg^{2+} (all of which operate as inhibitors) (Szabo, Bernardi et al. 1992). Shortly thereafter, the mitochondrial megachannel turned out to exhibit a voltage-dependent behavior, in thus far resembling VDAC (Szabo and Zoratti 1993). In support of a critical role for VDAC in MPT, purified VDAC molecules

reconstituted in planar bilayers or proteoliposomes were shown to form a dimeric channel that exhibited electrophysiological properties compatible with those of the mitochondrial megachannel (Szabo, De Pinto et al. 1993). Such an unexpected link between a protein of the outer mitochondrial membrane, VDAC, and a phenomenon that involves the inner mitochondrial membrane (i.e., MPT) casted suspicion on the actual composition of the mitochondrial megachannel, raising the possibility that it would be constituted by several proteins, not just one. Further supporting this hypothesis, a ligand of the peripheral benzodiazepine receptor, which was already known to involve VDAC, ANT and a third component (McEnery, Snowman et al. 1992), was found to elicit currents from otherwise electrically silent mitoplasts.

In 1996 the supramolecular nature of the PTPC was confrimed, when it was documented (in the rat brain) the presence of a complex comprising VDAC, ANT, hexokinase 1 (HK1) and creatine kinase, mitochondrial 1 (CKMT1) and exhibiting MPT like electrical activity upon reconstitution in liposomes (Beutner, Ruck et al. 1996; Beutner, Ruck et al. 1998). Based on its interacting partners (including VDAC and ANT) (Crompton, Virji et al. 1998) as well as on its pharmacological profile (Marsh 1977), CYPD was soon suspected to have a central role in MPT. In the late 1990s, purified ANT molecules reconstituted in proteoliposomes were found to form an oligomeric channel exhibiting PTPC-like functional properties (Ruck, Dolder et al. 1998). Cumulatively, these findings inspired a first PTPC model according to which MPT would be mediated by a supramolecular entity assembled at the interface between the inner and outer mitochondrial membrane by the physical and functional interaction of VDAC, ANT, HK1 and CKMT1. In line with its suborganellar localization (the mitochondrial matrix), CYPD was considered by this model as a regulator of the PTPC, but not as one of its pore-forming subunits.

Robust genetic data generated in the mid-2000s significantly challenged most components of its model. Thus, the simultaneous knockout of the genes coding for two distinct ANT isoforms, that is, Slc25a4 (encoding Ant1) and Slc25a5 (encoding Ant2), failed to abolish the ability of murine hepatocytes to succumb to several MPT inducers, including the Ca^{2+} ionophore Br-A23187, in a CsA inhibitable manner (Kokoszka, Waymire et al. 2004).

Similarly, the simultaneous genetic inactivation of three distinct VDAC isoforms, namely, VDAC 1, VDAC 2 and VDAC 3, neither altered the propensity of murine fibroblasts to die when challenged with hydrogen peroxide (an MPT inducer), nor did it influence the ability of their mitochondria to undergo MPT in response to Ca^{2+} (Baines, Kaiser et al. 2007).

At odds with these relatively minor effects, the standalone deletion of Ppif turned out to mediate major MPT inhibitory and cytoprotective effects, in vitro as well as in vivo, in

several models of acute ischemic injury (Basso, Fante et al. 2005). In particular, the absence of CYPD was shown to markedly increase the amount of Ca^{2+} ions required to trigger MPT and to render this process completely insensitive to CsA.

Taken together, these data apparently demonstrate that ANT and VDAC are dispensable for both the execution and the regulation of MPT, while CYPD has a crucial role in the process.

Moreover, it seems unlikely that CYPD, which is mainly localized within the mitochondrial matrix, would constitute the actual pore-forming component of the PTPC. In line with this notion, CYPD is currently viewed as the major gatekeeper of MPT, regulating the opening of the PTPC but not lining up the pore that physically allows for the entry of low molecular weight solutes into the mitochondrial matrix. This said, the possibility that CYPD may change conformation and become able to form pores in the inner mitochondrial membrane during MPT, similar to what BAX does in the course of mitochondrial outer membrane permeabilization (MOMP) (Desagher, Osen-Sand et al. 1999), has not yet been formally excluded.

Inorganic phosphate has been identified very early as an MPT-promoting metabolite (Tedeschi, Hegarty et al. 1965), suggesting that the PTPC would possess a specific binding site. In physiological conditions, inorganic phosphate is transported across the inner mitochondrial membrane by members of the SLC protein family, including SLC25A3 (best known as PHC or PiC) and SLC25A24 (also known as APC1) (Palmieri 2004). Although PiC imports inorganic phosphate into mitochondrial matrix coupled to either the co-import of H^+ ions or the export of OH^- ions, APC1 mediates this process along with the export of ATP and Mg^{2+} ions. In 2003, APC1 was suggested to be responsible for the MPT-promoting activity of inorganic phosphate via an indirect effect on the mitochondrial pool of ATP and ADP (Hagen, Lagace et al. 2003), a notion that has not been confirmed. Rather, it seems that APC1 responds to increases in cytosolic Ca^{2+} levels by operating in reverse mode, thus favoring the mitochondrial uptake of ATP and ADP and inhibiting MPT (Traba, Del Arco et al. 2012). In 2008 PiC was shown to bind CYPD and ANT1 in cellula, an interaction that was potentiated by MPT-inducing conditions and inhibited by CsA (Leung, Varanyuwatana et al. 2008). Along similar lines, a high-throughput genetic screen unveiled that PiC overexpression promotes mitochondrial dysfunction coupled to apoptotic cell death (Alcala, Klee et al. 2008). Also in this study PiC was found to interact with ANT1 (as well as with VDAC1), especially in the presence of MPT inducers. Moreover, the small-interfering RNA-mediated depletion of PiC exerted cytoprotective effects. Together with previous data indicating that the reconstitution of liposomes with

purified PiC molecules results in the formation of relatively unspecific pores (Schroers, Kramer et al. 1997), these findings pointed to PiC as to the possible pore-forming unit of the PTPC. This hypothesis is incompatible with recent results indicating that a consistent reduction in PiC levels does not alter the ability of isolated mitochondria to undergo MPT in response to Ca^{2+} ions (Varanyuwatana and Halestrap 2012). Thus, either PiC does not participate into the PTPC in a significant manner, or very small amounts of PiC are sufficient to mediate MPT. As a corollary, this suggests that the cytoprotective effects of PiC depletion may not stem from the modulation of MPT. Although the ability of PiC to influence mitochondrial dynamics may be involved in this process (Pauleau, Galluzzi et al. 2008), the exact molecular mechanisms by which PiC promotes cell death under some circumstances remain to be elucidated.

Regulatory components

Several proteins have been shown to regulate the activity of core PTPC units (that is, VDAC, ANT and CYPD). These regulatory components, which encompass cytosolic as well as mitochondrial proteins, appear to interact with the PTPC backbone in a highly dynamic manner (Verrier, Deniaud et al. 2004).

The translocator protein (18 kDa) (TSPO), a protein of the outer mitochondrial membrane, constitutes the benzodiazepine binding component of the so-called peripheral benzodiazepine receptor, an oligomeric complex involving VDAC and ANT (McEnery, Snowman et al. 1992). The physiological role of TSPO in steroid biosynthesis was described as early as in 1989 (Mukhin, Papadopoulos et al. 1989), and only a few years later circumstantial evidence implicating TSPO in MPT began to accumulate. For the most part, these studies reported the ability of a series of endogenous (for example, protoporphyrin IX) (Pastorino, Simbula et al. 1994) and exogenous (for example, PK11195, Ro5–4864, diazepam) (Chelli, Falleni et al. 2001) TSPO agonists to elicit MPT in isolated mitochondria. In line with this notion, the incubation of purified mitochondria with a TSPO-blocking antibody reportedly inhibits several manifestations of MPT (Azarashvili, Grachev et al. 2007). This said, the effects of TSPO ligands on cell death exhibit a great degree of variability, ranging from cytoprotective (Klaffschenkel, Waidmann et al. 2012), to overtly lethal (Campanella, Szabadkai et al. 2008). Such a context dependency may stem from several causes, including (but presumably not limited to) model intrinsic variables (including the expression levels of TSPO and other benzodiazepine receptors) and the concentration of TSPO-modulatory agents used, possibly linked to off-target effects (Gonzalez-Polo, Carvalho et al. 2005).

Various kinases have been shown to physically and/or functionally interact with core PTPC units (at least in specific tissues, such as the brain), including CKMT1 (which is localized in the mitochondrial intermembrane space), HK1, HK2 as well as glycogen synthase kinase 3β (GSK3β) and protein kinase Cε (PKCε) (Verrier, Deniaud et al. 2004). Some of these kinases, including CKMT1, HK1 and HK2 do not phosphorylate protein substrates, implying that their MPT-modulatory activity originates either from their physical interaction with core PTPC components or from their ability to catalyze metabolic reactions. Besides binding VDAC1 and ANT1 (Beutner, Ruck et al. 1996; Beutner, Ruck et al. 1998), CKMT1 phosphorylates creatine to generate phosphocreatine, a reaction that is tightly coupled to oxidative phosphorylation (and hence to the availability of ATP and ADP) (Dolder, Walzel et al. 2003). It remains to be formally demonstrated whether the MPT-modulatory activity of CKMT1 originates from its physical interaction with PTPC components or its catalytic activity.

HKs catalyze the rate-limiting step of glycolysis, converting glucose into glucose-6-phosphate in an ATP-dependent manner (Huertas, Maletz et al. 1976). Both HK1 and HK2 interact with multiple VDAC isoforms, hence gaining a preferential access to ATP exported from mitochondria (Pastorino and Hoek 2008). This configuration (that is, the binding of HKs to VDAC) is associated with an optimal flux through glycolysis as well as with major cytoprotective effects (Pastorino and Hoek 2003). Accordingly, the administration of cell-permeant peptides or chemicals that competitively displace HK2 from VDAC1 has been shown to kill several types of cells upon MPT (Smeele, Southworth et al. 2011; Galluzzi, Kepp et al. 2008). However, it remains unclear to which extent such a cytotoxic response reflects a direct modulation of the PTPC by HK2 rather than an indirect effect on the availability of antioxidants (cancer cells exploit glycolysis to boost the pentose phosphate pathway, which is critical for the regeneration of NAD(P)H and hence reduced glutathione) (Galluzzi, Kepp et al. 2013). The fact that the MPT-inducing activity of peptides disrupting the HK2/VDAC1 interaction is inhibited by CsA and bongkrekic acid, as well as by the ablation of Ppif, but not by that of VDAC1 and VDAC3 (Chiara, Castellaro et al. 2008), suggests that the PTPC-regulatory function of HKs mainly stems from a metabolic effect. Further supporting this notion, HK1 has recently been found to exert major cytoprotective effects in MPT-unrelated paradigms of death (Schindler and Foley 2013).

Contrarily to CKMT1 and HKs, GSK3β and PKCε exert MPT-modulatory functions that have been linked (at least partially) to their ability to phosphorylate core PTPC components (Pastorino, Hoek et al. 2005; Baines, Song et al. 2003; Takuma, Phuagphong

et al. 2001). For instance, active GSK3β has been reported to phosphorylateVDAC1, resulting in the MPT-stimulatory displacement of HK2 (Pastorino, Hoek et al. 2005) and VDAC2, promoting the consumption of ATP by ischemic mitochondria (a process that is also expected to promote MPT) (Das, Wong et al. 2008), while GSK3β phosphorylated on Ser9 (that is inactive) appears to inhibit the PTPC by physically disrupting the ANT1/CYPD interaction (Nishihara, Miura et al. 2007). Recently, the activation of GSK3β has also been linked to the MPT-triggering phosphorylation of CYPD (Whitehead and Hespell 1990). However, formal evidence supporting the notion that GSK3β directly phosphorylates CYPD is lacking. PKCε has been reported to phosphorylate VDAC1, yet this post-translational modification appears to promote, rather than destabilize, HK2 binding (Baines, Song et al. 2003). However, as the activation of PKCε by a synthetic peptide has been associated with the inactivating dephosphorylation of GSK3β (Korzick, Kostyak et al. 2007), it is not clear whether the effect of PKCε on the VDAC1/HK2 interaction in cellula actually reflects a direct phosphorylation event or a GSK3β-dependent signaling circuitry.

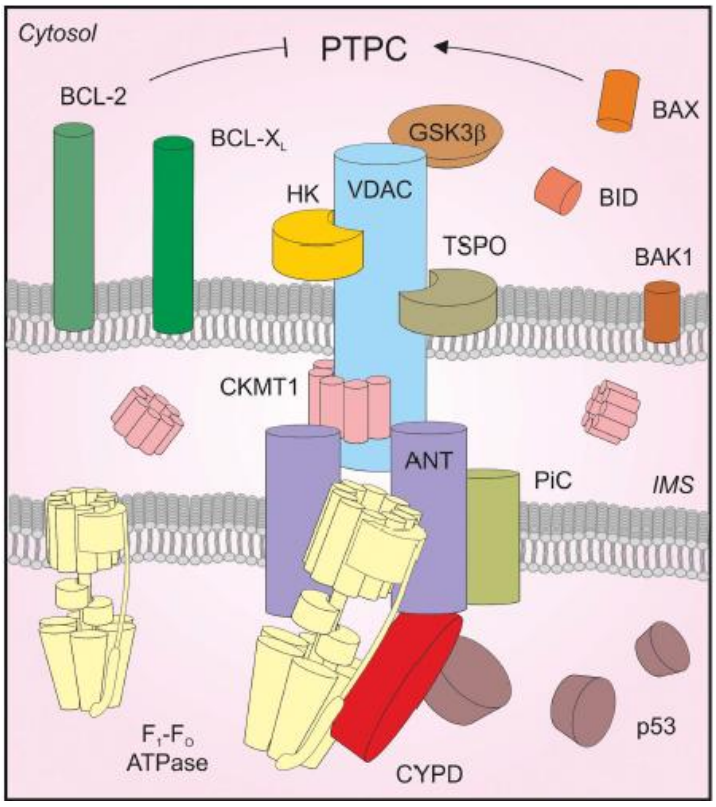

Figure 2. Possible configuration of the PTPC. MPT is mediated by the opening of a supramolecular entityassembled at the juxtaposition between mitochondrial membranes. Such a large multiprotein complex is commonly known as PTPC. Structural and functional studies performed throughout the past two decades suggest that multiple mitochondrial and cytosolic proteins intervene in the formation or regulation of the PTPC, yet the actual pore-forming unit of the complex remains elusive. These proteins include (but are not limited to): various isoforms of VDAC, ANT and HK, CYPD, PiC, TSPO, CKMT1, GSK3β, p53, as well as several members of the Bcl-2 protein family. The precise composition of the PTPC, however, remains elusive. Recent data indicate that the mitochondrial ATP synthase, in particular, the c subunit of the F_O domain, has a critical role in MPT. Whether the c subunit truly constitutes the pore-forming unit of the PTPC, however, has not yet been formally demonstrated.

As a matter of fact, the activation of several upstream signal transducers, including AKT1, mammalian target of rapamycin (mTOR), protein kinase A and protein kinase, cGMP-dependent, type I (PRKG1, best known as PKG) reportedly converge on the inactivation of

GSK3β, hence mediating MPT-inhibitory effects (Juhaszova, Zorov et al. 2004; Pediaditakis, Kim et al. 2010).

Of note, the core units of the PTPC have been shown to interact with several components of the machinery that control MOMP, including both pro- and anti-apoptotic members of the Bcl-2protein family as well as p53. BCL-2 and BCL-2-like 1 (BCL-2L1, best known as BCL-XL) have been proposed to inhibit MPT by regulating the opening state of VDAC1 (Shimizu, Narita et al. 1999; Vander Heiden, Chandel et al. 1999). Whether the MPT-modulatory activity of anti-apoptotic BCL-2 family members originates from an increase or a decrease in VDAC1 conductance remains a matter of debate. Irrespective of this uncertainty, BAX, BAK1 and BCL-2-like 11 (BCL-2L11, a BH3-only protein best known as BID) reportedly promote MPT-driven apoptosis by interacting with ANT1 and/or VDAC1 (Marzo, Brenner et al. 1998; Zamzami, El Hamel et al. 2000; Narita, Shimizu et al. 1998). Along similar lines, BCL-2-associated agonist of cell death (BAD, another BH3-only protein) has been shown to trigger a VDAC1-dependent, BCL-XL-responsive mechanism of MPT (Roy, Madesh et al. 2009). In this context, however, MPT appears to result from the BAD-dependent displacement of BCL-XL from VDAC1 rather than from a physical BAD/VDAC1 interaction (Roy, Madesh et al. 2009). Finally, by sequestering the BAX-like protein BAK1, VDAC2 reportedly exerts MOMP-inhibitory functions (Cheng, Sheiko et al. 2003). Thus, the molecular machineries for MOMP and MPT engage in complex, mutually regulatory crosstalk.

Recent data indicate that a pool of p53 localized to the mitochondrial matrix participate in MPT-driven regulated necrosis by interacting with CYPD (Vaseva, Marchenko et al. 2012). These findings add to an increasing amount of data arguing against the classical apoptosis/necrosis dichotomy. BAX and BAK1 are indeed being implicated in several paradigms of necrotic, as opposed to apoptotic, cell death, (Karch, Kwong et al. 2013) perhaps reflecting their ability to regulate mitochondrial dynamics, or Ca^{2+} homeostasis (Marchi, Patergnani et al. 2014). Further studies are required to obtain precise insights into this issue. In summary, in spite of a significant experimental effort, the precise molecular composition of the PTPC remains elusive (Figure 2). Accumulating evidence indicate that the mitochondrial ATP synthase, the multiprotein complex that catalyzes the synthesis of ATP while dissipating the chemiosmotic gradient generated by the respiratory chain across the inner mitochondrial membrane, constitutes a central PTPC component.

3. Molecular composition of mitochondrial ATP synthase

The mitochondrial ATP synthase is a large multiprotein complex consisting of a globular domain that protrudes into the mitochondrial matrix (F_1 domain, also known as soluble component) and an inner mitochondrial membrane-embedded domain (F_O domain), which are interconnected by a central and a lateral stalk. Owing to this molecular arrangement, the ATP synthase is also known as F_1F_O-ATPase (Yoshida, Muneyuki et al. 2001).

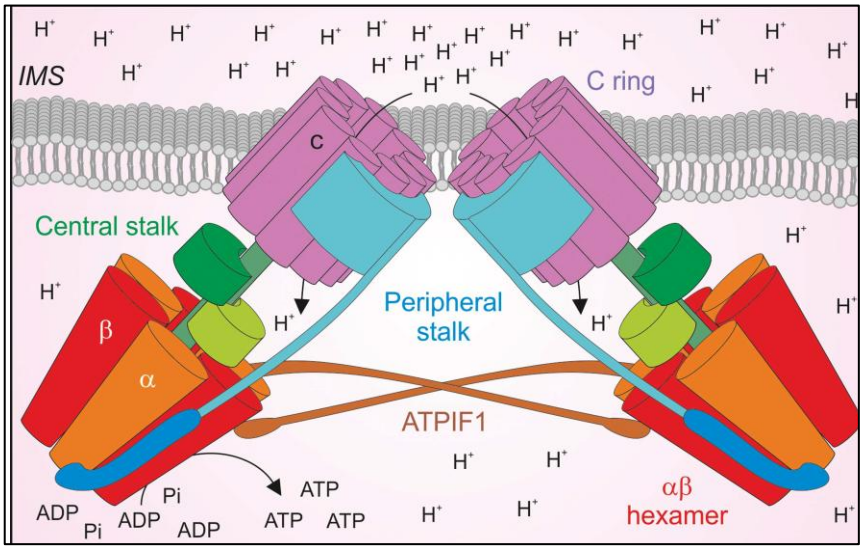

Figure 3. Molecular and supramolecular organization of the mammalian ATP synthase

Mammalian ATP synthases contain 15 different subunits: α, β, γ, δ, ε, a, b, c, d, e, f, g, A6L, F6 and O (also known as oligomycin sensitivity-conferring protein, OSCP) forming a fully functional holoenzyme with a total molecular weight of ~ 600 kDa. The α, β, γ, a and c subunits exhibit a high degree of homology to their chloroplast and bacterial counterparts. Moreover, the overall topology of the mammalian ATP synthase, as well as that of its F_1 and F_O components taken individually, are highly conserved across evolution (Devenish, Prescott et al. 2008), (Okuno, Iino et al. 2011). The mammalian F_1 domain is composed of three α/β dimers and interacts with one copy of the γ, δ and ε subunits (central stalk) as well as with the b, d, F6 and O subunits (peripheral stalk), providing a physical bridge between the soluble and proton-translocating (F_O) components of the holoenzyme (Rubinstein, Walker et al. 2003).

The F_O domain contains a ring-shaped oligomer of c subunits stabilized by binding of cardiolipin, a lipid that is highly enriched in (if not confined to) the inner mitochondrial membrane (Jonckheere, Smeitink et al. 2012). Of note, the number of c subunits composing the so-called c-ring varies to a significant extent across species (10 in humans) (Okuno, Iino et al. 2011). These components of the F_O domain are highly hydrophobic and

contain a critical carboxyl group (most often as part of a Glu or Asp residue) that is directly involved in the translocation of H^+ ions across the inner mitochondrial membrane (Lightowlers, Howitt et al. 1988). The remaining constituents of ATP synthase, that is, the a, e, f, g andA6L subunits, are also part of the F_O domain and interact with the c-ring. In particular, the a subunit provides a physical dock for the b subunit, while A6L appears to bridge F_O to other components of the peripheral stalk (Okuno, Iino et al. 2011) (Figure 3).

4. Potential pore sites of the mitochondrial F_1F_O ATP synthase

Thus far two main sites of possible pore-formation in mitochondrial F_1F_O ATP synthase have been proposed: the monomer–monomer interface of the dimer (Giorgio, von Stockum et al. 2013; von Stockum, Giorgio et al. 2015; Carraro, Giorgio et al. 2014) and the c-ring by itself and in the context of mitochondrial F_1F_O ATP synthase (Bonora, Bononi et al. 2013; Alavian, Beutner et al. 2014).

The dimer proposal (Figure 4A) is based on electrophysiological recordings of a black membrane that yielded currents in agreement with the known electrophysiological properties of the PTP after addition of mitochondrial F_1F_O ATP synthase dimers that were excised and extracted from blue native gels. No PTP-like currents were observed after the addition of monomeric F_1F_O ATP synthase extracted from the same blue native gel. Given, however, that bovine F_1F_O ATP synthase comprises 17 different subunits of which the two F_O subunits DAPIT and 6.8 kDa are easily lost during extraction of this fragile multi-subunit membrane complex from the inner mitochondrial membrane, a straightforward alternative explanation is the loss of PTP specific subunits during extraction from the excised gel bands or reconstitution into the black membrane. In this context it is worth mentioning that the bovine F_OF_1 subunits DAPIT and 6.8 kDa were recognized as constituents of the full complex only relatively recently (Meyer, Wittig et al. 2007), demonstrating how sensitive the full F_1F_O ATP synthase complex is to extraction procedures and the loss of native lipid. However, both subunits are essential to the full complex in vivo (Ohsakaya, Fujikawa et al. 2011; Fujikawa, Ohsakaya et al. 2014) and were present in 2D crystals in which only monomeric bovine F_1F_O ATP synthase was present (Jiko, Davies et al. 2015). The dimerization interface was visualized for the first time at the α-helical level for the F_1F_O ATP synthase from the unicellular colorless green algae Polytomella spec (Allegretti, Klusch et al. 2015).

The interface does not show any obvious pore-forming site. However, the Polytomella spec interface is unique and to date structures of the dimerization interface of the bovine or drosophila enzyme have not been reported and for the yeast dimer not yet published.

Therefore, a more thorough examination of the monomer–monomer interface as a potential pore-forming site remains a task for the future.

An alternative proposal for a pore-forming entity within the components that make up the mitochondrial F_1F_O ATP synthase is its proton transporting c-ring (Figure 4B).

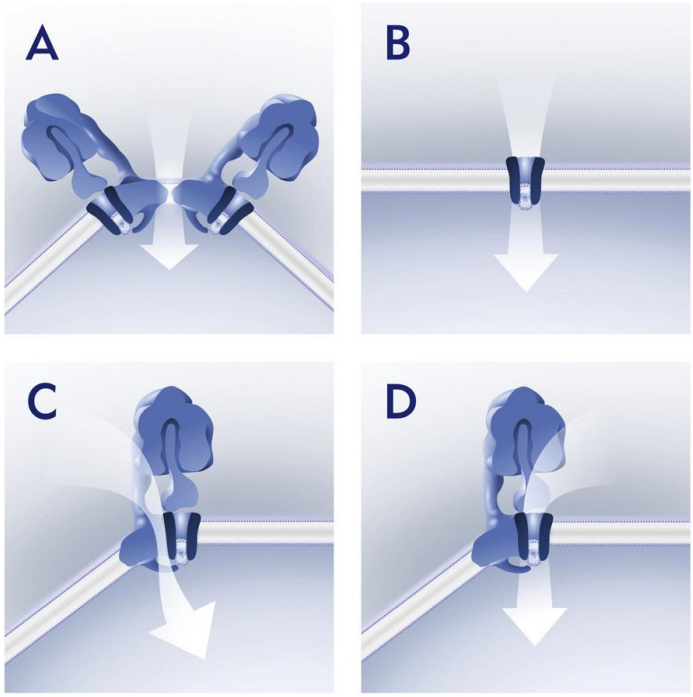

Figure 4. Potential pore-forming sites of the mitochondrial F_1F_O ATP synthase. (A) The dimerization interface of the F_1F_O ATP synthase dimer. (B) The lumen of the lipid plug sealed c-ring by itself. (C) The interface between the c-ring and the aqueous half-channel harboring a-subunit. (D) The lumen of the c-ring in the context of the F_1F_O ATP synthase

This proposal is based on our studies that examined PTP formation after depletion of the c-subunit mediated by small interfering RNA knock-down (Bonora, Bononi et al. 2013). Fortuitously, the c-ring is structurally the best characterized sub-complex of the F_1F_O ATP synthase membrane domain, including numerous high resolution X-ray crystal structures (Pogoryelov, Yildiz et al. 2009) (Symersky, Pagadala et al. 2012). F_1F_O ATP synthase c-rings consist of multiple copies of c-subunits arranged as a circle with a subunit copy number and diameter varying between species (8–15), but not between F_1F_O ATP synthase complexes of the same species (Pogoryelov, Klyszejko et al. 2012). The lumen of the c-ring is void of protein and proton tightness is enabled by the presence of lipids filling its lumen. The presence of c-ring lumenal lipids has been demonstrated in vivo for the Escherichia coli enzyme (Oberfeld, Brunner et al. 2006) and in vitro for reconstituted rotor rings (Meier, Matthey et al. 2001). Interestingly, the only high resolution X-ray structure of a rotor ring that visualized some but not all lumenal lipids showed them to be shifted to the p-side of the rotor ring (Murata, Yamato et al. 2005). This finding is in line with the p-side protruding lipid plug in reconstituted c-rings, as detected by atomic force microscopy (Matthies, Preiss et al. 2009), molecular dynamics simulations of membrane embedded c-rings (Krah, Pogoryelov et al. 2010) and the density protruding from c-rings in cryo-EM single particle reconstructions of intact F_1F_O ATP synthases (Allegretti, Klusch et al.

2015). The pore like shape of the rotor ring with a diameter roughly matching the predicted pore diameter of the PTP makes the c-ring an obvious candidate for a potential pore-forming site. In this context, it is noteworthy that in an evolutionary scenario proposed by Mulkidjanian and colleagues the rotor ring was proposed to have evolved from a polymer conducting pore as part of a RNA translocase, over the pore of a protein translocase to a cation transporting c-ring (Mulkidjanian, Makarova et al. 2007). This homology pattern based evolutionary scenario has subsequently been bolstered by structural studies on the flagellar motor and the Thermusthermophilus V-ATPase (Kishikawa, Ibuki et al. 2013). Any proposal for the c-ring as the PTP itself has to explain how the many modulating molecular players interact with it and importantly how either the lipid plug is removed or the diameter of the c-ring substantially widened; and how all of this occurs in a reversible manner and while exhibiting several sub-states of conductance. Since CyPD as the only bona fide binding partner of the PTP was not shown to interact with the c-ring, but rather binds to the OSCP, the c-ring by itself appears too simple to allow for regulation and modulation. Therefore, the c-ring in the context of either monomeric or dimeric F_1F_O ATP synthase is a more likely candidate for a physiological relevant site of pore formation. In the intact mitochondrial F_1F_O ATP synthase the central stalk (CS) makes tight contact with the c-ring at multiple sites, but it does not seal it off from bulk solution and keeps the c-ring's lumen connected to the matrix (Stock, Leslie et al. 1999).

That leaves the lipid plug as the only barrier to pore formation. Conformational rearrangement of c-subunits accompanied by diameter widening of the c-ring has been suggested as a way to c-ring pore-formation (Alavian, Beutner et al. 2014). In line with the idea of a diameter change in the c-ring, large scale rearrangements have been proposed as a way to switch gears for the T. thermophiles V-ATPase (Zhou, Morgner et al. 2011) and normal mode analysis suggests that c-rings are able to deform substantially (Saroussi, Schushan et al. 2012). Direct structural evidence for both types of flexibility, however, has not been reported yet. On the contrary, X-ray crystallography performed on numerous c-rings in detergent rather suggests c-rings to be rigid in their architecture, which does not seem to allow for larger movements of individual subunits or alpha helices. If the crystal structure based perceived rigidity is perhaps at least partially the result of the embedding detergent micelles' high dielectric environment remains to be seen (Tani, Mitsuma et al. 2009).

A further potential site for pore formation is the interface between the a-subunit and the c-ring (Figure 4C). In the cryo-EM structure of the Polytomella F_OF_1 ATP synthase dimer deep invagination of the membrane at the interface of the c-ring and the a-subunit have

been visualized (Kuhlbrandt and Davies 2016) rendering this idea more appealing. However, mitochondria of ρ0 cells lacking mitochondrial DNA which encodes the a- and A6L subunits are able to form the PTP (Masgras, Rasola et al. 2012) and hence it is generally thought that the a- and A6L subunits are not part of the PTPC.

Finally a new model, the death finger model (Figure 4D), was described. In this model, movement of a p-side density that connects the lipid-plug of the c-ring with the distal membrane bending F_O domain allows reversible opening of the c-ring and structural cross-talk with OSCP and the catalytic (αβ)3 hexamer (Gerle 2016).

Here, we present data indicating that MPT involves the dissociation (not the association) of F_1F_O ATP synthase dimers in combination with the formation of poorly selective pores across the IMM by C-rings.

Results

1. MPT is associated with dissociation of F_1F_O ATP synthase dimers

The current literature suggests that experimental conditions that promote F_1F_O ATP synthase dimerization are associated with a reduced cellular propensity for PTPC opening and consequent MPT (Masgras, Rasola et al. 2012; Daum, Walter et al. 2013). We set out to test the relationship between MPT induction and F_1F_O ATP synthase dimerization status in several primary: human adult dermal fibroblasts (HADFs), mouse embryonic fibroblasts (MEFs) and immortalized cell lines: human embryonic kidney HEK293T cells, human cervical carcinoma HeLa cells, human non-small cell lung carcinoma A549 cells, mouse NIH-3T3 fibroblasts.

To test PTPC opening, we employed the conventional calcein/Co^{2+} quenching assay (Bonora, Morganti et al. 2016) upon treatment of cells with 1 µM ionomycin plus 1 mM Ca^{2+} (Fig 5A, 5B). To investigate F_1F_O ATP synthase dimerization in physiological conditions, blue native gel electrophoresis was employed, followed by immunoblotting to detect ATP synthase alpha subunit 1, (ATP5A1) (Fig 5C, 5D). As positive and negative control for dimers detection we used rat hearth mitochondria treated with n-Dodecyl β-D-maltoside (DM) or digitonin (Dig) respectively (Fig 5C and 6A). Indeed the aggressive DM detersion the poorer preservation of F_1F_O ATP synthase dimers during isolation compared to Dig (Minauro-Sanmiguel, Wilkens et al. 2005; Wittig and Schagger 2008). Different cell lines exhibited rather distinct calcein quenching rates (Fig 5B). Similarly, the relative abundance of F_1F_O ATP synthase dimers (i.e., the ratio between dimers and monomers) varied quite considerably with cell type (Fig 5D). Intriguingly, calcein quenching rates and the relative abundance of F_1F_O ATP synthase dimers by the Pearson's method exhibited a tendency toward negative correlation (Fig5E), suggesting that increased F_1F_O ATP synthase dimerization is associated with low MPT sensitivity. To obtain further insights into this issue, we purified rat liver mitochondria, placed them in an energization buffer (which contains all substrates for $\Delta\psi_m$ preservation and ATP synthesis), and we exposed them to control conditions or CsA prior to triggering MPT with 100 µM Ca^{2+}. In setting, MPT-associated mitochondrial swelling was monitored as a decrease in the diffraction of light at 540 nm of the preparation (Fig 5F). Mitochondria were then assessed for the relative abundance of F_1F_O ATP synthase dimers by blue-native electrophoresis and ATP hydrolysis in-gel activity assay (Fig 5G). MPT induction by Ca^{2+} ions correlated with a partial accumulation of F_1F_O ATP synthase monomers over dimers, and this could be completely prevented by the pre-administration of CsA (Fig 5F, 1H).

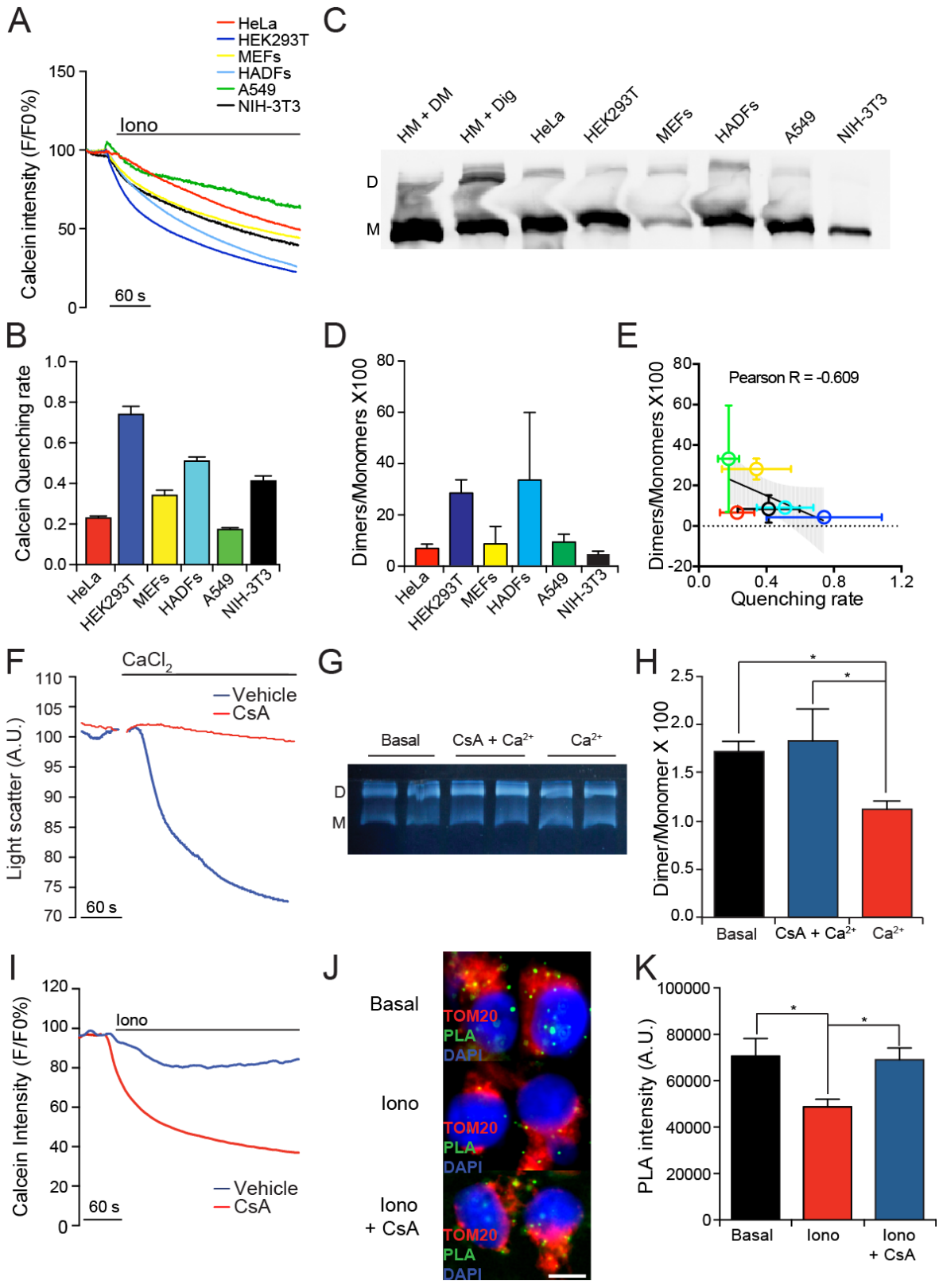

Fig5. Correlation of dissociation of F_1F_O ATP synthase with MPT

◄Fig 5. Correlation of dissociation of F_1F_O ATP synthase with MPT
(A) Representative calcein/Co^{2+} quenching traces and **(B)** quenching rate quantification of HeLa cells, HEK293T cells, MEFs, HADFs, A549 cells and NIH-3T3 fibroblasts treated with 1 µM ionomycin. **(C)** Representative immunoblotting for the detection of the ATP5A1 subunit followed after Blue Native PAGE and **(D)** quantification of F_1F_O ATP synthase dimers (D) and monomers (M) in HeLa cells, HEK293T cells, MEFs, HADFs, A549 cells and NIH-3T3 fibroblasts maintained in control conditions. Rat hearth mitochondria (HM) in presence of Dodecyl β-D-maltoside (DM) or digitonin (Dig) were used as negative or positive control for dimeric form respectively. **(E)** Correlation between calcein quenching rate upon stimulation with ionomycin and relative abundance of F_1F_O ATP synthase dimers in basal conditions, in HeLa cells, HEK293T cells, MEFs, HADFs, A549 cells and NIH-3T3 fibroblasts maintained in control conditions. Pearson R coefficient of correlation is reported. **(F)** Representative traces of mouse liver mitochondria undergoing MPT in response to 100 µM $CaCl_2$ alone or in the presence of 1 µM cyclosporine A (CsA). **(G)** In gel activity assay followed after Blue Native PAGE and **(H)** quantification of F_1F_O ATP synthase dimers (D) and monomers (M) in mouse liver mitochondria in basal conditions or after MPT induction as in panel F. **(I)** Representative calcein/Co^{2+} quenching traces in HEK293T treated with 1 µM Iono, alone or in the presence of 1.6 µM CsA. **(J)** Representative images and **(K)** quantification of PLA assays for F_1F_O ATP synthase dimers in HEK293T maintained in basal conditions or driven in MPT as in panel I. data were shown as means ± SEM; n = 3, *p<0.05 (ANOVA plus unpaired Student's t test). Scale bar = 10 µm.

We thus set up a procedure to verify the levels of F_1F_O ATP synthase dimers *in cellula* by developing a dedicated proximity ligation assay (PLA) (Fredriksson, Gullberg et al. 2002). In this setting, antibodies specific for ATP synthase subunit D (ATP5H) were conjugated with either + or – PLA probes (Fig 6 B-C), and then used as a cocktail to stain HEK293T. As result of the PLA procedure HEK293T displayed a considerable amount of dotted staining colocalyzing with the mitochondrial protein translocase of outer mitochondrial membrane 20 (TOMM20) (Fig 6E). As a negative control ATP5H expression was interfered for using a mixture of specific siRNA sequences, in this condition, only a minor amount of PLA signal was detected (Fig 6E-G). Considering these results and the fact that F_1F_O ATP synthase requires specific subunits to dimerize and that dimers can spontaneously arrange to higher order complexes, we concluded that our PLA assay was specific to detect levels of dimeric/oligomeric F_1F_O ATP synthase levels. Thus after PLA validation, we tested the effect undergoing MPT in response to ionomycin plus Ca^{2+}, alone or in the presence of CsA. Even if only a minor amount of PLA signal was localized out of mitochondria, the PLA measurement signal was limited to the mitochondrial area, to avoid artefactual results. Efficient and CsA-sensitive MPT induction was verified by the calcein/Co^{2+} quenching assay (Fig 5I), whereas the F_1F_O ATP synthase dimerization status was conservatively evaluated by the PLA (Fig 5J). This system allows for the visualization of heterologous proximity between the + and – probe (while the proximity between +/+ and –/– probes remains undetected). Irrespective of the intrinsic underestimation of the relative abundance of F_1F_O ATP synthase dimers associated with this approach, MPT was accompanied by a significant decrease in the PLA signal that did not occur in the presence of CsA (Fig 5K). These findings suggest that PTPC opening and consequent MPT correlate

with the destabilization of F_1F_O ATP synthase dimers, and that such as dissociation can be blocked by the MPT inhibitor CsA.

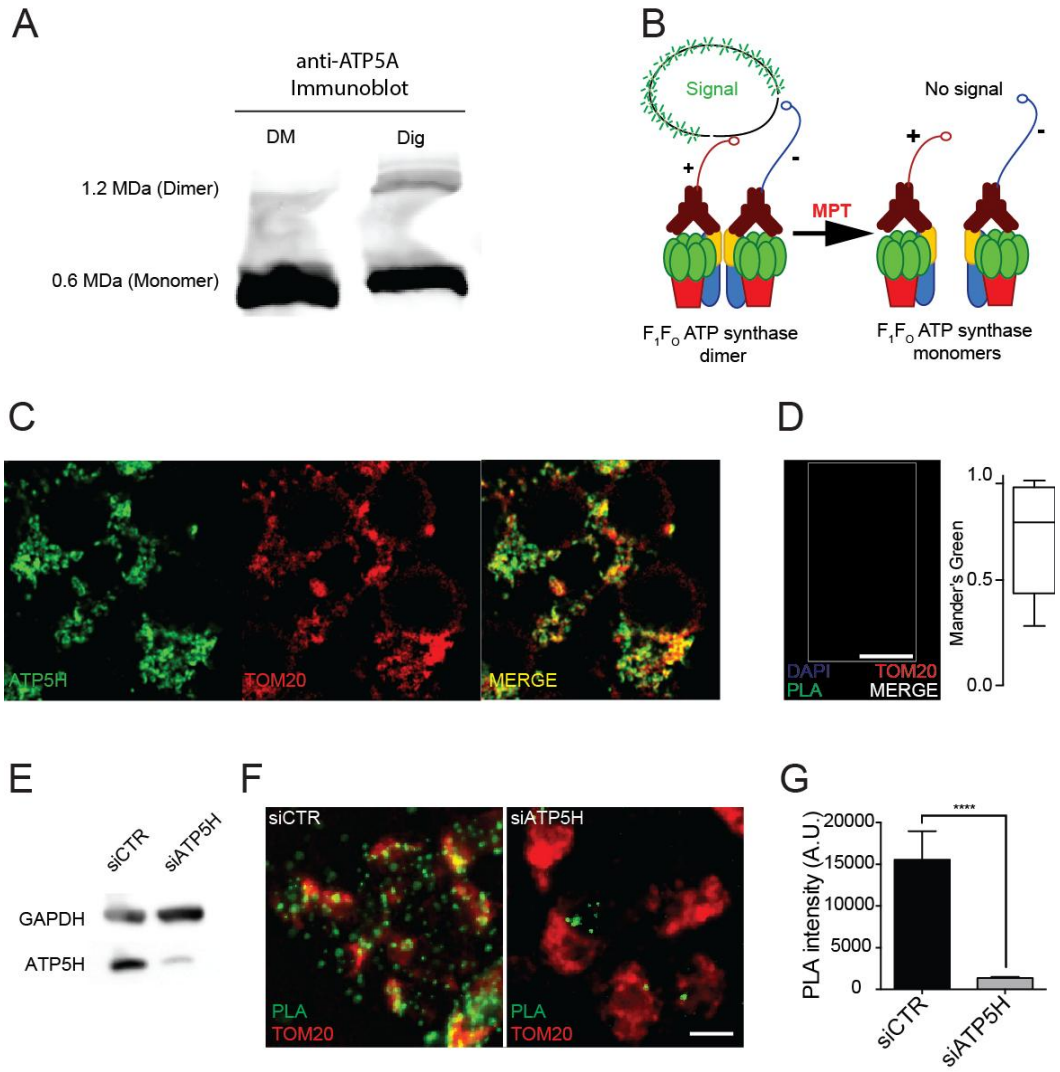

Fig 6.Validation of F_1F_O ATP synthase dimerization status
(**A**) Higher resolution image of F_1F_O ATP synthase dimers and monomers isolated from rat hearth mitochondria (HM) by the use of n-Dodecyl β-D-maltoside (DM) or digitonin (Dig), separated by blue native gel elctrophoresys and detected by immunostaining of ATP5A. (**B**) Schematic representation of PLA assay setting. In physiological conditions (left), the mitochondrial F_1F_O ATP synthase can form dimers or higher order oligomers. In this setting, antibodies specific for ATP5H can bring + and – PLA probes in proximity to each other, allowing for rolling-circle amplification of a detectable DNA product. In the course of MPT (right), as F_1F_O ATP synthase dimers dissociate, the distance between + and – PLA probes conjugated to ATP5H-targeting antibodies is excessive for rolling-circle amplification to occur. In this specific system, detection is highly conservative as both the + and the – PLA probes are conjugated with ATP5H-targeting antibodies, but + and + (or – and –) probes in proximity do not allow for rolling-circle amplification. (**C**) Representative images of immunoreactivity of the anti- ATP5H antibody used for the PLA assay and its colocalization with the mitochondrial marker TOMM20. (**D**) 3D volume rendering of a representative HEK 293T cells stained for DNA (DAPI, blue), mitochondria (TOMM20, red) and F_1F_O ATP synthase dimers (PLA, green). Statistic of PLA colocalization with TOMM20 on the right side (bars: max and min value; box: 10^{th} and 90^{th} percentile; line: median). (**E**) Assessment of transfection efficiency in HEK293T cells transfected with a control siRNA (siCTR) or a siRNA targeting ATP5H (siATP5H) for 96 h. GAPDH levels were monitored to ensure equal lane loading. **(F, G)** Representative images (**F**) and quantification (**G**; means ± SEM; n = 3) of PLA assays for F_1F_O ATP synthase dimers in HEK293T cells transfected with a siCTR or siATP5H for 96 h *p<0.001 (unpaired Student's t test). Scale bar = 10 µm.

2. Stabilization of F_1F_O ATP synthase dimers by ATPIF1 inhibits MPT

Since CYPD binds to the peripheral stalk of the F_1F_O ATP synthase in a CsA-sensitive manner (Giorgio, Bisetto et al. 2009), we speculate that such an interaction provokes a general rearrangement that promotes dimer destabilization (at least of part of the F_1F_O ATP synthase pool). If PTPC opening involves the dissociation of F_1F_O ATP synthase dimers, artificially stabilizing dimers can be expected to inhibit MPT. To test this prediction, we harnessed HEK293T engineered to transiently overexpress ATPase inhibitory factor 1 (ATPIF1), a subunit of the F_1F_O ATP synthase that is known to promote dimerization (Garcia, Morales-Rios et al. 2006). Overexpressed ATPIF1 could be readily visualized by immunofluorescence microscopy and perfectly co-localized with mitochondrial protein translocase of outer mitochondrial membrane 20 (TOMM20) (Fig 7A).

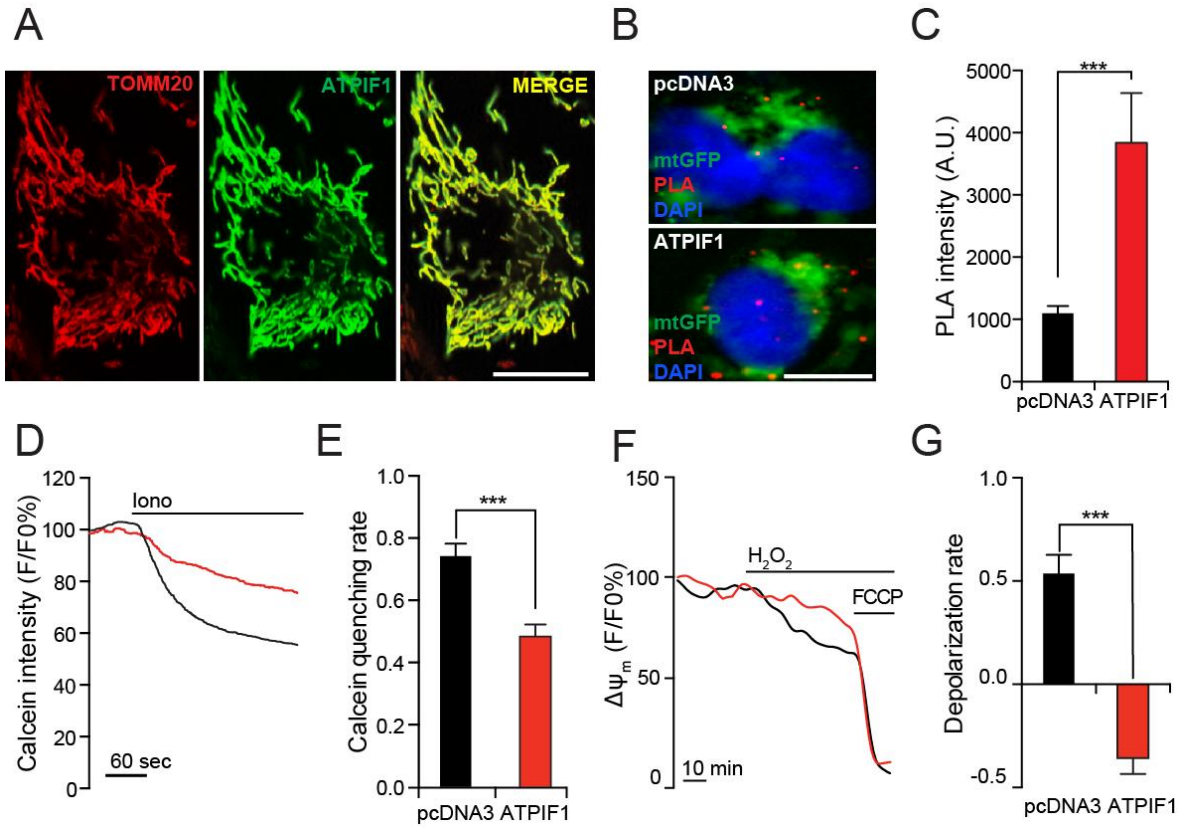

Fig 7. Stabilization of F_1F_O ATP synthase dimers by ATPIF1 inhibits MPT.
(A) Representative colocalization of ATPIF1 with TOMM20 in HEK293T cells transfected with a plasmid for ATPIF1 overexpression. **(B)** Representative images and **(C)** quantification of PLA assays for F_1F_O ATP synthase dimers in HEK293T transfected with an empty vector (pcDNA3) or with a plasmid for the overexpression of ATPIF1 and co-transfected with a plasmid coding for mtGFP. **(D)** Representative calcein/Co^{2+} quenching traces and **(E)** quenching rate quantification in HEK293T transfected as in **B**, **C** and treated with 1 µM ionomycin (Iono). **(F)** Representative mitochondrial transmembrane potential ($\Delta\psi_m$) recordings and **(G)** depolarization rate quantification in HEK293T transiently as in **B**, **C** and exposed to 500 µM H_2O_2. 1 µM carbonyl cyanide 4-(trifluoromethoxy)phenylhydrazone (FCCP) was employed as control for depolarization. Data were shown as means ± SEM; n = 3. Scale bars = 10 µm.***p<0.001 unpaired Student's *t* test.

Moreover, HEK293T overexpressing ATPIF1 did not exhibit signs of mitochondrial deterioration, including fragmentation (Fig 8A-8C), total mass reduction (Fig8A, 8D), and depolarization (Fig 8E, 8F) as compared to HEK293T transfected with an empty vector. In addition, co-expressing ATPIF1 with a luciferase directed to the mitochondrial matrix demonstrated that ATPIF1 did not significantly alter mitochondrial ATP content in HEK293T, neither in basal conditions, nor upon inhibition of ATP synthesis with 75 µM N,N-dicyclohexylcarbodiimide (DCCD) (Fig 8G, 8H).

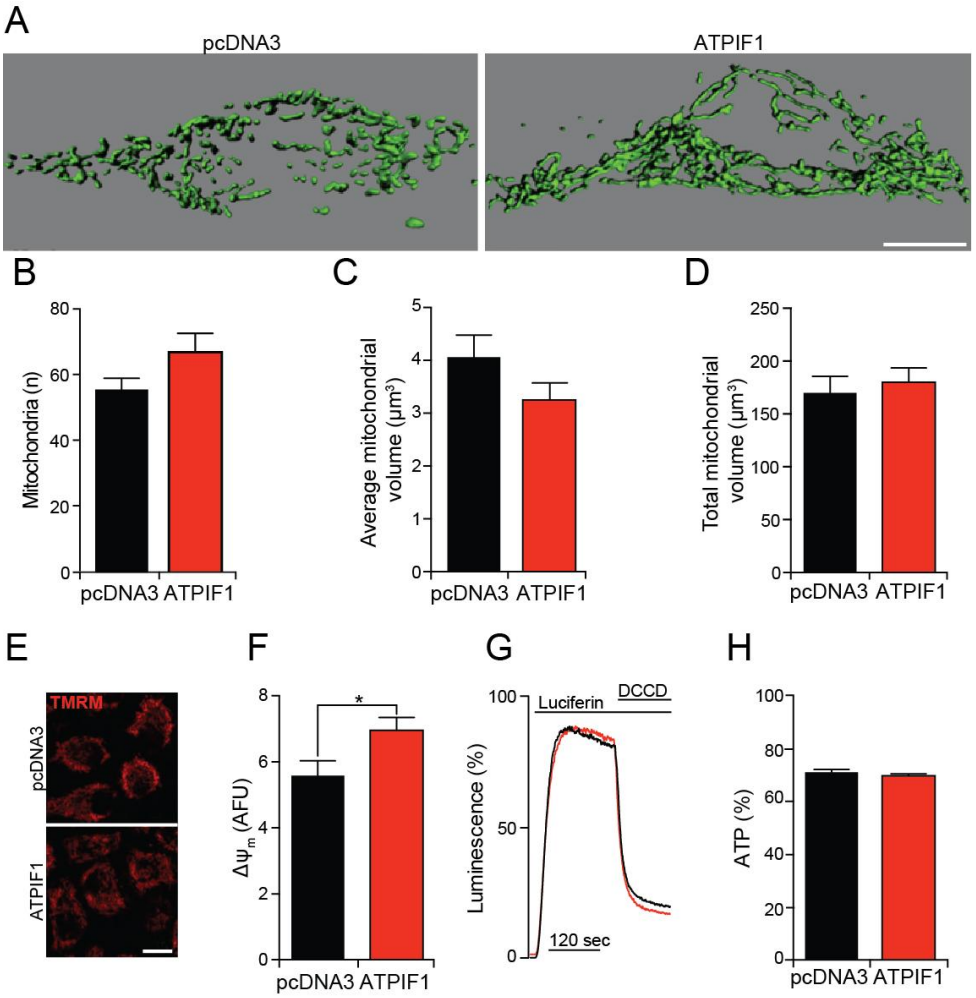

Fig 8. Mitochondrial parameters in ATPIF1-overexpressing HEK293T cells.
(**A-D**) Representing rendering (A) and quantification of mitochondrial morphological parameters (**B-D**; means ± SEM; n = 3) in HEK293T cells transiently transfected with an empty vector (pcDNA3) or with a plasmid for the overexpression of ATPIF1. Scale bar = 10 µm.
(**E, F**) Representative images (E) and quantification (F; means ± SEM; n = 3) of TMRM staining in HEK293T cells transiently transfected with an empty vector (pcDNA3) or with a plasmid for the overexpression of ATPIF1. *p<0.05 (ANOVA plus unpaired Student's t test). Scale bar = 10 µm.
(**G, H**) Representative traces (G) and quantification (H; means ± SEM; n = 3) of mitochondrial ATP-dependent light emission in HEK293T cells transiently transfected with an empty vector (pcDNA3) or with a plasmid for the overexpression of ATPIF1. 75 µM N,N-dicyclohexylcarbodiimide (DCCD) were employed to completely inhibit mitochondrial ATP synthesis at the end of the assay.

HEK293T overexpressing ATPIF1 manifested a drastic increase in the relative abundance of F_1F_O ATP synthase dimers as determined by PLA signal overlapping mitochondrial

GFP (mtGFP) (Fig 7B, 7C), prompting us to test their sensitivity to MPT elicited by 1 µM ionomycin plus 1 mM Ca^{2+}. Conventional calcein/Co^{2+} quenching assays revealed that ATPIF1-overexpressing HEK293T indeed display an increased resistance to MPT induction by ionomycin plus Ca^{2+} as compared to their control counterparts (Fig 7D, 7E). Since one of the major consequences of the MPT is mitochondrial depolarization, we performed long-term confocal imaging on control and ATPIF1-overexpressing HEK293T cells treated with the MPT-inducer hydrogen peroxide (H_2O_2), upon staining with the $\Delta\psi_m$-sensitive probe tetramethylrhodamine methyl ester (TMRM). Control cells (transfected with an empty pcDNA3-based vector) treated with 500 µM H_2O_2 experienced relatively slow mitochondrial depolarization, which could be virtually prevented by ATPIF1 overexpression (Fig 7F, 7G).

3. Modulation of F_1F_O ATP synthase dimers via ATP5I impacts on MPT

To corroborate these observations, we evaluated MPT sensitivity after manipulating ATP synthase subunitE (ATP5I), critical for dimerization (Arselin, Giraud et al. 2003). Transfecting HEK293T with a small-interfering RNA (siRNA) ATP5I led to >97% reduction in ATP5I levels after 96 hours (Fig 9A). Per se, ATP5I depletion considerably sensitized HEK293T cells to MPT induction by ionomycin plus Ca^{2+} (Fig 9B, 9C).

Next, we tested whether overexpressing ATP5I would have any effect on PTPC opening in conditions that are known to sensitize cells to MPT. To this aim, we took advantage of the fact that overexpressing the c subunit of the F_1F_O ATP synthase not only promotes (at least some extent of) spontaneous MPT, but also potently sensitizes cells to MPT induction by ionomycin plus Ca^{2+} (Bonora, Bononi et al. 2013). In yeast a critical residue required that allows ATP5I to promote dimers stability was characterized (Arselin, Giraud et al. 2003). We transposed this mutation to the human ATP5I gene and generated a glycine-to-leucine substitution ($ATP5I^{G26L}$) mutant. Thus, we co-transfected HEK293T with cDNAs for the overexpression of ATP5G1 (one of the human isoforms of the c subunit) together with either wild-type ATP5I or $ATP5I^{G26L}$, and monitored the relative abundance of F_1F_O ATP synthase dimers, MPT sensitivity and mitochondrial depolarization rate.

Upon co-transfection, HEK293T expressed high levels of ATP5G1 and ATP5I or $ATP5I^{G26L}$, which properly co-localized at mitochondria (Fig 9D). The overexpression of either ATP5I or $ATP5I^{G26L}$ seems to restore the moderate morphological alterations imposed by ATP5G1 overexpression on the mitochondrial network, although in a statistically non-significant manner (Fig 10A-10D).

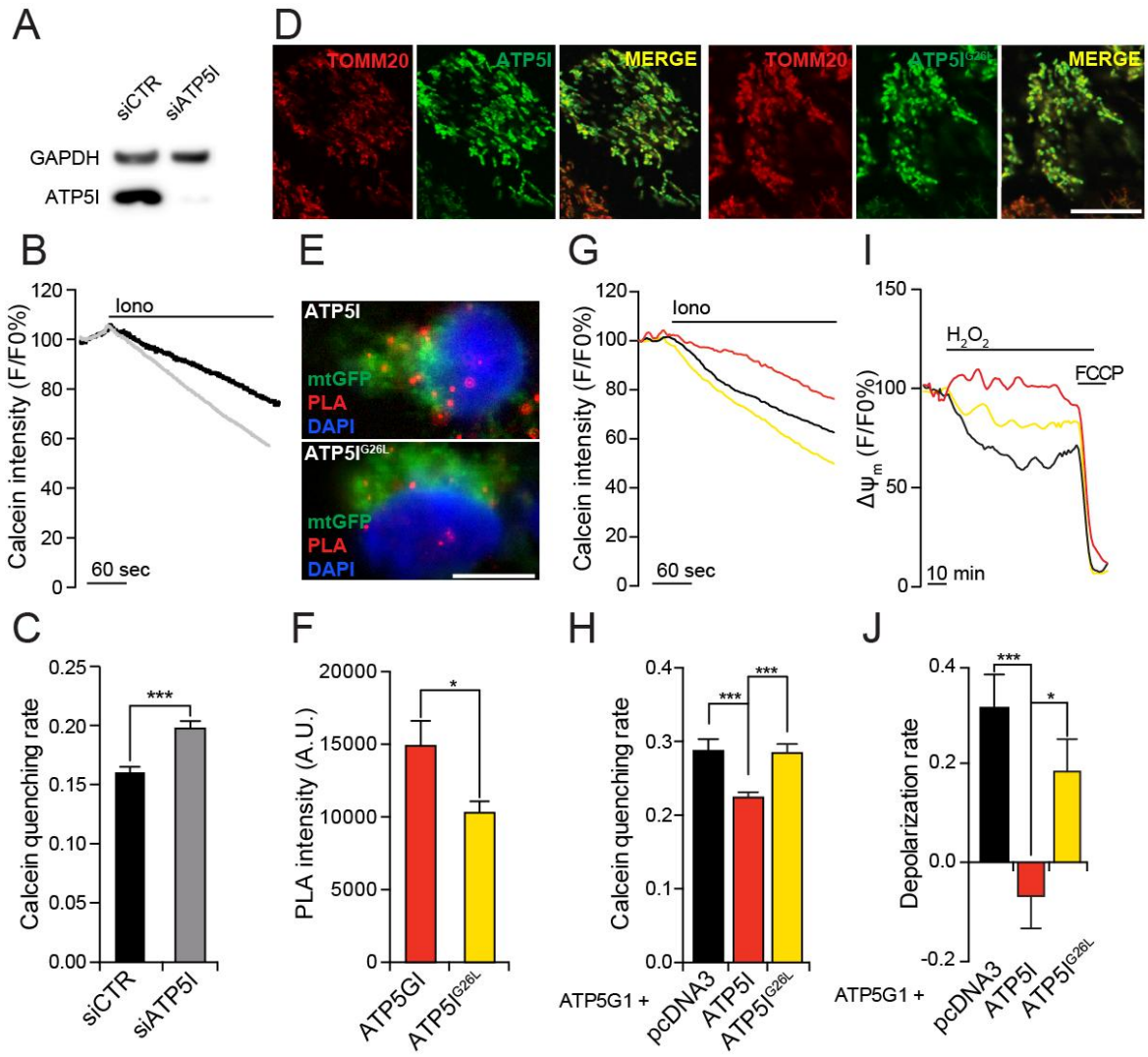

Fig9. Modulation of F1FO ATP synthase dimers via ATP5I affects MPT
(A) Assessment of transfection efficiency in HEK293T cells transfected with a control siRNA (siCTR) or a siRNA targeting ATP5I (siATP5I) for 96 h. GAPDH levels were monitored to ensure equal lane loading. Representative calcein/Co^{2+} quenching traces **(B)** and quenching rate quantification **(C)** in HEK293T cells transfected with siCTR or siATP5I for 96 h, and then treated with 1 µM ionomycin (Iono). Means ± SEM; n = 3. **(D)** Representative colocalization of ATP5I or ATP5IG26L with TOMM20 in HEK293T cells transfected with constructs for ATP5I or ATP5IG26L overexpression, respectively. Representative images **(E)** and quantification **(F)** of PLA assays for F_1F_O ATP synthase dimers in HEK293T cells transfected with plasmids for the overexpression of ATP5I or ATP5IG26L and co-transfected with a plasmid coding for mtGFP. Means ± SEM; n = 3. *p<0.001 (unpaired Student's t test). **(G)** Representative calcein/Co2+ quenching traces and **(H)** quenching rate quantification (means ± SEM; n = 3) in HEK293T co-transfected with an ATP5G1-encoding construct and an empty vector (pcDNA) or with plasmids for the overexpression of ATP5I or ATP5IG26L and treated with 1 µM Iono. **(I)** Representative mitochondrial transmembrane potential (Δψm) recordings and (**J**) depolarization rate quantification (means ± SEM; n = 3) in HEK293T transfected as in G, H and exposed to 500 µM H_2O_2. 1 µM carbonyl cyanide 4-(trifluoromethoxy)phenylhydrazone (FCCP) was added as control for depolarization. Scale bars = 10 µm.*p<0.05, ***p<0.001 (ANOVA plus unpaired Student's t test).

Conversely, ATP5I (but not $ATP5I^{G26L}$) remarkably increased $\Delta\psi_m$in HEK293T co-overexpressing ATP5G1 (Fig 10E, 10F), although this had no impact on mitochondrial ATP content (Fig 10G, 10H). Importantly, the overexpression of ATP5I, but not $ATP5I^{G26L}$, increased the relative abundance of F_1F_O ATP synthase dimers in ATP5G1-

overexpressing HEK293T (Fig 9E, 9F), while limiting their sensitivity to MPT induction by ionomycin plus Ca^{2+} (Fig 9G, 9H). Along similar lines ATP5I (but less so $ATP5I^{G26L}$) prevented mitochondrial depolarization in HEK293T by 500 µM H_2O_2 (Fig 9I, 9J).

Altogether, these data indicate that stabilizing F_1F_O ATP synthase dimers (by two genetically distinct approaches) limits PTPC opening and consequent MPT and demonstrate that the dissociation of F_1F_O ATP synthase dimers is a cause, not a consequence, of MPT.

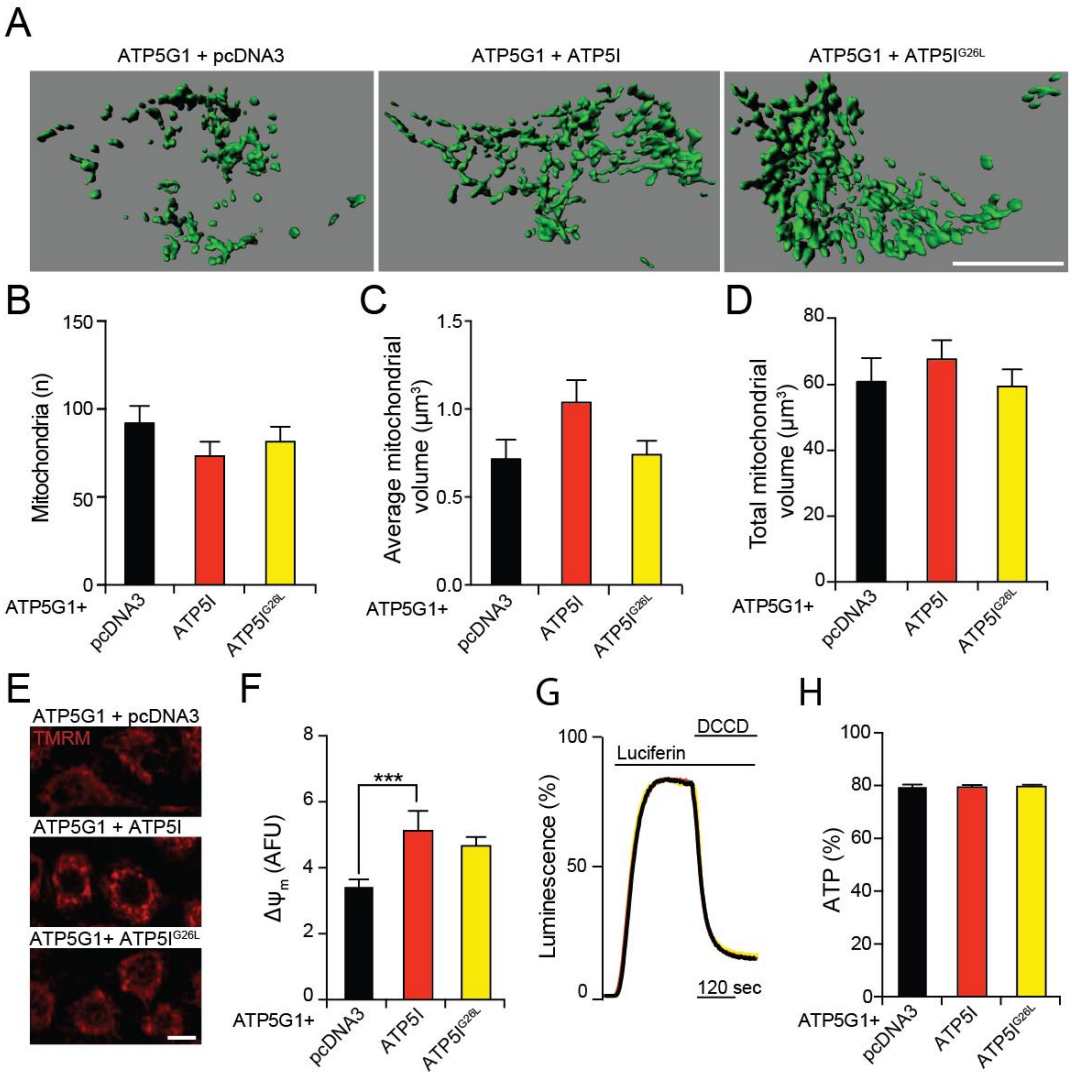

Fig 10. Mitochondrial parameters in ATP5G1- and ATP5I-cooverexpressing HEK293T cells.
(**A-D**) Representing rendering (A) and quantification of mitochondrial morphological parameters (**B-D**; means ± SEM; n = 3) in HEK293T cells transiently transfected with a construct for the overexpression of ATP5G1 plus an empty vector (pcDNA3) or a plasmid for the overexpression of ATP5I or ATP5IG26L. Scale bar = 10 µm. (**E, F**) Representative images (E) and quantification (F; means ± SEM; n = 3) of TMRM staining in HEK293T cells transiently transfected with a construct for the overexpression of ATP5G1 plus an empty vector (pcDNA3) or a plasmid for the overexpression of ATP5I or ATP5IG26L. **p<0.001 (ANOVA plus unpaired Student's t test). Scale bar = 10 µm. (**G, H**) Representative traces (**G**) and quantification (H; means ± SEM; n = 3) of mitochondrial ATP-dependent light emission in HEK293T cells transiently transfected with a construct for the overexpression of ATP5G1 plus an empty vector (pcDNA3) or a plasmid for the overexpression of ATP5I or ATP5IG26L. 75 µM N,N-dicyclohexylcarbodiimide (DCCD) were employed to completely inhibit mitochondrial ATP synthesis at the end of the assay.

4. C-ring conformation affects PTPC opening and consequent MPT

Since MPT apparently involves the disassembly of F_1F_O ATP synthase dimers, we hypothesized that the c subunit might contribute to PTPC opening in a subsequent step of the process as part of C-rings. We previously demonstrated that depleting the c subunit with sRNAs is sufficient to inhibit MPT (Bonora, Bononi et al. 2013). Along similar lines, Alavian and collaborators reported that substitution of a residue in the highly conserved glycine zipper domain of the c subunit results in a deformation of C-rings that is paralleled by increased MPT sensitivity (Alavian, Beutner et al. 2014). The glycine rich domain displays extraordinary conservation across species, possibly because the symmetric organization of glycines allows for the tight disposition of c subunits within C-rings (Pandini, Kleinjung et al. 2015). Indeed, substituting glycine residues with alanines increased the distance between c subunits in C-rings from *I. tartaricus*, and substituting G25 with serine dramatically reduced the stability of the complex (Pogoryelov, Klyszejko et al. 2012).

To test whether C-rings are determinant in PTPC opening, we transposed the G25S mutation identified by Pogoryelov *et al.* to the human c subunit, generating the $ATP5G1^{G83S}$ mutant. In addition, we created an ATP5G1 variant in which all key glycines were substituted with leucines ($ATP5G1^{4GL}$), as for the findings from Alavian and colleagues (Alavian, Beutner et al. 2014). Bioinformatic studies based on the RaptorX web server (Kallberg, Wang et al. 2012) predicted that both $ATP5G1^{G83S}$ and $ATP5G1^{4GL}$ would exhibit a structural deformation at the level of the first helix (Fig11A). Transfecting HEK293T with cDNAs encoding ATP5G1, $ATP5G1^{G83S}$ or $ATP5G1^{4GL}$ resulted in robust mitochondrial expression of wild-type or mutant ATP5G1, (Fig11B) and did not affected the dimerization status of F_1F_O ATP synthase as assessed by PLA signal overlapping mitochondrial GFP (mtGFP) (Fig 11C, 11D). $ATP5G1^{4GL}$-overexpressing HEK293T were more sensitive to MPT induction than HEK293T

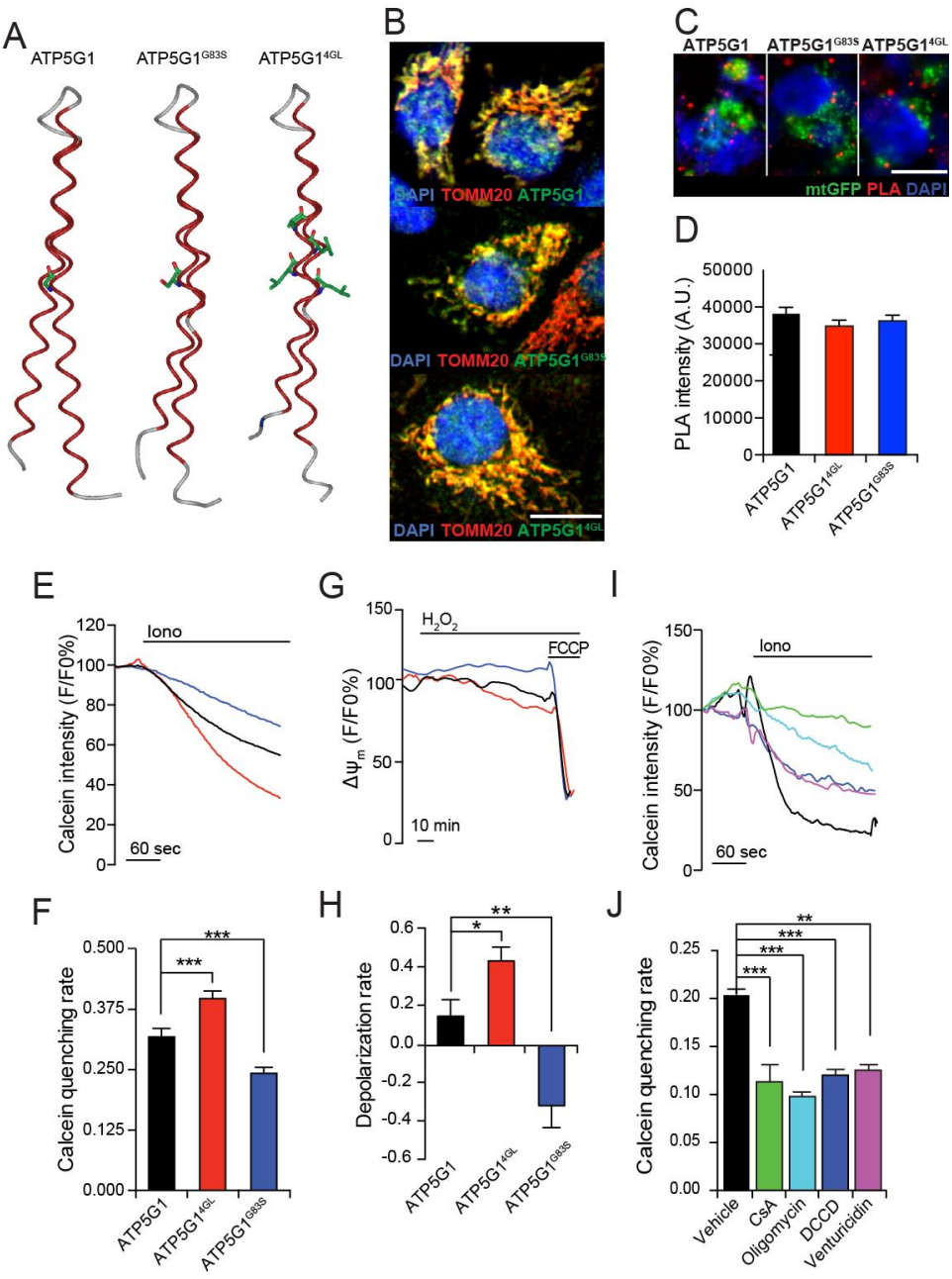

Fig 11. C-ring conformation affects PTPC opening and consequent MPT

(A) Bioinformatic prediction of the alterations imposed by the G83S and the 4GL mutations on ATP5G1 structure. **(B)** Representative colocalization of ATP5G1, ATP5G1^{G83S} or ATP5G1^{4GL} with TOMM20 in HEK293T cells transfected with constructs for ATP5G1, ATP5G1^{G83S} or ATP5G1^{4GL} overexpression, respectively. Scale bar = 10 µm. **(C)** Representative images and **(D)** quantification of PLA assays for F_1F_O ATP synthase dimers in HEK293T cells transfected with plasmids for the overexpression of ATP5G1, ATP5G1^{G83S} or ATP5G1^{4GL} and co-transfected with a plasmid coding for mtGFP. **(E)** Representative calcein/Co^{2+} quenching recordings and **(F)** quenching rate quantification in HEK293T transfected as in C, D and then treated with 1 µM ionomycin. **(G)** Representative mitochondrial transmembrane potential (Δψm) readings and **(H)** depolarization rate quantification in HEK293T cells transfected as in C, D and then exposed to 500 µM H_2O_2. 1 µM carbonyl cyanide 4-(trifluoromethoxy)phenylhydrazone (FCCP) was employed at the end of the assay as a positive control for depolarization. **(I)** Representative calcein/Co^{2+} quenching traces and **(J)** quenching rate quantification in HEK293T cells pre-treated with 1.6 µM cyclosporine A (CsA), 10 µM oligomycin, 15 µM N,N-dicyclohexylcarbodiimide (DCCD) or 10 µM venturicidin, and then exposed to 1 µM Iono.Data were shown as means ± SEM; n = 3 *p<0.05, **p<0.01, ***p<0.001 (ANOVA plus unpaired Student's t test).

overexpressing the wild-type protein. Conversely, the overexpression of ATP5G1^{G83S} increased the ability of HEK293T to resist the MPT induction by ionomycin and Ca^{2+} (Fig 11E, 11F). Along similar lines, ATP5G1^{4GL} accelerated, while ATP5G1^{G83S} retarded, mitochondrial depolarization driven by 500 µM H_2O_2 (Fig 11G, 11H). These results suggest that the glycine zipper domain of the c subunit plays a central role in PTPC opening.

To validate this notion, we harnessed the fact that some of the most potent inhibitors of the F_1F_O ATP synthase bind to a unique pocket of the C-ring, which is partially formed by the c subunit glycine zipper domain (Symersky, Osowski et al. 2012). In particular, we tested whether the C-ring-targeting agents oligomycin, venturicidin, and DCCD would affect the sensitivity of HEK293T to MPT induction by ionomycin plus Ca^{2+} in calcein/Co^{2+} quenching assays. Indeed, oligomycin, venturicidin, and DCCD reduced calcein quenching rate as efficiently as CsA (Fig 11I, 11J), corroborating the notion that C-rings have a key role in PTPC opening.

5. Critical role of C-rings in MPT

To determine whether the dissociation of F_1F_O ATP synthase dimers or the rearrangement of C-rings constitutes the driver of MPT, we co-transfected HEK293T with cDNAs coding for ATPIF1 and ATP5G1 or ATP5G1^{4GL}, and determined their sensitivity to MPT induction by ionomycin plus Ca^{2+} in calcein/Co^{2+} quenching assays. Surprisingly, the overexpression of ATPIF1 (which stabilizes F_1F_O ATP synthase dimers) limited the sensitization of HEK293T to MPT imposed by the overexpression of ATP5G1 or ATP5G1^{4GL} (Fig 12A, 12B) suggesting that the dissociation of F_1F_O ATP synthase dimers is required for C-rings to assume a conformation compatible with PTPC opening. Along similar lines, the depletion of ATP5I (which destabilizes F_1F_O ATP synthase dimers) retained the ability to facilitate MPT induction by ionomycin plus Ca^{2+} even when ATP5G1was overexpressed, an effect that was lost in ATP5G1^{G83S}-overexpressing cells (Fig 12C, 12D). Alltoghether these data suggests that a proper C-ring conformation is required for MPT induction once F_1F_O ATP synthase dimers have dissociated, strengthening the role for the C-ring in the formation of PTPC.

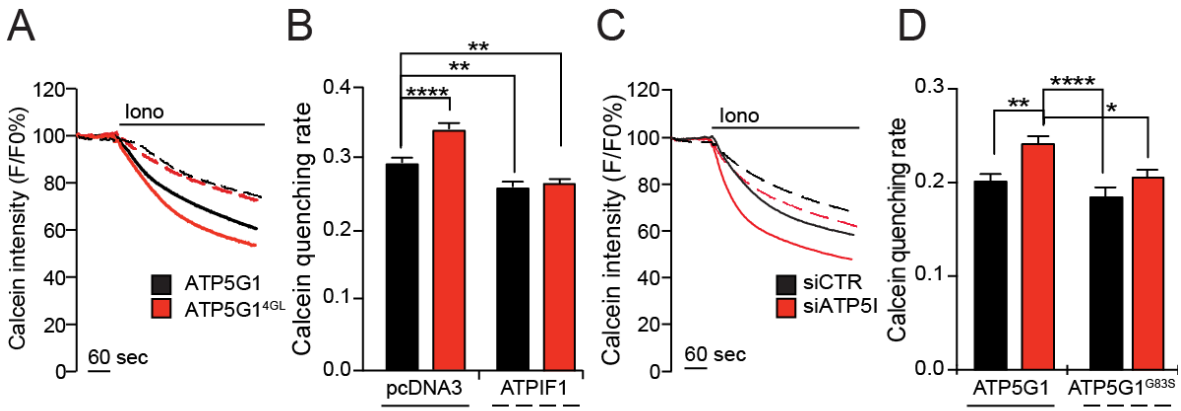

Fig12. Critical role of C-rings in MPT.
(A) Representative calcein/Co^{2+} quenching recordings and **(B)** quenching rate quantification in HEK293T transfected with an empty plasmid or with a construct for the overexpression of ATPIF1, combined with an ATP5G1-or an $ATP5G1^{4GL}$-encoding plasmid, and then treated with 1 µM ionomycin (Iono). **(C)** Representative calcein/Co^{2+} quenching recordings and **(B)** quenching rate quantification in HEK293T transfected with a control siRNA (siCTR) or with a siRNA specific for ATP5I (siATP5I), combined with an ATP5G1-or an $ATP5G1^{G83S}$-encoding plasmid, and then treated with 1 µM Iono. Data were shown as means ± SEM; n = 3 *p<0.05, **p<0.01, ****p<0.0001 (ANOVA plus unpaired Student's t test).

Discussion

MPT-driven regulated necrosis is an established etiological factor in pathological conditions including acute ischemic episodes of the brain, heart and kidney (Galluzzi, Blomgren et al. 2009; Linkermann, De Zen et al. 2012; Ong, Samangouei et al. 2015). Thus, the elucidation of the precise molecular composition and mode of action of the PTPC constitutes a key step for the development of novel neuro-, cardio- or nephroprotective strategies. In the past decade, it has become clear that the mitochondrial F_1F_O ATP synthase plays a central role in MPT (Giorgio, Bisetto et al. 2009; Bonora, Bononi et al. 2013; Giorgio, von Stockum et al. 2013; Alavian, Beutner et al. 2014; Azarashvili, Odinokova et al. 2014) although the detailed mechanisms remain a matter of debate (Izzo, Bravo-San Pedro et al. 2016).

Here, we demonstrated that PTPC opening and consequent MPT correlate with the destabilization of F_1F_O ATP synthase dimers, and that such as dissociation can be blocked by the MPT inhibitor CsA. Since CYPD binds to the peripheral stalk of the F_1F_O ATP synthase in a CsA-sensitive manner (Giorgio, Bisetto et al. 2009), we speculate that such an interaction provokes a general rearrangement that promotes dimer destabilization. To understand whether the dissociation of F_1F_O ATP synthase dimers was a driver or MPT or rather as simple consequence, we employed two genetically distinct approaches to improve dimer stability, namely, the overexpression of ATPIF1 or ATP5I (Arnold, Bauer et al. 1997; Garcia, Morales-Rios et al. 2006). With both interventions, PTPC opening (as measured by calcein/Co^{2+}quenching assays) as well as mitochondrial depolarization (as monitored with the $\Delta\psi_m$-sensitive probe TMRM) were inhibited. Conversely, the siRNA-mediated downregulation of ATP5I (which destabilizes F_1F_O ATP synthase dimers) neatly sensitized cells to MPT induction. These data demonstrate that the dissociation of F_1F_O ATP synthase dimers is a cause, not a consequence, of MPT.

We next focused on the role of C-rings on PTPC opening, taking advantage of site-directed mutagenesis to alter the glycine zipper domain of the c subunit. This domain displays extraordinary conservation across species, possibly because the symmetric organization of glycines allows for the tight disposition of c subunits within (and hence dictates the architectural organization of) C-rings (Pandini, Kleinjung et al. 2015). Indeed, substituting various glycine residues with alanines increased the distance between c subunits in C-rings from *I. tartaricus*, and substituting G25 with serine dramatically reduced the stability of the complex (Pogoryelov, Klyszejko et al. 2012). Individually mutating 4 distinct glycine residues in the c subunit of HEK293T cells to valine has recently been shown to favor PTPC opening (Alavian, Beutner et al. 2014), which we also observed when the same

residues were concomitantly substituted with leucine. Conversely, the G83S substitution strongly inhibited the activity of the PTPC, as did several distinct C-ring-targeting agents. Taken together, these observations suggest that PTPC opening requires a specific C-ring conformation.

Interestingly, the overexpression of ATPIF1 inhibited PTPC opening not only upon overexpression of wild-type ATP5G1 (which we previously demonstrate to favor MPT) (Bonora, Bononi et al. 2013), but also upon overexpression of the ATP5G1^{4GL} variant. This suggests that the dissociation of F_1F_O ATP synthase dimers is required for C-rings to assume a conformation compatible with PTPC opening. Moreover, ATP5G1^{G83S}-overexpressing cells were desensitized to PTPC opening even upon the siRNA-mediated depletion of ATP5I (which promotes dimer destabilization), strengthening the notion that proper C-ring conformation is required for MPT induction once F_1F_O ATP synthase dimers have dissociated.

In conclusion, our data supports a model according to which PTPC opening and consequent MPT involves the dissociation of F_1F_O ATP synthase dimers and the acquisition of a permissive conformation by C-rings.

Material and Methods

Chemicals, cell cultures and transfections.

Unless otherwise noted, chemicals were purchased from Sigma-Aldrich, cell culture media and supplements from Thermo Fischer Scientific and plasticware from Corning Life Sciences. Human embryonic kidney HEK293T cells, human cervical carcinoma HeLa cells, human non-small cell lung carcinoma A549 cells, human adult dermal fibroblasts (HADFs), mouse NIH-3T3 fibroblasts, and mouse embryonic fibroblasts (MEFs) were grown in Dulbecco's modified Eagle's medium (DMEM) supplemented with 10% fetal bovine serum (FBS), 100 units/mL penicillin G sodium and 100 µg/mL streptomycin sulfate. For RNA interference, HEK293T cells were transfected with a commercial control siRNA (AllStars Negative Control siRNA) or with a set of siRNAs specific for ATP5I (siATP5I) (SI04272905; SI04299232; SI00308112; SI04155228), all from Qiagen, by means of the HiPerfect® transfection reagent (Qiagen), as per manufacturer's instructions. For transient overexpression experiments, a pCMV6-Entry-based plasmid coding for MYC-tagged ATP5G1 (RC200292) or ATP5I (RC215565) under the control of the CMV immediate early promoter was obtained from OriGene. The gene encoding ATP5G1^{G83S} and ATP5G1^{4GL} cloned into pCMV6-Entry was synthesized by Blue Heron Biotechnology, Inc. The gene encoding mutant ATP5I^{G26L} cloned into pCMV6-Entry was synthesized by Bio-Fab Research. For the quantification of mitochondrial ATP levels, a VR1012-based construct encoding a mitochondrially-targeted variant of the *Photinus pyralis* luciferase under the control of the CMV immediate early promoter was employed. A pcDNA3-based plasmid coding for a mitochondrially-targeted variant of GFP (mtGFP) under the control of the CMV immediate early promoter was employed for the evaluation of mitochondrial ultrastructure. Plasmid (co-)transfections were performed via the standard Ca^{2+}-phosphate technique.

*Proximity ligation assays***.**

Cell were fixed in 4% PFA for 10 min at 37°C, washed in PBS, placed in a jar containing 1 mM EDTA buffer (pH 8.0) for 20 min at 100°C (to improve the epitope-antibody binding) and then placed at room temperature for additional 10 min. Thereafter, cells were permeabilized with 0.05% Triton X-100 for 10 min at 37°C, and unspecific binding sites were blocked by incubating cells in 0.05% Triton X-100 supplemented with 2% bovine serum albumin (BSA) for 45 min at 37°C. Upon overnight incubation with ATP5H-specific antibodies (ab110275, from Abcam) previously conjugated to + or - PLA oligonucleotide probes (antibody dilution 1:100; 4°C), as per the instructions of Duolink In

Situ®Probemaker kits (Sigma-Aldrich), detection was performed as follows. A ligation-ligase solution was added to each sample for 30 min at 37 °C, washed twice for 2 min with Duolink In Situ® Wash Buffer A, an amplification-polymerase solution was added for 100 min at 37°C and washed twice for 10 min with 1x Duolink In Situ® Wash Buffer A. Eventually, slides were stained with Duolink In Situ® Detection Reagent Green or Red, mounted using DAPI-containing Duolink In Situ® Mounting Medium, and protein proximity was evaluated on on a Axiovert 200M fluorescence microscope equipped with a 40X water immersion objective (N.A. 1.2, from Carl Zeiss Microscopy, LLC) as a function of global green signal intensity.

Calcein/Co^{2+} quenching assays.

PTPC opening was assayed as previously described (Attached A). Briefly HEK293T cells were loaded with 1 mMcalceinacetoxymethyl ester and Co^{2+} as instructed by the Image-IT® LIVE Mitochondrial Transition Pore Assay Kit (Thermo Fischer Scientific). Cells were then imaged based on 490 ± 20 nm excitation and 525 nm longpass emission filters on a Axiovert 200M fluorescence microscope equipped with a 40X water immersion objective (N.A. 1.2, from Carl Zeiss Microscopy, LLC). Finally, images were analyzed with MetaMorph® (Molecular Devices), and quenching rate was calculated as the slope of the fluorescence trace over a period of 60 sec after stimulation.

Quantification of mitochondrial ATP.

HEK293T cells expressing a mitochondrially-targeted variant of the *Photinus pyralis* luciferase were perfused with a modified Krebs–Ringer buffer containing 125 mM NaCl, 5 mM KCl, 1 mM Na_3PO_4, 1 mM $MgSO_4$, 1 mM $CaCl_2$, 20 μM luciferin, and 20 mM HEPES buffer (pH 7.4) at 37°C, and luciferin-dependent luminescence was monitored with a customized luminometer (Elettrofor), as previously described (Jouaville, Pinton et al. 1999).

Mitochondrial swelling.

Mitochondria were isolated from the mice livers according to conventional procedures and placed in energized buffer containing respiratory substrates. Thereafter, 100 μM $CaCl_2$ alone or upon pre-treatment with 1 μM CsA was used to promote PTPC opening, which was followed spectrometrically by measuring 90 °C light scattering at 540 nm.

Quantification of mitochondrial transmembrane potential.

$\Delta\psi_m$ was assayed as previously described (Attached A). Briefly HEK293T cells were loaded with 1 nM TMRM (Thermo Fischer Scientific) in Krebs-Ringer buffer supplemented with 250 μM sulfinpyrazone, then placed in a humidified chamber at 37°C and imaged with a LiveScan Swept Field Confocal Microscope (Nikon Instruments, Inc.) equipped with a 60× oil immersion (N.A. 1.4, from Nikon Instruments, Inc.) every 30 sec for 30 min. TMRM fluorescence was analyzed by means of the NIS Elements software package (Nikon Instruments, Inc.), and depolarization rate were calculated as the slope of the fluorescence trace over a period of 10 min after stimulation.

Analysis of mitochondrial morphology.

Mitochondrial morphology was assayed as previously described (Attached A). Briefly, HEK293T cells expressing a mitochondrially-targeted variant of GFP, were imaged with an IX-81 automated epifluorescence microscope (Olympus) equipped with a 60X oil immersion objective (N.A. 1.35, from Olympus) and an ORCA-R2 CCD camera (Hamamatsu Photonics K.K.). Selected cells were followed over time, and z-stacks were subjected to digital deconvolution by means of a Wiener deconvolution filter and a theoretical point-spread function provided by the Xcellence software package (Olympus). GFP^+ objects were quantified with the "3D object counter" plug-in of the open-source Fiji software (freely available at http://fiji.sc/), whereas 3D representations were obtained with the "3D Viewer" plug-in.

Blue-native and SDS-PAGE.

Cells or mitochondrial pellets were lysed in 50 mMBis-Tris buffer supplemented with 1 M aminocaproic acid (pH 7.0). Upon protein content quantification by means of the Protein Assay Kit (Bio-Rad), digitonin (3 mg/mg total protein) was added to the samples; lysates were incubated on ice for 30 min, and then centrifuged at 14000 g for 20 min to remove insolubilized material. Thereafter, native lysates were combined with 5% Serva Blue G and 60 μg of proteins was loaded and separated on a freshly prepared 5-12% polyacrylamide gel. As an internal standard, 40 μg of proteins from mouse liver mitochondria were used. At the end of the run, the gel was equilibrated in 25 mM Tris buffer supplemented with 192 mM glycine and 0.1% SDS (pH 8.3) for 30 min, followed by conventional transfer on polyvinyldifluoride (PVDF) membranes (Bio-Rad) and immunoblotting with antibodies specific for ATP5A1 (ab14748, from Abcam) and secondary donkey anti-mouse antibodies labeled with IRdye (Li-Cor, Biosciences) (primary 1:1000, secondary 1:5000; both in TBS supplemented with 0.1% Tween and 5% BSA). Detection was performed with the Odyssey infrared Imaging System (Li-Cor Biosciences). Signal intensity was analyzed in Image™

Studio Lite (Li-Cor Biosciences). As an alternative, gels were stained with a $Pb(NO_3)_2$ solution in the presence of ATP, and directly visualized according to previously published procedures.

Immunoblotting.

Immunoblotting was performed as previously described, with minor modifications. In brief, cells were washed, harvested and lysed in RIPA buffer (50 mM Tris-HCl pH 7.8, 150 mM NaCl, 1% IGEPAL CA-630, 0.5% sodium deoxycholate, 0.1% SDS, 1mM dithiothreitol) supplemented with 1 mM phenylmethylsulfonyl fluoride and Complete Protease Inhibitor Cocktail® (Roche Diagnostics Corp.). Thereafter, protein extracts (30 µg/lane) were separated on precast 4-12% SDS-PAGE gels (Thermo Fischer Scientific), electrotransfered onto PVDF membranes (Bio-Rad) and probed with antibodies specific for ATP5I (ab12221, from Abcam) of GAPDH (#2118, from Cell Signaling Technology). Finally, membranes were incubated with appropriate HRP-labeled secondary antibodies (Thermo Fischer Scientific). A conventional chemiluminescent substrate (#34080, from Thermo Fischer Scientific) and the ImageQuant LAS 4010 (GE Healthcare) were employed for detection.

Immunofluorescence microscopy.

Immunofluorescence microscopy was performed according to standard procedures. Briefly, cells were fixed in 4% PFA for 20 min at room temperature, washed three times in PBS and permeabilized with 0.1% Triton X-100 for 5 min at room temperature. Thereafter, unspecific binding sites were blocked by incubating cells in PBS supplemented with 2% BSA (blocking buffer) for 1 h at room temperature. Cells were then incubated overnight at 4°C with primary antibodies specific for TOMM20 (1:100 in blocking buffer, from Santa Cruz SC-11415), ATP5I (1:100 in blocking buffer, from Abcam 122241), ATPIF1 (1:100 in blocking buffer, from Abcam 110277) or ATPG51 (1:100 in blocking buffer, from Abcam 181243). Finally, primary antibodies were revealed by means of appropriate AlexaFluor 488® or AlexaFluor 594® conjugates (Thermo Fischer Scientific). Images were acquired with a LSM 510 confocal microscope (Carl Zeiss Microscopy, LLC) through a Plan-Apochromat 63x/1.4 oil objective (Carl Zeiss Microscopy, LLC).

Statistical procedures.

Unless otherwise indicated, assays were performed in triplicate independent instances, yielding comparable results. Data, which are presented as means ± SEM, were analyzed with Microsoft Excel (Microsoft Co.). Statistical significance was determined by means of

one-way or two-way ANOVA followed by two-tailed unpaired Student's *t* tests. *p* values <0.05 were considered statistically significant

Chapter 2. Regulation of autophagy and PKCβ levels by PML is essential for MDSC high glucose-dependent adipogenesis

Abstract

The promyelocytic leukemia protein (PML) is a well-known oncosuppressor directly involved in human tumor development. Recently several reports have demonstrated an unexpected and critical role of PML in stem cell biology and in metabolism regulation.

In this study, the role of PML in high glucose dependent adipogenesis of muscle derived mesenchymal stem cells (MDSCs) was investigated. We showed that the genetic and pharmacological deletion of PML impaired the adipogenic differentiation of MDSCs, suggesting that PML plays a crucial role in adipogenic differentiation process.

In agreement with current studies reporting that autophagic mechanism are involved in mesenchymal stem cell differentiation, here PML is been shown to regulate adipogenic differentiation through its ability to modulate autophagic levels. Indeed pharmacological modulation of autophagy was reported to reverse the effects on adipogenesis due to deletion of PML.

Moreover, for the first time, we identify that PML can act as PKCβ regulator. PKCβ is necessary for high glucose dependent adipogenesis, indeed its mRNA and protein levels increased in WT-MDSCs after addiction of Hg medium, but not in PMLKO-MDSCs. The overexpression of PKCβ in PMLKO-MDSCs is demonstrated to restore adipogenic differentiation.

These finding could help to understand the molecular mechanism of adipogenic process in order to suggest novel therapeutic strategies for metabolic and obesity-related disorders.

Introduction

1. PML, multiple function protein

The promyelocytic leukemia (PML) gene was first identified as a fusion partner of the human retinoic receptor alpha (RARα) as the result of a chromosomal translocation discovered in acute promyelocytic leukemia (APL) (de The, Lavau et al. 1991; Rowley 1982; Kakizuka, Miller et al. 1991). PML proteins dimerize through the RBCC domains and then multimerize to form multiprotein sub-nuclear structures called PML-nuclear bodies (PML-NBs), which have three major biological functions. First, PML-NBs operate as a nuclear sponge for proteins, accumulating and releasing proteins under normal conditions, and sequestering foreign or misfolded proteins in pathological conditions. Second, PML-NBs form catalytic surfaces for the post-translational modification of proteins by sumoylation, ubiquitination, phosphorylation or acetylation. Third, PML-NBs serve as active sites for specific nuclear functions such as transcriptional regulation or heterochromatin formation. Through these functions, PML-NBs orchestrate biological processes, including DNA damage response, apoptosis, senescence and angiogenesis in various tissues (Lallemand-Breitenbach and de The 2010; Bernardi and Pandolfi 2007).

The roles of PML and PML-NBs in solid tumors and leukemia pathogenesis has been deeply investigated, indeed PML is reported to explicate its functions through modulation of the activity of p53 (Bernardi, Scaglioni et al. 2004), Atk (Trotman, Alimonti et al. 2006), HIF1α (Bernardi, Guernah et al. 2006), or mitochondrial regulatory pathways (Giorgi, Ito et al. 2010). However little is known about the role of this tumor suppressor in stem cell biology or the mechanisms of its regulation of metabolism.

2. PML in stem cell biology

In the last years, a new possible role for PML as regulator of stem cell biology has emerged. Ito et al. showed a critical role of PML in the stem cells of the hematopoietic system, demonstrating that deletion of PML leads to loss of quiescence in hematopoietic stem cells, resulting in their transient amplification and subsequent exhaustion. Moreover they defined a critical role for PML in the maintenance of leukemia-initiating cells (LICs) in disease models of chronic myeloid leukemia (CML), and presented a new therapeutic approach based on targeting quiescent LICs by pharmacological inhibition of PML. Indeed, PML is often elevated in patients with CML, and these higher levels have been shown to correlate with poor clinical outcomes. In addition, PML-deficient LICs become exhausted with time, and are incapable of generating CML in transplanted animals. Interestingly, inhibition of PML by arsenic trioxide (Ato) disrupted LICs maintenance and

sensitized LICs to anti-leukemic therapy with little adverse effect on normal hematopoietic stem cells (Ito, Bernardi et al. 2008).

Much less it is known about stem cells located outside the hematopoietic system, such as mesechymal stem cell (MSCs). Human MSCs are an important type of adult stem cells and have multiple differentiation activities and high self-renewal potential. The ease of isolation and availability of MSCs make them attractive tools for potential use in cell transplantation therapy and tissue repair (Chen, Wang et al. 2012; Satija, Gurudutta et al. 2007). However, the mechanisms of the self-renewal and multiple differentiation capabilities of MSCs have not been fully elucidated, thus limiting the use of these powerful tools.

Recently, many research groups have investigated the regulation of MSCs proliferation and differentiation, and several important regulatory pathways have been revealed. In particular, the role of the Wnt signaling pathway on the fate of MSCs has been established. However, the effects of Wnt signaling can induce different or even opposite biological functions (Chen, Wang et al. 2012; Ling, Nurcombe et al. 2009). In the differentiation process of MSCs, the role of Wnt signaling is dependent on the level of the signals, and high levels of Wnt promote osteogenesis of MSCs, whereas low levels inhibit osteogenesis (De Boer, Wang et al. 2004). Thus, the complex effect of Wnt signaling is context-dependent and is closely related to its target genes (Ling, Nurcombe et al. 2009). Interestingly, Shtutman et al (Shtutman, Zhurinsky et al. 2002) reported that PML gene can function as a target of the Wnt signaling pathway, and its gene product is involved in the regulation of various cell functions. In addition Sun et al in 2013 revealed a previously unknown role of PML in the regulation of cell proliferation and osteogenic differentiation of MSCs. Briefly, PML regulates MSCs as an inhibitor of cell proliferation, but promotes osteogenic differentiation, which is associated with the upregulation of integrin-binding sialoprotein (bone sialoprotein) IBSP (Sun, Fu et al. 2013).

3. Adipocyte differentiation

Adipose tissue is characterized by a marked cellular heterogeneity including adipocytes, fibroblasts, endothelial cells and a combination of small MSCs, T regulatory cells, macrophages and preadipocytes in various stages of development. In particular preadipocytes have the ability to proliferate and differentiate into mature adipocytes, conferring adipose tissue a constant functional plasticity, which determines its ability to expand throughout the entire lifespan. Indeed, analysis of adipocyte turnover using carbon-14 dating has shown that adipocytes area dynamic and highly regulated population of cells.

New adipocytes form constantly to replace lost adipocytes, such that approximately 50% of adipocytes in the human subcutaneous fat are replaced every 8 years (Spalding, Arner et al. 2008).

The first hallmark of the adipogenesis process in vitro is the dramatic alteration in cell shape as the cells convert from fibroblastic to spherical shape; however adipogenesis is a multi-step process involving a cascade of transcription factors and cell-cycle proteins regulating gene expression and leading to adipocyte development.

Transcriptional regulation of adipocyte differentiation

A summary of main transcriptional regulators is presented in figure 13

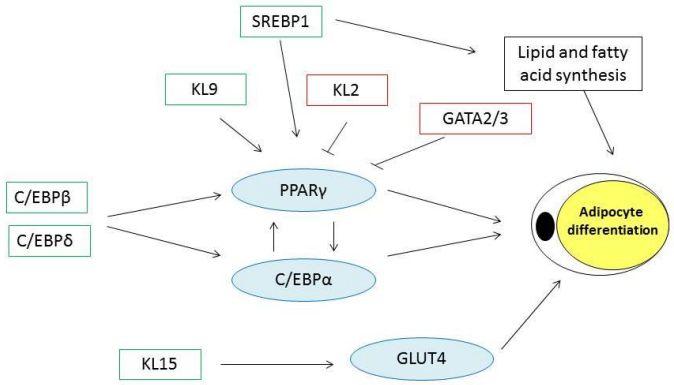

Figure 13. Schematic summary of main transcriptional regulators of adipogenic process. Activators as labeled by green boxes, inhibitors by red boxes.

The first stage of adipogenesis consists of the transient dramatic induction of C/EBP-β and C/EBP-δ, (stimulated in vitro by hormonal differentiation cocktail) (Ramji and Foka 2002) which begin to accumulate within 24 hours of adipogenesis induction (Tang, Otto et al. 2003). At this stage cells re-takes cell cycle and in the conversion from G1 to S stage, C/EBP-β is hyperphosphorylated and sequentially activated by glycogen synthase kinase-3 β and mitogen-activated protein kinase (MAPK). Then, both C/EBP-β and C/EBP-δ directly induce expression of PPAR-γ and C/EBP-α, the key transcriptional regulators of adipocyte differentiation (Tang, Gronborg et al. 2005).

PPAR-γ and C/EBP-α initiate positive feedback to induce their own expression and also activate a large number of downstream target genes whose expression determines the adipocyte differentiation. After few days C/EBP-α protein initiates to accumulate and to be phosphorylated by the cyclin D3, inducing a proliferation inhibition effect on the cells, which allow beginning final differentiation phase of adipogenesis (Wang, Shi et al. 2006).

PPAR-γ is a member of the nuclear receptor superfamily of ligand-activated transcription factors and is a prerequisite for the differentiation of both brown and white adipocytes

(Kajimura, Seale et al. 2008). All the studies performed on PPAR-γ gain and loss of function models confirmed that PPAR-γ is both necessary and sufficient for fat formation (Farmer 2006). Ectopic expression of C/EBP-α in fibroblasts can induce adipogenesis only in the presence of PPAR-γ (Freytag, Paielli et al. 1994). Accordingly, PPAR-γ ectopic expression can induce adipogenesis in mouse embryonic fibroblasts lacking C/EBP-α, but C/EBP-α cannot rescue adipogenesis when PPAR-γ is not expressed, showing that PPAR-γ is a master regulator of adipogenesis (Rosen, Hsu et al. 2002).

In addition to PPAR-γ and C/EBPs, several other transcription factors are likely to play an important role in the molecular control of adipogenesis.

The Kruppel-like factors (KLFs) are a large family of C_2H_2 zinc-finger proteins that regulate apoptosis, proliferation and differentiation. The range of KLF genes that are expressed in adipose tissue, the variability in their expression patterns during adipocyte differentiation and their effects on adipocyte development and gene expression indicate that a cascade of KLFs function during adipogenesis. For example, KLF15 promotes adipocyte differentiation (Mori, Sakaue et al. 2005) and induces expression of the insulin-sensitive GLUT-4 (Gray, Feinberg et al. 2002). KLF5 is induced early during adipocyte differentiation by C/EBP-β and C/EBP-δ and activates the PPARγ promoter, functioning in concert with the C/EBPs. KLF6 inhibits the expression of preadipocyte factor-1 (Pref-1) in 3T3-L1 cells and fibroblasts. Although overexpression of KLF6 is not sufficient to promote adipocyte differentiation, cells with reduced amounts of KLF6 show decreased adipogenesis (Li, Yea et al. 2005). Recently, KLF9 has been reported as a key pro-adipogenic transcription factor through regulation of PPARγ expression with C/EBP-α at the middle stage of adipogenesis. The expression of KLF9 was markedly upregulated during the middle stage of 3T3-L1 adipocyte differentiation and inhibition of KLF9 by RNAi impaired adipogenesis (Pei, Yao et al. 2011). However, not all KLFs promote adipocyte differentiation, for instance KLF2 represses the PPARγ promoter (Wu and Lingrel 2005).

Sterol regulatory element binding transcription factor 1 (SREBP1) was identified as a pro-adipogenic basic helix–loop–helix transcription factor that induces PPAR-γ expression (Kim, Sarraf et al. 1998). SREBP1 also mediates the induction of lipid biosynthesis by insulin in adipocytes increasing the gene expression of the main lipogenic genes, as fatty acid synthase and acetyl-CoA carboxylase (Kim, Wright et al. 1998).

Cyclic AMP response element-binding protein (CREB) also seems to have a possible role in the control of adipogenesis. CREB expression in 3T3-L1 preadipocytes is necessary and

sufficient to induce adipogenesis, whereas silencing of CREB expression blocks adipogenesis (Reusch, Colton et al. 2000; Zhang, Klemm et al. 2004).

Many transcription factors repress adipogenesis, including several members of the GATA - binding and forkhead families, Forkhead Box O1 (FOXO1) and Forkhead Box A2 (FOXA2). GATA2 and GATA3, two members of the GATA family of transcription factors which are zinc-finger DNA-binding proteins involved in developmental processes, are expressed in preadipocytes and downregulated during terminal maturation (Tong, Dalgin et al. 2000). Forced expression of GATA2 reduces adipogenesis, and GATA2-deficient embryonic stem cells displayed enhanced adipogenic potential. Constitutive expression of GATA2 and GATA3 blunts adipocyte differentiation and traps cells at the preadipocyte stage. This inhibitory effect on adipogenesis could be mediated through reduced PPARγ promoter activity (Tong, Tsai et al. 2005).

Extranuclear regulation of adipocyte differentiation

In addition to several transcriptional regulators also extranuclear factors play to orchestrate adipocyte differentiation. In table below the main extranuclear regulators of adipocyte differentiation are reported.

Insulin and IGF-1 signaling	The loss of individual insulin-receptor substrate (IRS) proteins inhibits adipogenesis	(Smith, Wise et al. 1988), (Bluher, Michael et al. 2002)
AKT1/2 and mTOR	Downstream effectors of insulin action cascade involved in adipogenesis	(Garofalo, Orena et al. 2003; Kim and Chen 2004)
Thyroid hormone	Plays a central role in normal development, differentiation and metabolic homeostasis. T3 induced adipogenesis through TR a 1-induced lipogenic gene expression, whereas TR a 2 antagonizes T3 action.In obese subjects, subcutaneous fat, with higher expression of TR a 1, is more T3 responsive than visceral fat.	(Ortega, Moreno-Navarrete et al. 2009)
Glucocorticoids	Potent inducers of adipogenesis in vitro, and hypercortisolism. Associated with obesity and disturbances in fat tissue distribution. Activate the expression of C/EBP-δ and PPARγ	(Wu, Bucher et al. 1996; Joyner, Hutley et al. 2000)
MAPK family members	ERK1 is required in the proliferative phase of differentiation, and blockade of ERK activity in 3T3-L1 cells or in mice inhibits adipogenesis. p38 MAPK is required for adipogenesis in 3T3-L1 but not in primary preadipocytes.	(Bost, Aouadi et al. 2005; Aouadi, Laurent et al. 2006)
Fibroblast growth factors (FGFs)	FGF1, FGF2 and FGF10, show proadipogenicactivity on human preadipocytes, and their neutralization inhibits adipogenesis	(Hutley, Shurety et al. 2004)

Anti-adipogenic factors

The Wnt family of secreted glycoproteins acts through autocrine or paracrine mechanisms to influence the development of many cell types. Wnt completely blocks induction of the key adipogenic transcription factors C/EBPα and PPARγ. In contrast, inhibition of Wnt

signalling in preadipocytes results in spontaneous differentiation, indicating that preadipocytes produce endogenous Wnt that is a potent inhibitor of differentiation. Ectopic expression of the Wnt gene potently represses adipogenesis (Ross, Hemati et al. 2000). In particular, the constitutive expression of WNT10b, a gene which is highly expressed in preadipocytes and downregulated during the course of differentiation, inhibits adipogenesis (Longo, Wright et al. 2004). Ectopic expression of WNT10b stabilizes free cytosolic β-catenin and is a potent inhibitor of adipogenesis. β-catenin functions as a Wnt effector, binds to the androgen receptor and is translocated to the nucleus in response to testosterone where it interacts with the TCF/LEF transcription factors to inhibit adipogenesis. Loss of β-catenin in myometrial tissue causes its conversion to adipose tissue, which shows that the Wnt-β-catenin pathway is an important regulator of adipogenesis and mesenchymal cell fate in vivo (Kanazawa, Tsukada et al. 2005; Singh, Artaza et al. 2006).

The transforming growth factor β (TGF-β) superfamily members, TGF-β, bone morphogenetic protein (BMP) and myostatin regulate the differentiation of many cell types, including adipocytes. TGF-β is a cytokine that stimulates preadipocyte proliferation and inhibits adipogenesis in vitro. TGF-β and its signalling components are expressed in cultured adipocytes and adipose tissue. Transgenic overexpression of TGF-β impairs the development of adipose tissue (Clouthier, Comerford et al. 1997). Blockade of endogenous TGF-β signalling by inhibition of SMAD3 increases adipogenesis. SMAD3 binds to C/EBPs and inhibits their transcriptional activity (Choy and Derynck 2003). Exposure of multipotent mesenchymal cells to BMP4 commits these cells to the adipocyte lineage, allowing them to undergo adipose conversion. The effects of BMP2 are more complex and are dependent on the presence of other signaling molecules. BMP2 stimulates adipogenesis of multipotent C3H10T1/2 cells at low concentrations, but favors chondrocyte and osteoblast development at higher concentrations. Myostatin, positively or negatively regulates adipogenesis in vitro, depending on the type of cell and culture conditions (Rebbapragada, Benchabane et al. 2003).

Pref-1 is a transmembrane protein that belongs to a family of epidermal-growth factor-like repeats containing proteins and is activated by proteolytic cleavage (Villena, Kim et al. 2002). Pref-1 cleavage releases an extracellular moiety that inhibits adipogenesis, possibly through interaction with Notch. Expression of Pref-1 is high in preadipocytes and normally declines during differentiation, and forced Pref-1expression in 3T3-L1 cells blocks adipogenesis. A soluble form of Pref-1 is sufficient to decrease adipose tissue mass and insulin sensitivity (Lee, Villena et al. 2003). Pref-1is implicated in the regulation of

adipogenesis by FOXA2 (Wolfrum, Shih et al. 2003), KLF6 (Li, Yea et al. 2005) and KLF2 (Wu, Srinivasan et al. 2005).

4. Autophagy

Macroautophagy (herein referred to as autophagy) is an evolutionarily conserved cellular process by which cells sequester a portion of their cytoplasm and organelles into double-membraned vesicles called autophagosomes that subsequently fuse with lysosomes for degradation of the enclosed materials (He and Klionsky 2009), (Fig 14).

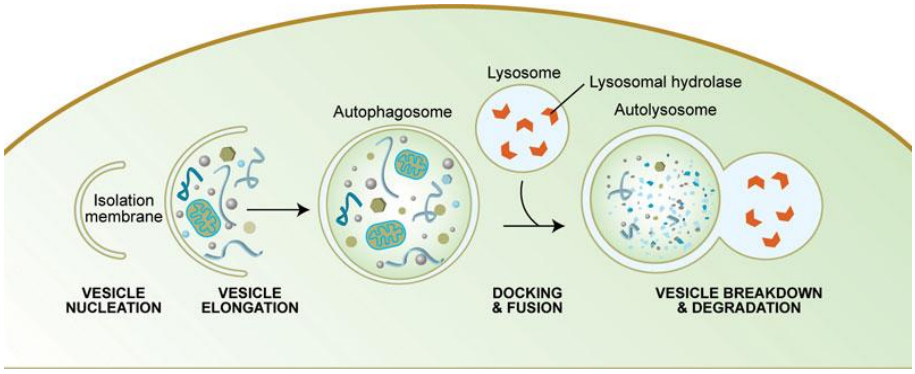

Figure 14: Schematic diagram of the steps of autophagy.
Autophagy begins with the formation of the phagophore or isolation membrane (vesicle nucleation step). The concerted action of the autophagy core machinery proteins at the phagophore assembly site (PAS) is thought to lead to the expansion of the phagophore into an autophagosome (vesicle elongation). The autophagosome can engulf bulk cytoplasm nonspecifically, including entire organelles, or target cargos specifically. When the outer membrane of the autophagosome fuses with an endosome (forming an amphisome before fusing with the lysosome) or directly with a lysosome (docking and fusion steps), it forms an autophagolysosome. Finally, the sequestered material is degraded inside the autophagolyosome (vesicle breakdown and degradation) and recycled.

Autophagosome formation is controlled by a series of protein complexes acting sequentially, including the ULK1-ATG13-RB1CC1/FIP200-C12orf44/ATG101 complex for autophagy induction, the class III phosphatidylinositol (PtdIns) 3-kinase complex (including BECN1, ATG14/ATG14L/Barkor, PIK3R4/VPS15, PIK3C3/VPS34 and AMBRA1) for initiation of autophagosomes, and the ATG12–ATG5-ATG16L1 complex and the MAP1LC3A/LC3 (ATG8 homolog)–phosphatidylethanolamine (PE) complex (both ubiquitin-like conjugation systems) for the extension and closure of the autophagosome double membranes (Fig. 15). Besides these core components, a number of other autophagy-related (ATG) genes characterized in yeast, and their mammalian orthologs, are also required for autophagy (Mizushima and Levine 2010). In addition, studies using proteomics approaches identified many other proteins in extensive networks that connect various cellular processes and signaling pathways to the autophagy machinery (Behrends, Sowa et al. 2010). Upon autophagosome maturation and the fusion of its outer membrane with the lysosome membrane, the contents as well as the inner membrane of

autophagosomes are degraded to generate amino acids and other cellular building blocks for recycling by the cell. Besides this recycling function in response to nutrient or energy starvation, autophagy is increasingly recognized as a quality control mechanism for both proteins and organelles.

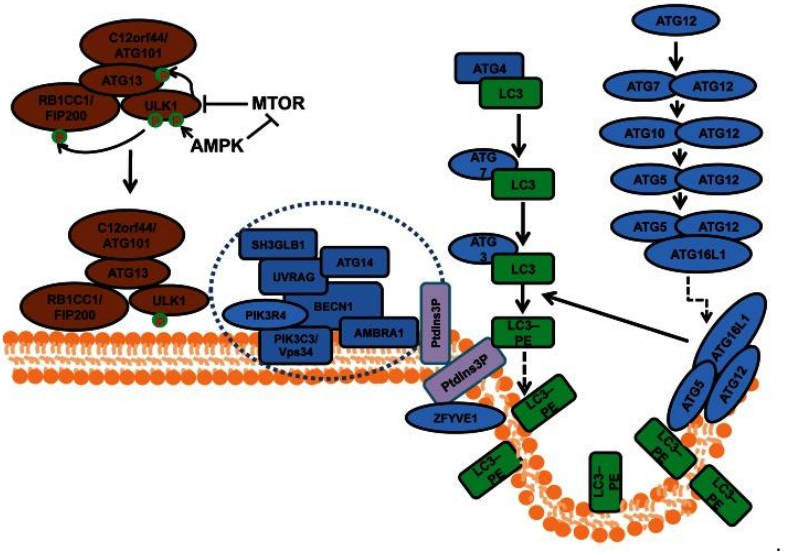

Figure 15. The process and regulation of autophagosome formation in mammalian cells
Mammalian autophagosome formation is induced by the activation of the ULK1 which is promoted by suppression of MTOR complex 1 (MTORC1) under starvation conditions or AMPK (both directly as well as by repressing MTORC1) in low-energy states. Once the activated ULK1 complex translocates to part of the endoplasmic reticulum (or possibly other intracellular membranes), it coordinates with the class III phosphatidylinositol-3-phosphate (PtdIns3P) kinase complex (including PIK3C3, BECN1, PIK3R4/p150, AMBRA1, UVRAG, ATG14 and SH3GLB1) for the initiation of autophagosomes upon formation of PtdIns3P and recruitment of double ZFYVE 1. Two ubiquitin-like systems including the ATG12–ATG5-ATG16L1 complex and the LC3–phosphatidylethanolamine (PE) conjugation system (including ATG3, ATG4, ATG7 and MAP1LC3) will then promote the elongation of phagophore membranes for the formation of autophagosomes.

Although originally classified as a type of programmed cell death, autophagy is more widely viewed as a basic cell survival mechanism to combat environmental stressors. Autophagy genes were initially identified in yeast and were found to be necessary to circumvent nutrient stress and starvation. Subsequent elucidation of mammalian gene counterparts has highlighted the importance of this process to normal development (Hale, Ledbetter et al. 2013). So autophagy is crucial for maintaining cellular homeostasis as well as remodeling during normal development, and dysfunctions in autophagy have been associated with a variety of diseases such as cancer, inflammatory bowel diseases and neurodegenerative diseases (Mizushima and Komatsu 2011; Rubinsztein, Marino et al. 2011).

A hallmark of cellular defects in neurodegenerative diseases is the accumulation of ubiquitinated protein aggregates (or inclusion bodies), which is normally cleared by the ubiquitin-proteasome degradation system as well as autophagy for larger aggregates (Rubinsztein 2006; Mizushima and Klionsky 2007). The accumulation of large protein

aggregates has been linked to increased neuronal apoptosis and axonal degeneration, accounting for the phenotypes in neurodegenerative diseases. In cancer, defective autophagy has been linked to increased DNA damage and gene mutations, leading to increased tumorigenesis (Mathew, Karantza-Wadsworth et al. 2007), as well as to the reduced proliferation of tumor cells during cancer progression and metastasis (Wei, Wei et al. 2011; Kimmelman 2011).

In contrast to the amount of data derived from studies of somatic cells and disease models, the role of autophagy in the maintenance and function of stem cells is poorly understood. Both embryonic and various tissue stem cells play essential roles in development, tissue renewal and certain disease processes. Many stem cells are also long lived and persist throughout the adult life of an organism, thus the quality control mechanisms and maintenance of cellular homeostasis would be crucial for the maintenance of these cells. Thus, autophagy is expected to play an important role in the normal function of stem cells and associated diseases. Indeed, consideration of the available data suggests that the unique properties of stem cells (self-renewal, pluripotency, differentiation and quiescence) are dependent on the activation of the autophagic process (Phadwal, Watson et al. 2013; Vessoni, Muotri et al. 2012). First, the processes of self-renewal and differentiation both require a strict control of cellular remodeling that involves protein turnover and lysosomal degradation of organelles (Zeng and Zhou 2008). Second, the elimination and turnover of damaged macromolecules and organelles are essential to preserve the pluripotency of long-lived stem cells during their lengthy periods of quiescence (Coller, Sang et al. 2006). Third, basal autophagy is a homeostatic process that mediates quality control, clearance of altered and damaged intracellular proteins and organelles, and cellular remodeling through degradation of structural components (Guan, Simon et al. 2013).

5. Autophagy and mesenchymal stem cells

The knowledge of autophagy's role in MSCs relies on the observation that primary human bone marrow MSCs have high levels of constitutive autophagy, which decrease when these cells differentiate into osteoblasts (Oliver, Hue et al. 2012), a feature also observed when bone marrow MSCs isolated from GFP-LC3 mice undergo osteoblast differentiation (Liu, Fang et al. 2013).

Recently, it has been proposed that MSCs are in a state of arrested autophagy, showing the accumulation of autophagosome, which rapidly undergoes autophagic degradation. The balance of autophagy seems to be the key for an efficient MSC differentiation and function. Upon induction of osteogenic differentiation, LC3II expression is lost within 12h.

By contrast, during adipogenic differentiation, treatments with rapamycin led to inhibition of adipocyte formation while autophagosome blockade by bafilomycin accelerated fat accumulation (Nuschke, Rodrigues et al. 2014).

On the other hand, it has been proposed that autophagyis important for avoiding senescence of MSCs cultured in vitro. MSCs undergo senescence, after few cycles of replication in vitro, and these senescent cells maintain their characteristic metabolic modification and remain viable for long periods. It has been observed that senescent rat MSCs increased their basal autophagy activity, showing a greater number of autophagic vacuoles and increased the expression levels of LC3, ATG7 and ATG12. Pharmacological inhibition of autophagy with bafilomycin A1 and 3-MA reduced the expression levels of senescence-related proteins, suggesting that autophagy is activated during senescence for maintaining the senescent state of MSCs (Zheng, Hu et al. 2014).

There is growing evidence for a pivotal role of autophagy in MSCs-derived cells, such as adipocytes, chondrocytes, and osteoblasts/osteocytes. Adipose specific deletion of Atg7 leads to decreased adipose mass and enhanced insulin sensitivity, with autophagy playing an important role, as suggested by the observation that autophagy-deficient primary Atg5ko MEFs exhibit reduced efficiency in adipogenesis (Baerga, Zhang et al. 2009; Singh, Xiang et al. 2009; Zhang, Goldman et al. 2009). Autophagy has also proved important in chondrocytes, where silencing of Becn1 results in enhanced chondrocyte death while 3-MA administration renders the chondrocytes refractory to killing, suggesting that sustained autophagy promotes cell death (Bohensky, Shapiro et al. 2007). In this context, autophagy may act both as cytoprotective and a pro-death process, possibly involved in the onset and/or progression of diseases. In fact, autophagy regulatory proteins such as ULK1, BECN1, and LC3A prove to be constitutively expressed in normal human articular cartilage, whereas their expression is reduced in osteoarthritis chondrocytes and cartilage (Carames, Taniguchi et al. 2010).

Osteocytes have also have been shown to utilize autophagy for their homeostasis. It has been reported that glucocorticoid (GC) treatment dose-dependently decreased antioxidant gene expression, with low GC doses activating autophagy, whereas high-dose increased apoptosis, suggesting autophagy as mechanism to survive GC exposurestress (Jia, Yao et al. 2011). Osteoblasts, the precursor of osteocytes, activate autophagy during their differentiation. Accordingly, osteoblast-specific deletion of RB1CC1/FIP200 led to osteopenia in mice as well as to defective osteoblast terminal differentiation in both primary bone marrow and calvarial osteoblasts in vitro. Administration of autophagy inhibitors 3-MA and chloroquine recapitulates the phenotype observed when FIP200 is

deleted, suggesting that autophagy is important in supporting osteoblast differentiation (Liu, Fang et al. 2013). The data available as of today support the idea that autophagy activation is important in cultured bone marrow MSCs, but does not completely clarify the role played by autophagy in processes such as stemness maintenance, self-renewal and differentiation. Thus, many questions still remain unanswered.

Results

1. PML is essential for high glucose dependent adipogenic differentiation.

In order to determine the involvement of PML in adipogenic process we decided to perform experiment in muscle derived stem cells (MDSCs) obtained from newborn WT and PMLKO mice. These cells can be isolated from the skeletal muscle of 5 days C57BL/6mice and selected by the preplate technique, which is based on the properties of distinct cell populations to selective adhesion to the culture plate at different time points (optimized from (Lavasani, Lu et al. 2013); a schematic representation is shown in Figure 16.

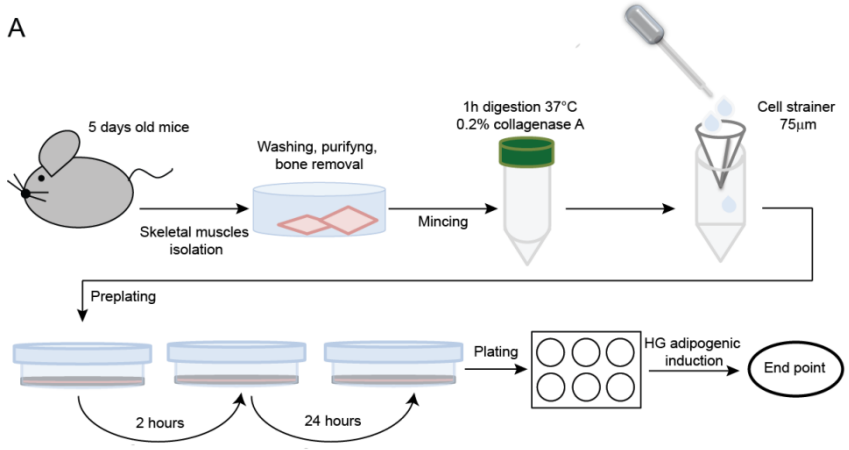

Figure 16. Schematic representation of MDSCs isolation by preplate technique. 5 days old mice were sacrificed and the skeletal muscles were isolated. After washes and bone removal the muscles were minced and digested for 1 hour at 37°C by 0.2% collagenase A 0.2%. Using a 75 µm cell strainer obtained cells were purified from the undigested tissue and plated. After 2 hours the suspension containing MDSCs were plated in a new dish and that passage was repeated after 24 hours. Cells able to attach after 24 hours are defined MDSCs and used for all the experiments of this paper.

Moreover we have reported that high-glucose (Hg) concentration, one of the most common conditions leading to an increase in adipose tissue in vivo (Chuang, Yang et al. 2007), could affect MDSCs differentiation into mature adipocytes in vitro (Aguiari, Leo et al. 2008).

Activation of adipocyte commitment was reported to be induced by a cascade of key transcriptional factors, among which the master regulator is PPARγ (Tontonoz, Hu et al. 1994). So, to assess the adipogenic potential of WT-MDSCs and PMLKO-MDSCs the PPARγ protein levels were detected by immunoblot. As shown in Fig 17A and 17B, PPARγ protein levels in WT-MDSCs increased following the addition of Hg for 7 days, unlike the PMLKO-MDSC in which PPARγ protein levels remained unaltered from low-glucose (Lg) to Hg condition.

Furthermore PPARγ directs the expression of a multiplicity of genes that are responsible for the fully adipocyte differentiation, including glucose transporter 4 (GLUT4), which

contribute to the creation and maintenance of the adipocyte phenotype (Smas and Sul 1995; Spiegelman, Choy et al. 1993). With the expression of this protein, cells acquire a capacity for insulin-stimulated glucose transport, and lipid droplets begin to appear in the cytoplasm and over time coalesce into fewer major droplets in the cells.

As expected, under Hg condition the GLUT4 protein levels increased in WT-MDSCs, but the same effects was showed in PMLKO-MDSCs (Fig 17A and 17C). After all, the basal levels of GLUT4 in Lg condition were minor in PMLKO-MDSCs compared to WT-MDSCs, and after the addition of Hg the total GLUT4 protein levels did not reach the WT-MDSCs levels. That should suggest that PMLKO-MDSCs were able to feel the increase in glucose concentration, confirmed by the increment of GLUT4 protein, but the impairment in PPARγ protein expression did not allow the adipogenic process.

During adipogenesis, differentiating cells start to accumulate lipids in their cytosol which can be detected by oil red O (ORO) staining.

The number of ORO positive cells is a marker for adipogenic differentiation and, as shown in figure 17D and 17E, the PMLKO-MDSCs cultured in Hg were unable to accumulate lipid and so differentiate in contrast with the WT-MDSCs. Indeed the percentage of ORO positive cells increased from 1.3 to 16.9 in WT-MDSCs while from 1.25 to 2.7 in PMLKO-MDSCs.

To confirm that PML deletion can prevent adipogenic differentiation, the PML protein levels were pharmacologically decreased in WT-MDSCs by arsenic trioxide (Ato), typically used in APL therapy to degrade the PML-RARα (Lallemand-Breitenbach, Zhu et al. 2001). We confirmed that Ato treatment is able to drastically reduce the PML protein levels in our model (Fig 17A) and that, due to this reduction, the adipogenesis process was prevented (Fig 17A-E). Indeed PPARγ and GLUT4 protein levels did not increase after Hg addition and the number of ORO positive cells was significantly reduced respect to untreated condition.

In addition, in order to understand if PML deletion can prevent or only delay the adipogenic differentiation, the accumulation of lipid drops was followed for 21 days. Data shown that percentage of ORO positive WT-MDSCs in Hg constantly increased, while PMLKO-MDSCs were unable to differentiate.

The adipogenic deficiency shown in PMLKO-MDSCs was not only associated on the number of cells able to differentiate but also to a deficiency of lipid drop formation.

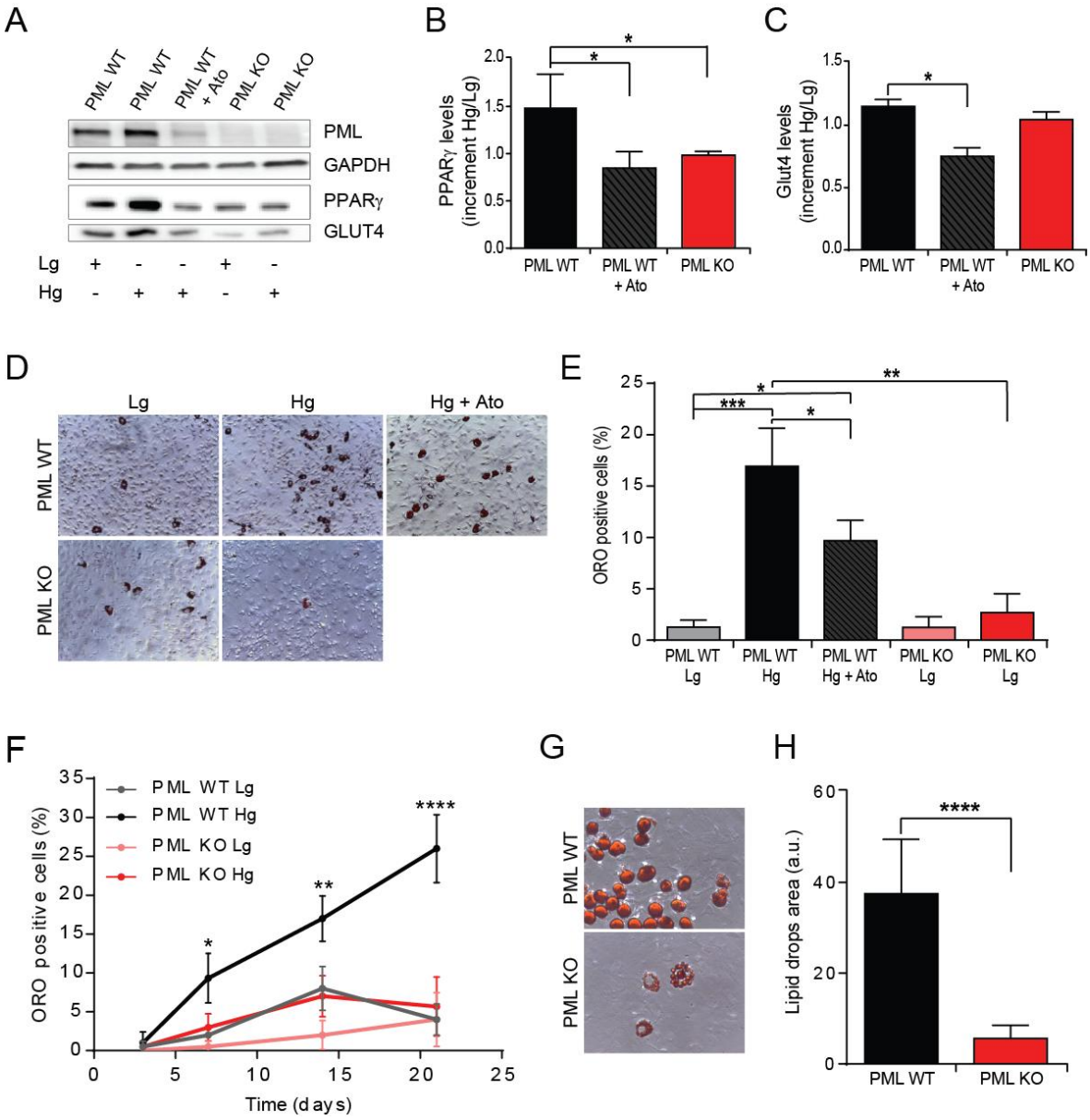

Figure 17. PML is essential for high glucose dependent adipogenic differentiation.
(**A**) Representative immunoblot of PML, GAPDH, PPARγ and GLUT4 proteins levels in WT and PMLKO MDSC. Where indicated they were cultured in 5mM glucose (Lg), 25 mM glucose (Hg) and 25 mM glucose plus 500 nM arsenic trioxide (Ato) for 7 days. The adipogenic differentiation was shown as increment of ratio Hg/Lg of PPARγ (**B**) and GLUT4 (**C**) levels and as lipid drops accumulation (**D-H**). (**D**) Representative images and (**E**) quantification of lipid drops by Oil Red O (ORO) staining, shown as % of positive cells on total cells. Magnifications 10X. (F) Quantification of lipid drops accumulation in PML WT and PML KO MDSC cultured in Lg or Hg for 3, 7, 14 and 21 days. Data were shown as % mean ± stdev. ANOVA test (**G**) Representative images and (H) quantification of lipid drops area in PML WT and PML KO MDSC cultured in Hg for 21 days. Magnifications 40X. Data were shown as % mean ± stdev. Student's t-test.

As shown in figure 17G and 17H, after 21 days of Hg adipogenic induction, the few PMLKO-MDSCs able to differentiate showed small lipid drops and not all the cytosol was filled by the lipid drop as in the WT-MDSCs, sustaining the hypothesis that PML is essential for a correct high glucose dependent adipogenic differentiation.

2. PML deletion increases autophagy levels

Macroautophagy (termed autophagy in this manuscript) is a bulk degradation process that occurs sequestrating proteins and organelles into double-membrane vesicles called autophagosomes and their subsequent degradation through the fusion of autophagosomes with lysosomes (Xie and Klionsky 2007). By selectively degrading harmful protein aggregates or damaged organelles, autophagy maintains intracellular homeostasis and plays essential quality control functions within the cell (Mizushima and Komatsu 2011).

Recently we demonstrated that PML represses the autophagic process (Missiroli, Bonora et al. 2016) in primary mouse embryonic fibroblasts and in vivo. Here we confirmed the role of PML as regulator of autophagy levels in our experimental model.

The autophagy protein microtubule-associated protein 1 light chain 3 (MAP1LC3A, best known as LC3) is in the cytosol as LC3-I form, until it is cleaved in LC3-II, its membrane-bound form, which is localized to autophagosomes. Detection of the conversion of LC3-I to LC3-II via immunoblotting confirmed that PMLKO-MDSCs and WT-MDSCs treated with Ato contained higher levels of LC3-II than WT-MDSCs (Fig 18A and 18B).

Another key marker to detect autophagy activity is p62/SQSTM1. p62 acts as a receptor for ubiquitinated cargoes and delivers them and itself to the autophagosome leading to subsequently degradation (Komatsu, Waguri et al. 2007). The levels of p62 in PMLKO-MDSCs and in WT-MDSCs treated with Ato decreased compared to WT-MDSCs (Fig 18A and 18C).

In addition, autophagosomes were detected in live imaging experiments as fluorescent cytoplasmic dots that concentrated LC3fused to GFP. The number of GFP-LC3-positive dots was higher in PMLKO-MDSCs and WT-MDSCs treated with Ato respect to WT-MDSCs (Fig 18D). Taken together, these data confirmed that the deletion of PML increased autophagy levels.

Treatment with Ato is reported to can modulate autophagic machinery, leading to an increase in both p62 and LC3-II levels, indicating a block in the autophagic process (Ren, Xie et al. 2011). To make sure of the correct activity, the autophagic flux was challenged by treatment with NH_4Cl, an inhibitor of autophagic flux. The accumulation of LC3-II

after NH_4Cl administration (Fig 18E) demonstrated that in our experimental conditions the autophagic flux was not blocked.

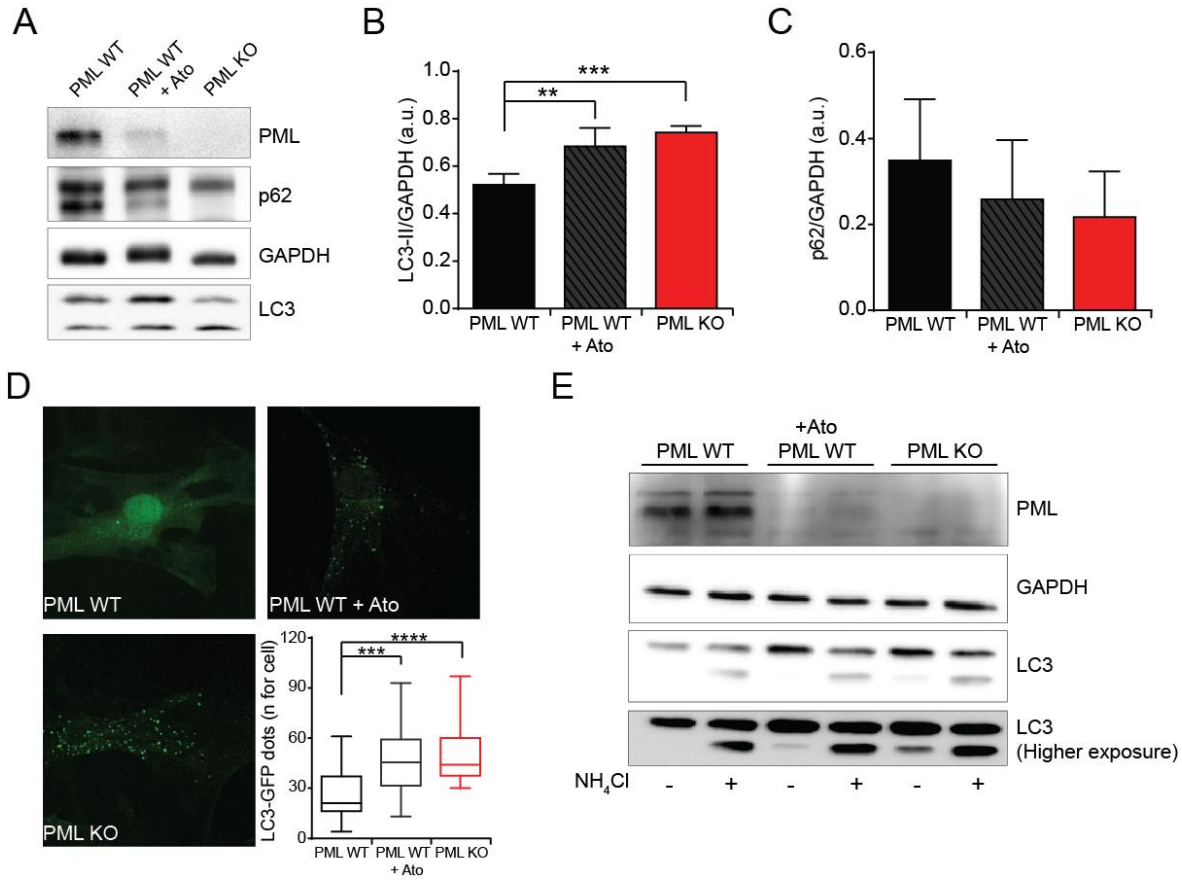

Figure 18. PML deletion increases autophagy levels.
PML WT and PML KO MDSC were cultured in 25 mM glucose (Hg) and, where indicated, 25 mM glucose plus 500 nM arsenic trioxide (Ato) for 7 days. (**A**) Representative immunoblot of PML, p62, GAPDH and LC3 protein levels, quantification of (**B**) LC3II/GAPDH and (**C**) p62/GAPDH relative protein levels. Data were shown as % mean ± stdev. ANOVA test. (**D**) Representative images and quantification of LC3 clustering in MDSC infected with GFP-LC3 virus. Magnifications 60X. (**E**) Analysis of autophagic flux. Representative immunoblot of PML, GAPDH and LC3 protein levels after addition, where indicated, of NH_4Cl 20 mM for 1 hour

3. Autophagy modulation affects Hg adipogenic differentiation

Among its myriad of cellular and developmental functions, mTOR has emerged as a key regulator of lipid metabolism and adipogenesis in recent years. The adipogenic function of mTORC1 in vivo is evidenced by the reduced and increased adiposity in S6K1KO (Um, Frigerio et al. 2004; Carnevalli, Masuda et al. 2010) and 4ebp1/2KO mice (Le Bacquer, Petroulakis et al. 2007) and by the lean phenotype of adipose-specific Raptor KO mice (Polak, Cybulski et al. 2008). A positive regulatory role of mTOR in adipogenesis has also been established in preadipocyte differentiation in vitro through the effects of rapamycin. Indeed upon rapamycin inhibition of mTORC1 or depletion of S6K1, the essential input from mTORC1 to PPARγ was shown to be abrogated, resulting in inhibition of adipogenesis (Yoon, Zhang et al. 2013).

This link between mTOR regulation (and consequent autophagy levels regulation) and adipogenesis should explain the different phenotypes showed after deletion or reduction of PML levels in MDSC.

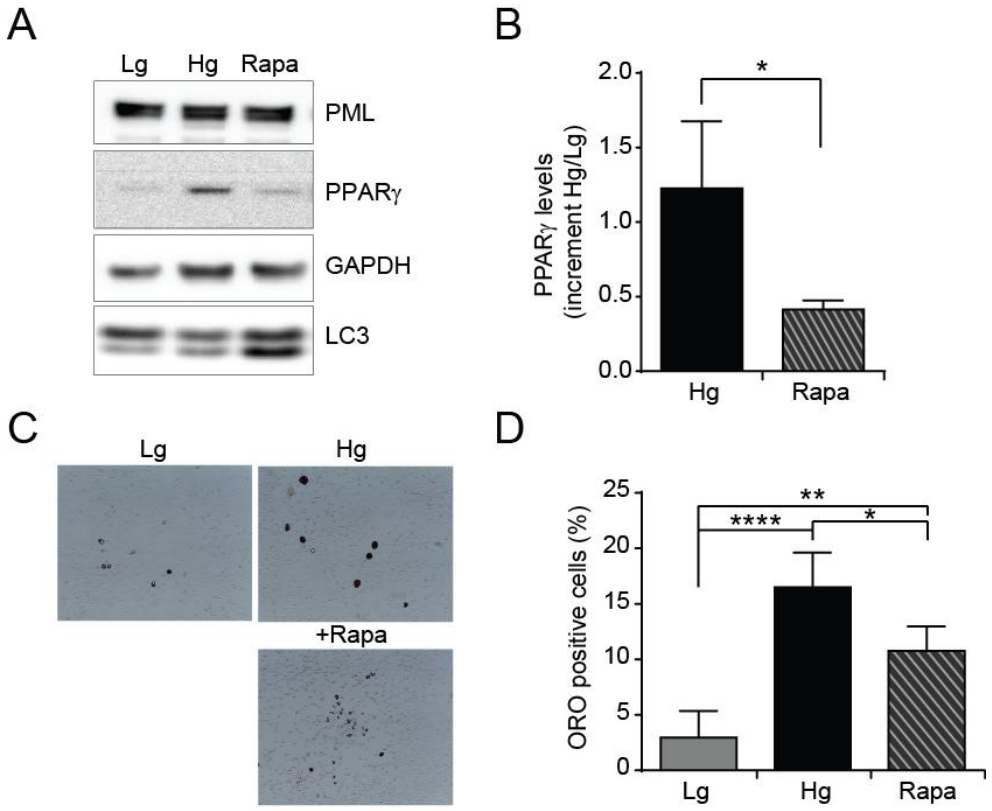

Figure 19.Autophagy induction correlates with adipogenic defects
(**A**) Representative immunoblot of PML, PPARγ GAPDH, and LC3 proteins levels in WT-MDSC. Where indicated they were cultured in 5mM glucose (Lg), 25 mM glucose (Hg) and 25 mM glucose plus 100nM Rapamycin (Rapa) for 7 days. The Rapa effect on autophagy was detected by LC3-II accumulation and the adipogenic differentiation was shown as increment of ratio Hg/Lg of PPARγ levels (**B**), data were shown as % mean ± stdev. Student's t-test. (**C**) Representative images and (**D**) quantification of lipid drops by Oil Red O (ORO) staining, shown as % of positive cells on total cells. Magnifications 10X. Data were shown as % mean ± stdev. ANOVA test.

To confirm this hypothesis WT-MDSCs were treated by rapamycin to mimic the high autophagic levels showed in PMLKO-MDSCs. Rapamycin was added to Hg for 7 days in WT-MDSCs confirming its effect on autophagic levels, as showed by the increase of LC3-II conversion (Fig 19A). Following rapamycin treatment the PPARγ protein levels did not increase (Fig 19A and 19B), and consequently the % of ORO positive cells in WT-MDSCs significantly decreased (Fig 19C and 19D) compared to WT-MDSCs cultured in Hg condition. The lipid droplets accumulation was not completed blocked, suggesting on one hand the non-toxic effect of rapamycin on the cell culture, and on the other hand that autophagy levels can be a modulator of adipogenic process.

On the other hand, we tried to inhibit autophagy in PMLKO-MDSCs. Clozapine, a second generation antipsychotic drug, was reported to inhibit autophagosome turnover resulting in

a dysfunctional autophagic process, including impaired lysosomal fusion (Park, Chung et al. 2012). We decided to use this inhibitor due to its reported role in adipogenesis process; indeed treatment with clozapine increased adipogenesis by 37.4% during 3T3-L1 cell differentiation accompanied by increased SREBP-1, PPARγ, C/EBPα, LDLR and Adiponectin gene expression (Hu, Kutscher et al. 2010). We confirmed the inhibitory effect on autophagy in our *in vitro* model, as shown by the accumulation of LC3-I and LC3-II in PMLKO-MDSC cultured in Hg plus clozapine (Fig 20A). Inhibition of autophagosome turnover results in proceeding of adipogenesis in PMLKO-MDSCs, in which the PPARγ protein levels increased (Fig 20A) and cells were able to accumulate lipid drops (Fig 20B and 20C).

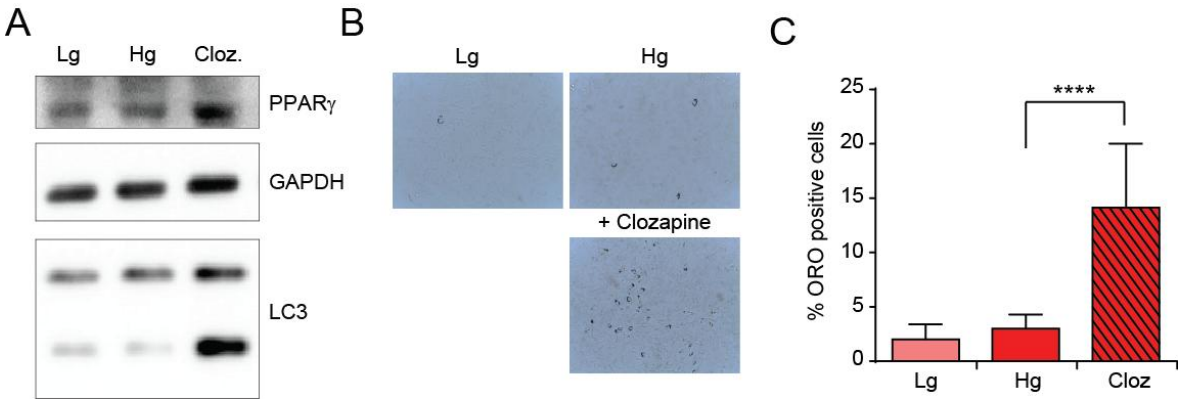

Figure 20.Inhibition of PML KO autophagy high levels restore adipogenic differentiation

(**A**) Representative immunoblot of PPARγ GAPDH, and LC3 proteins levels in PMLKO-MDSC. Where indicated they were cultured in 5mM glucose (Lg), 25 mM glucose (Hg) and 25 mM glucose plus 7.6 µM Clozapine (Cloz.) for 7 days. The Cloz effect on autophagy was detected by LC3-I and LC3-II accumulation. (**B**) Representative images and (**C**) quantification of lipid drops by Oil Red O (ORO) staining, shown as % of positive cells on total cells. Magnifications 10X. Data were shown as % mean ± stdev. ANOVA test

4. PKCβ levels regulation by PML allows high glucose dependent adipogenic differentiation

PKC family members play essential roles in a variety of physiological functions including cell metabolism, proliferation, differentiation, cell migration, and apoptosis (Clemens, Trayner et al. 1992; Gallicano, Yousef et al. 1997; Zhou, Wang et al. 2006). Several reports indicated that PKC isoforms may be involved in the regulation of adipocyte differentiation (Artemenko, Gagnon et al. 2005; Fleming, MacKenzie et al. 1998; McGowan, DeVente et al. 1996).

Moreover the specific isoform PKCβ was reported to inhibit autophagy (Patergnani, Marchi et al. 2013), indeed PKCβKO MEFs showed an increase in autophagic levels.

To assess the direct involvement of PKCβ in Hg-dependent differentiation process, the adipogenic potential in PKCβKO-MDSCs was analyzed. As shown in figures 21A and 21B the PKCβKO-MDSCs were unable to accumulate lipid droplets and so to differentiate following the administration of Hg. PKCβKO-MDSCs showed a phenotype similar to PMLKO-MDSCs, moreover we confirmed that autophagic levels in PKCβKO-MDSCs are higher respect to WT-MDSCs (Fig 21C), joining another common aspect with PMLKO-MDSCs. Starting from these observations, in searching for the molecular mechanism at the base of Hg-dependent adipogenesis, the PKCβ protein levels were detected in our experimental conditions. We showed that the pharmacologically and genetically deletion of PML was associated to PKCβ protein levels reduction (Fig 21D and 21E). In order to understand how PML could regulate PKCβ protein levels, we analyzed the mRNA relative levels of PKCβ; data showed a significant reduction in PKCβ mRNA expression in WT-MDSCs treated by Ato and in PMLKO-MDSCs compared to WT-MDSCs (Fig 21F), demonstrating a transcriptional regulatory role of PML on PKCβ during Hg-dependent adipogenic differentiation. To assess the direct role of PKCβ in this process we reintroduced PKCβ by virus infection in PMLKO-MDSCs. MDSCs can be infected by adenovirus carrying PKCβ-GFP and the efficiency of the transduction was confirmed by immunoblot analysis (Fig 21G). The transduction of PKCβ in PMLKO-MDSCs restored the ability of endogenous PKCβ to increase under Hg condition, as a positive feed-back. More important in PMLKO-MDSCs transduced by PKCβ the PPARγ levels increased. The restore of adipogenic potential in PMLKO-MDSCs transduced by the PKCβ virus was assessed by lipid drops accumulation. As shown in figure 21H and 21I the % of positive cells doubled in PMLKO-MDSC after the reintroduction of PKCβ, supporting the hypothesis that PKCβ regulated by PML plays a crucial role in Hg-dependent adipogenic differentiation.

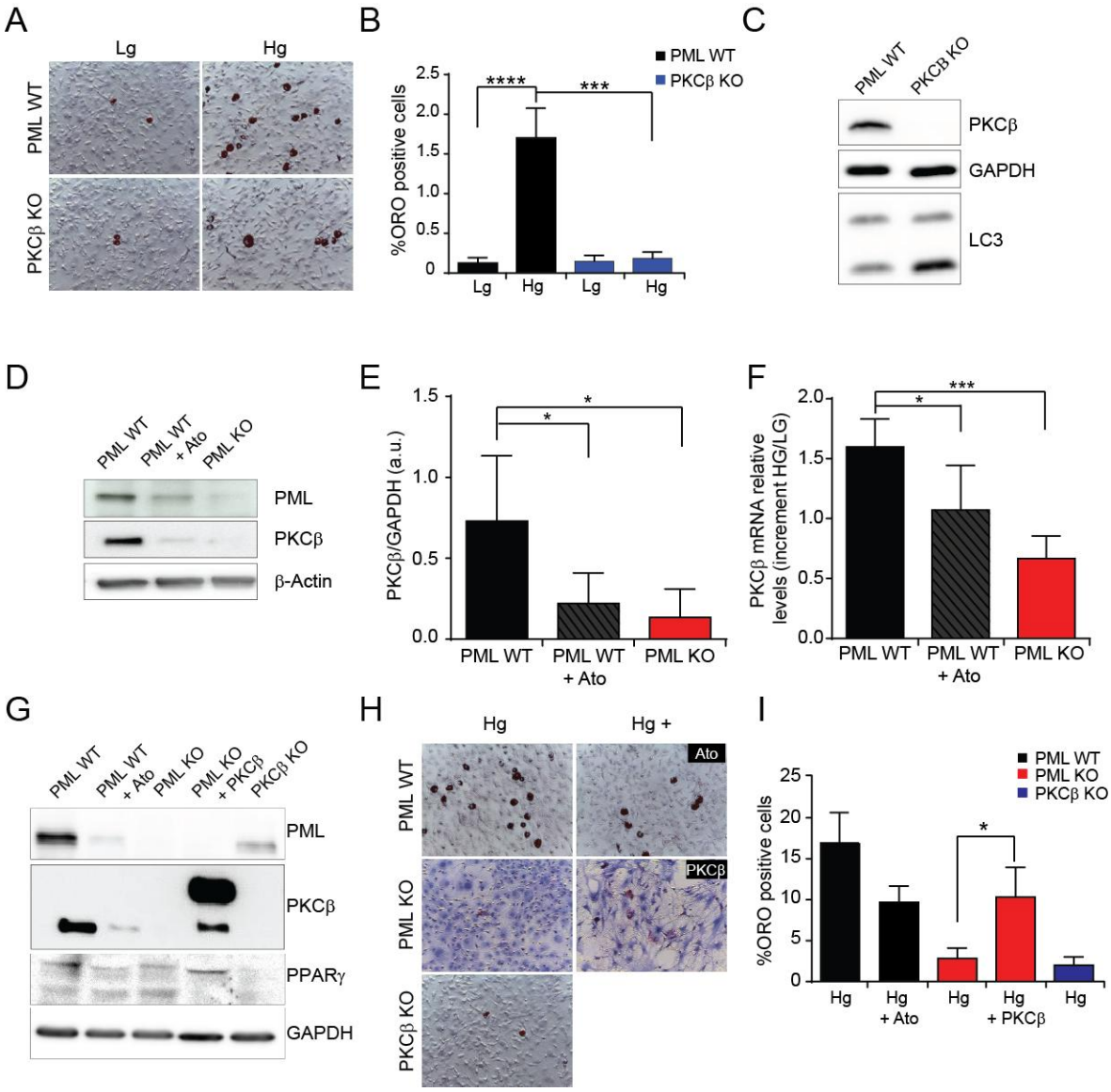

Figure 21. Lack of PKCβ expression in PML KO prevents high glucose dependent adipogenic differentiation.

(**A**) Representative images and (**B**) quantification of lipid drops by Oil Red O (ORO) staining in PMLWT and PKCβKO MDSC cultured in 5mM glucose (Lg) or 25 mM glucose (Hg). Data are showed as % of positive cells on total cells. Magnifications 10X. (**C**) Representative immunoblot of PKCβ, GAPDH and LC3 protein levels to detect autophagy levels.

(**D**) Representative immunoblot of PML, PKCβ and β-Actin proteins levels, (**E**) quantification of PKCβ protein levels and (**F**) PKCβ mRNA relative levels in PMLWT and PMLKO MDSC cultured in 25 mM glucose (Hg) and, where indicated, 25 mM glucose plus 500 nM arsenic trioxide (Ato).

(**G**) Representative immunoblot of PML, PKCβ, PPARγ and GAPDH protein levels inPMLWT, PMLKO and PKCβKO MDSC cultured in 25 mM glucose (Hg) and, where indicated, 25 mM glucose plus 500 nM arsenic trioxide (Ato) or infected with PKCβ virus for 7 days. (**H**) Representative images and (**I**) quantification of lipid drops by Oil Red O (ORO) staining inPMLWT, PMLKO and PKCβKO MDSC cultured in 25 mM glucose (Hg) and, where indicated, 25 mM glucose plus 500 nM arsenic trioxide (Ato) or infected with PKCβ virus for 7 days. Data were showed as % of positive cells on total cells. Magnifications 10X.

All data were shown as % mean ± stdev. ANOVA test

5. PML-PKCβ regulation is specific of Hg-dependent adipogenesis pathway

Controversial data are reported in literature about the role of PML in adipogenic differentiation and its role as metabolic regulator. Different groups published opposite data about the response of PML KO mice to diet induced obesity (Kim, Yang et al. 2011), (Cheng, Guo et al. 2013). They speculated that the composition of the diet may interact in a different manner in the diverse genetic backgrounds of the mice being studied. The animals consequently could develop distinct metabolic profiles that contribute to the varied phenotypes. Despite the different phenotypes observed in these studies, it is clear that PML is a critical metabolic regulator in the mouse and further investigation to dissect the mechanisms underlying the phenotypic differences caused by different diets and genetic backgrounds are necessary.

Moreover Kim et al showed that PML expression was highest in growing and confluent 3T3-L1 cells but decreased after adipogenic induction, and suggested that PML could be a negative regulator of adipogenic process (Kim, Yang et al. 2011). Since this data seemed to be in contrast with our results, we evaluated the role of PML during "classical" adipogenesis induction. The commercial mediums used to induce adipogenic differentiation in vitro are composed by insulin, 3-isobutyl-1-methylxanthine (IBMX), indomethacin and dexamethasone.

The accumulation of lipid drops was followed for 21 days after the addition of adipogenic cocktail in WT-MDSCs and PMLKO-MDSCs. The percentage of differentiated cells considerably increased respect to Hg-dependent differentiation condition, suggesting that a different pathway of the adipogenic process should be triggered. Moreover although at 7 days we showed that the percentage of ORO positive PMLKO-MDSCs were significantly less respect to the WT-MDSCs, this difference was recovered after a week (Fig 22A).

In addition the protein levels of PKCβ during Hg and classical adipogenic differentiation were revealed by immunoblotting analysis (Fig 22B). The PKCβ protein levels constantly increased in WT-MDSCs in Hg condition, whereas, as we supposed from our previous data, the same did not happened in PMLKO-MDSCs. Interestingly the addition of classical adipogenic cocktail did not affect clearly the PKCβ expression. From this data we supposed that the classical adipogenic cocktail could act directly activating the master regulator of transcription factors involved in adipogenesis, instead PML/PKCβ regulation could act upstream.

To validate this hypothesis PMLKO-MDSCs were cultured for 7 days in Hg plus troglitazone. Troglitazone is reported to be a full agonist of PPARγ in 3T3L1 adipocytes and to be able to stimulate PPARγ transcriptional activity (Camp, Li et al. 2000). PMLKO-

MDSCs treated with troglitazone were able to differentiate, as demonstrated by the lipid drops accumulation (Fig 22C and 22D) following the increase of PPARγ levels (Fig 22E). Moreover this process did not involve the PKCβ pathway; indeed following troglitazone administration the PKCβ protein levels did no increase.

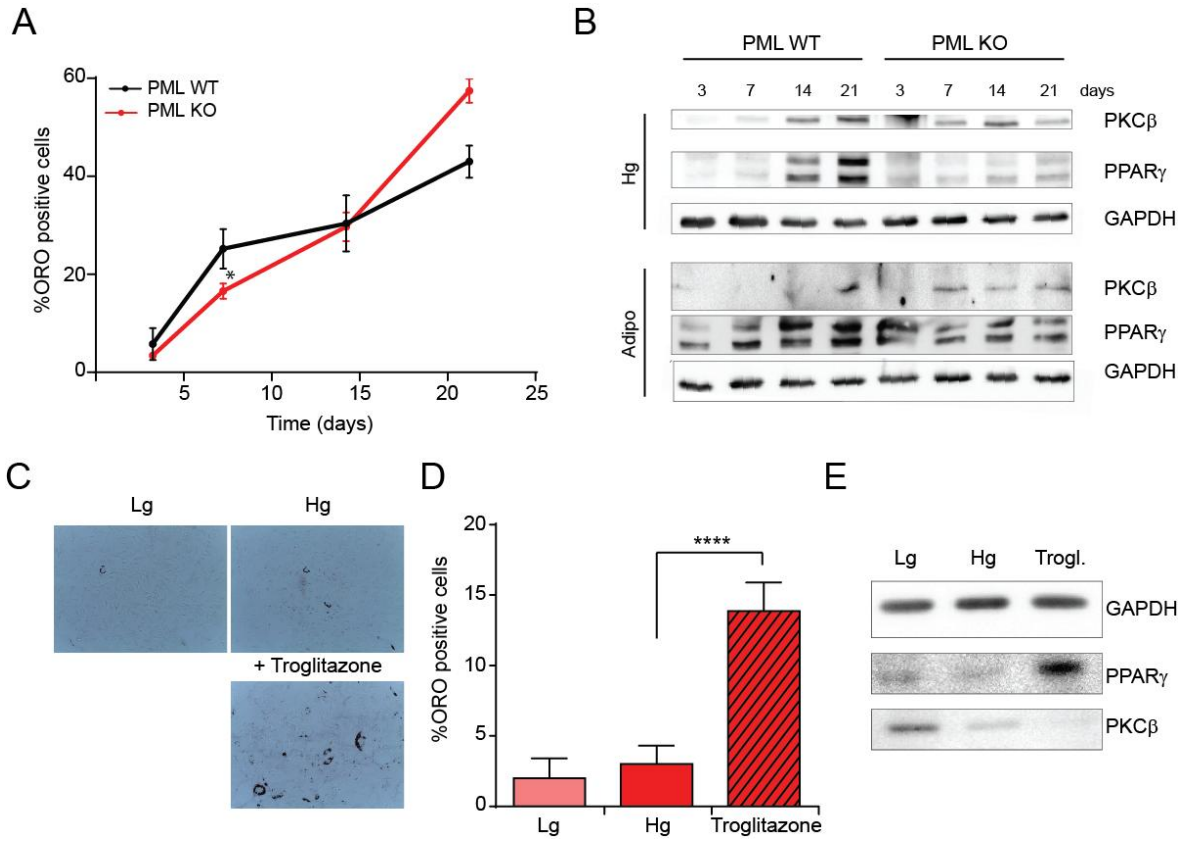

Figure 22.PML KO did not affect adipogenesis induced by classical cocktail
(**A**) Quantification of lipid drops accumulation in WT-MDSC and PMLKO-MDSC cultured in adipogenic cocktail medium (10 µg/mL insulin, 0,5 mM IBMX, 0,1 mM indomethacin, 1 µM dexamethasone) for 3, 7, 14 and 21 days. Data were shown as % mean ± SEM. Student's t-test. (**B**) Representative immunoblot of GAPDH, PPARγ and PKCβ proteins levels in WT-MDSC and PMLKO-MDSC cultured in Hg and adipogenic cocktail mediumfor 3, 7, 14 and 21 days. (**C**) Representative images and (**D**) quantification of lipid drops by Oil Red O (ORO) staining in PMLKO-MDSC cultured in 5mM glucose (Lg), 25 mM glucose (Hg) and 25 mM glucose plus 4.5µM troglitazone for 7 days. Data were showed as % of positive cells on total cells. Magnification 10X. (**E**) Representative immunoblot of GAPDH, PPARγ and PKCβ proteins levels in PMLKO-MDSC cultured in 5mM glucose (Lg), 25 mM glucose (Hg) and 25 mM glucose plus 4.5 µM troglitazone for 7 days.

Discussion

In this study, we showed that PML plays a crucial role in Hg-dependent adipogenic process. Indeed the genetic and pharmacological deletion of PML in MDSCs impaired PPARγ expression and lipid drops accumulation. Several reports have demonstrated an unexpected and critical role of PML in stem cell and progenitor cell biology, for instance PML is required for HSCs maintenance and NPCs differentiation (Regad, Bellodi et al. 2009; Ito, Bernardi et al. 2008). Yet, the role of PML in MSCs biology remains unknown. MSCs are multipotent cells with the potential to differentiate into a variety of cell lineages (Pittenger, Mackay et al. 1999). The biology of MSCs and their capacity to treat various diseases have therefore been extensively studied, as well as the potential roles of MSCs in managing the various components of metabolic syndrome (Tolar, Le Blanc et al. 2010; Bernardo, Pagliara et al. 2012). Obesity is considered the main culprit of metabolic syndrome. Severe obesity is due to an increase in adipocyte size combined with increased adipocyte number (Brook, Lloyd et al. 1972; Faust, Johnson et al. 1978; Hirsch and Batchelor 1976) and recent evidence suggests that MSCs are a major source of adipocyte generation, resulting in an increased adipocyte number (Matsushita 2016).

Different groups have reported that the expression of PML is relevant for the response to metabolic insults, nutritional disorders and obesity; but the results of their studies were contradictory, and a deeper investigation of the reasons of this have to be investigated.

Carracedo et al studied the consequences of high-fat diet (HFD) (60% of calories from fat) on adult WT and PML KO mice of a pure 129Sv genetic background. They showed that PML KO mice exhibited a significant increase in body weight and fat mass compared with WT mice. Moreover the augmented sensitivity to HFD-induced obesity was associated with parameters of metabolic syndrome, including exacerbated glucose intolerance and serum leptin levels (Carracedo, Weiss et al. 2012). In agreement, Kim et al showed that despite having normal food intake and activity levels, PML KO mice gained body weight faster and had more fat mass in the diet-induced obesity model compared to WT mice. Differently, they reported that PML KO mice did not show any significant metabolic defects (Kim, Yang et al. 2011).

Completely in contrast with this data, Cheng et al showed that PML KO mice exhibit altered gene expression in liver, adipose tissue, and skeletal muscle, an accelerated rate of fatty acid metabolism, abnormal glucose metabolism, constitutive AMP-activating kinase (AMPK) activation, and insulin resistance in skeletal muscle. They highlighted that increased rate of energy expenditure protects PML KO mice from the effects of obesity induced by a Western diet (Cheng, Guo et al. 2013).

Here we showed that PMLKO-MDSCs were unable to differentiate under Hg condition, whereas they did not show deficiency under classical adipogenic cocktail. This could suggest that different pathways are involved in adipogenesis, and as different cocktails *in vitro* show different results, also in *in vivo* a meticulous selection of suitable diet should be carried out. Indeed, they speculate that the composition of the diet may interact in a different manner in the diverse genetic backgrounds of the mice being studied (Cheng, Guo et al. 2013), but a deeper study has never been produced.

Interestingly in 2015 an evaluation of PML transcript abundance in a cohort of human liver biopsies from lean or morbidly obese subjects was published. This study revealed a significant PML up-regulation in obese individuals, and demonstrated that PML accumulates in hepatocytes in conditions of obesity (Carracedo, Rousseau et al. 2015). Moreover, obesity is associated to lipid accumulation in hepatocytes, termed steatosis (Fracanzani, Valenti et al. 2011); their results clearly demonstrated that PML expression significantly correlated with the extent of steatosis.

This observation might open an interesting mean of regulation of PML in the context of cancerous lesions, in which nutrient availability might impact on the expression of this protein and hence on the biology of the disease. Furthermore this highlights the involvement of PML in adipogenic process in different tissue, such as liver.

Supporting our results about the role of PML in adipogenesis process, Cheng et al in 2015 published a paper about the ability of Ato to inhibit adipogenic process in bone marrow MSC of aplastic anemia patients. The typical pathological feature of aplastic anemia is the rise in the number of fat cells and the reduction of osteoblasts in bone marrow. Both fat cells and osteobalsts in bone marrow are derived from MSCs. Generally, the adipogenic and osteogenic differentiation is a dynamic and balanceable process, and the imbalance of this process may participate in the occurrence and progress of many diseases. In this study they reported that Ato inhibits adipogenic differentiation and promotes osteogenic differentiation in the MSCs of aplastic anemia patients (Cheng, Liu et al. 2015). They did not correlate the effects to PML levels, but in agreement with data here showed this could explain the efficiency of the Ato therapy and provide new target for the treatment of aplastic anemia and other disease in which an imbalance of MSCs differentiation was observed.

Moreover we identified a primary role of Hg exposure in adipogenic differentiation creating a direct link between hyperglycemia and the increase in adiposity, which may play a key role in the progression of the metabolic dysfunction into, for example, an irreversible diabetic state.

It is clear that this process should be involved in many diseases and the understanding of the molecular mechanism of the process should provide new therapeutic targets.

We, for the first time, identified a correlation between PML, PKCβ and autophagy levels.

As reported in "introduction" section, there is growing evidence for a pivotal role of autophagy in MSCs-derived cells, such as adipocytes, chondrocytes, and osteoblasts/osteocytes. From this crucial point we started to investigate the possible molecular mechanism of PML KO imbalance of Hg-dependent adipogenic process.

We recently demonstrated that PML represses the autophagic process (Missiroli, Bonora et al. 2016) and here we confirm that PMLKO-MDSCs show high levels of autophagy respect to WT-MDSCs. We confirmed that the autophagic levels regulated by PML are the responsible of correct adipogenesis. Indeed the modulation of autophagy levels, in WT by Rapamycin and in PMLKO by Clozapine, is able to restore the effects due to PML background. Moreover we confirm that the autophagic process is directly involved in MSCs differentiation.

PKCβ shares several aspects with PML: PKCβ is involved in the regulation of adipocyte differentiation (Zhou, Wang et al. 2006), and it was reported to inhibit autophagy (Patergnani, Marchi et al. 2013). In addition PKCβ KO mice ate more food than WT mice daily, but gained less weight, suggesting that there are important alterations in energy expenditure and disposition (Bansode, Huang et al. 2008).

For that reasons we searched for PKCβ levels in our experimental models. We showed that PKCβ upregulationwas necessary for Hg-dependent adipogenic differentiation, and that PML deletion prevented PKCβ upregulation, resulting in adipogenesis impairment.

PKCβ has a role in differentiation by participating in the ERK signaling pathway (Lee, Kwak et al. 2003), and the activation of MEK/ERK signaling was reported to promote adipogenesis by enhancing PPARγ and C/EBPα gene expression during the differentiation of 3T3-L1 preadipocytes (Prusty, Park et al. 2002). If it is well established the possible role of PKCβ as regulator of adipogenic process, how PML could regulate PKCβ should be elucidated. On the base of our results we could only suggest that PKCβ is regulated at transcriptional levels by PML.

In conclusion, we suggested that during Hg-dependent adipogenesis PML is fundamental to maintain the correct levels of autophagy and to promote PKCβ expression in order to obtain correct differentiation. This new link between PML, autophagy and PKCβ could provide new therapeutic target for metabolic disease and disease characterized by an imbalance of MSCs differentiation process.

Future studies aimed at identifying how PML could regulate PKCβ should provide greater insight the molecular mechanism regulating the high glucose dependent adipogenic differentiation of MSCs.

Materials and Methods

Cell cultures

Primary cultures of muscle-derived stem cells (MDSCs) were prepared from newborn C57BL/6 WT, PML KO and PKCβ KO mice. 5 days old mice were sacrificed and the skeletal muscles were isolated. After washes and bone removal the muscles were minced and digested for 1 hour at 37°C by 0.2% collagenase A 0.2%. Using a 75 µm cell strainer obtained cells were purified from the undigested tissue and plated in DMEM Lg (5mM). After 2 hours the suspension containing MDSCs were plated in a new dish and that passage was repeated after 24 hours. Cells able to attach after 24 hours are defined MDSCs and used for all the experiments of this paper.

Adipogenic differentiation

For the high glucose dependent adipogenic differentiation DMEM Lg (5mM) was replaced with DMEM Hg (25mM) for 7 days or time indicated in the results.

For the classical adipogenic cocktail differentiation DMEM Lg (5mM) was replaced with DMEM Hg (25mM) plus 10 µg/mL insulin, 0,5 mM IBMX, 0,1 mM indomethacin, 1 µM dexamethasone for 3, 7, 14 and 21 days.

Oil Red O staining

Oil red O (Sigma-Aldrich) staining of the cytoplasmic droplets of neutral lipids was performed according to the standard procedure. Monolayer cultures were fixed by 10% paraformaldehyde for 10 min, washed with PBS, permeabilized by isopropanol for 5 min and let dry. Then Oil Red O working solution was added to well for 10 min at room temperature. After washing, stained cells were acquired by light microscopy. Magnifications 10X.

Immunoblotting

For immunoblotting, cells were scraped into ice-cold, phosphate buffered saline (PBS) and lysed in a buffer containing 50 mMTris-HCl pH 7.4, 150 mM NaCl, 1% Triton X-100, 0.2% SDS, protease, and phosphates inhibitor cocktail. After 30 min of incubation on iceand centrifugation at 2500 rpm 4°C for 5 min, proteins were quantified by the Lowry method and 15 µg of each sample were loaded on anacrilamide geland transferred to nitrocellulose membranes. After incubation with TBS–Tween-20 (0.05%) supplemented with 5% non-fat powdered milk for 1 h to saturate unspecific binding sites, membranes were incubated over night with primary antibodies. Finally, membranes were incubated with appropriate horseradish peroxidase (HRP)-labeled secondary antibodies (Thermo

Fischer Scientific), followed by detection by chemiluminescence (ThermoScientific), using ImageQuant LAS4000 (GE Healthcare).

Antibodies

For immunoblotting, the following primary antibodies were used: mouse anti-PML [MAB3738] (1:3000) from Millipore; rabbit anti-PPARγ [2435](1:1000) and rabbit anti-GAPDH [2118] (1:5000) from Cell Signaling; rabbit anti-GLUT4 [2213] (1:1000), rabbit anti-p62 [P0067] (1:1000), mouse anti-β-actin [A1978] (1:10000), rabbit anti-LC3B [L7543] (1:1000) from Sigma-Aldrich; PKCβ [ab32026] (1:1000) from Abcam.

Reagents and viral vectors

For pharmacological deletion of PML arsenic trioxide (Ato) 500 nM in DMEM Hg was used. NH_4Cl 20 mM for 1 hour was added to DMEM Hg to block autophagic flux. Rapamycin 100 nM was used to induce autophagy in WT-MDSC. Clozapine 7.6 µM was used to inhibit autophagy in PMLKO-MDSC. 4.5 µM troglitazone was used to induce PPARγ expression in PMLKO-MDSC. Were indicated cells were infected by GFP-LC3 virus and PKCβ virus.

Fluorescence microscopy and quantitative analysis of GFP-LC3 dots

Cells were cultured in a 24 mm glass coverslips and infected at 50% confluence by GFP-LC3 virus. After 36 h, images were takenon a Nikon LiveScan Swept Field Confocal Microscope (SFC) Eclipse Ti equipped with NIS-Elements microscope imaging software (Nikon Instruments). For each condition, the number of GFP-LC3 dots was counted in at least 15 independent visual fields.

Real-Time RT-PCR and Quantitative RT-PCR

Total RNA was extracted with TRIzol Reagent (Invitrogen, Carlsbad, CA, USA). RNAs were purified with RNeasy Mini Kit (Qiagen GmbH, Hilden, Germany), and DNase digestion was performed with RNase-Free DNase Set (Qiagen). The RNA quality and concentrationwere measured using the NanoDropTM ND-1000 (Thermo Scientific). For the first-strand cDNA synthesis, 1,000 ng of total RNA ofeach sample was reverse-transcribed with M-MLV Reverse Transcriptase (Invitrogen), following the manufacturer's protocol.

Real-time PCRs were carried out using the designedprimers at a concentration of 300 nM and FastStart SYBR GreenMaster (Roche Diagnostics, Mannheim, Germany) on a Rotor-Gene3000 (Corbett Research, Sydney, Australia). Thermal cycling conditionswere as follows: 10 min denaturation at 95°C, followed by 40 cycles of denaturation for 10 s at

95°C; annealing for 20 s at 60°C; and elongation for 30 s at 72°C. Values were normalized to the expression of the glyceraldehyde-3-phosphate dehydrogenase (GAPDH) internal reference.

Statistical analysis

The results were expressed as the mean ±SD. The probability of statistical differences between experimental groups was determined by the ANOVA test, results from treatments showing significant overall changes were subjected to post hoc Bonferroni tests. The Student's t-test was used to determine statistical significance between two groups.*p* values <0.05 were considered statistically significant. Different labels indicate *p<0.05, ** p<0.001, *** p<0.0001 and ****p< 0.00001.

Chapter 3. Mitochondria-nucleus communication in mesenchymal stem cell differentiation: key role of acetyl-CoA transport system

Abstract

Growing evidence shows that cellular metabolism underlies stem cell fate, including pluripotency, differentiation and reprogramming. In addition to generating ATP, through oxidative phosphorylation, mitochondrial metabolism provides the building blocks to support biomass, such as amino acid and lipids, and is involved in cell signaling in determining stem cells fate. Here, we investigated if and how the distribution and the physiology of mitochondria of adult mesenchymal stem cells derived from adipose tissue (ADSCs) could change during adipogenic and osteogenic commitment. We showed that mitochondrial mass and mitochondrial respiration increased, especially in the early phase of differentiation process.

We identified sites of contacts between mitochondria and nucleus, which increase in volume and number during differentiation process, suggesting that mitochondria could communicate with nucleus to orchestrate differentiation. Acetyl-coA is a key metabolite that could link metabolism with signaling, chromatin structure, and transcription. Here, we showed that inhibition of mitochondrial acetyl-CoA transport system impaired osteogenesis leading to a reduction of H3K9 acetylation, an epigenetic osteogenic marker.

These finding highlighted that mitochondria metabolites could play a key regulatory role in differentiation process which have to be deeply investigated and could suggest novel therapeutic strategies in field of regenerative medicine.

Introduction

1. Multipotent mesenchymal stem cells: adipose-derived stem cells

Promising bioengineering technologies, such as tissue engineering, which is an interdisciplinary field involving physicians, engineers, and scientists, may provide novel tools for reconstructive surgery. A number of conditions, such organ failure, tissue loss due to trauma, cancer abrasion, and congenital structural anomalies, can be treated by current clinical procedures/surgical strategies including organ transplantation, autologous tissue transfer, and the use of artificial materials; however, these treatments have potential limitations, including organ shortages, damage to healthy parts of the body during treatment, allergic reactions, and immune rejection. Recent developments in the emerging field of stem cell science, stem cell-associated growth factors, and regenerative medicine may allow the use of stem cells to repair tissue damage and, eventually, to replace organs. Stem cell candidates include embryonic stem cells (ESCs), induced pluripotent stem cells (iPSCs), and postnatal adult stem cells (Mizuno, Tobita et al. 2012).

ESCs are capable of extensive self-renewal and expansionand have the potential to differentiate into any type of somatic tissue (Lenoir 2000). These traits make human ESCs promising for future use in regenerative medicine. iPSCs are derived from differentiated cells such as skin fibroblasts and appear to have the same potential and properties; however, their generation is not dependent upon a source of embryos (Takahashi and Yamanaka 2006). As such, although the therapeutic potential of both ESCs and iPSCs is enormous due to their auto-reproducibility and pluripotentiality, there are still some limitations to their practical use: for example, cellular regulation of teratoma formation, ethical considerations, immuneconcerns regarding ESCs, and difficulties with genetic manipulation with respect to iPSCs (Ben-David and Benvenisty 2011).

In contrast, post-natal adult stem cells are, by their nature, immune compatible, and there are no ethical concerns related to their use. Mesenchymal stem cells (MSCs) are adherent fibroblast-like multipotent cells, which can differentiate into mesoderm cell lineages such as osteoblasts, chondrocytes, myoblasts and adipocytes (Pittenger, Mackay et al. 1999). Recently, it was demonstrated that MSCs could differentiate into cells in different germ layers, such as ectodermal neuronal-like cells as well as endodermal hepatocyte-like cells (Dezawa, Kanno et al. 2004). MSCs were first derived from bone marrow (BM) (Pittenger, Mackay et al. 1999).

The Mesenchymal and Tissue Stem Cell Committee of InternationalSociety for Cellular Therapy has defined human MSCs based on the following four criteria: (1) plastic-adherent and fibroblast-like cells; (2) the ability of osteogenic, chondrogenic and adipogenic

differentiation; (3) simultaneous expression of CD73, CD90 and CD105; (4) lack of expression of CD11b, CD14, CD19, CD34, CD45, CD79α and human leukocyte antigen-DR (Dominici, Le Blanc et al. 2006). MSCs are full of potential for cell therapies due to their multipotency and the therapeutic advantage of hypo-immunogenicity (Kassem and Abdallah 2008) and low tumorigenicity (Bauer, Dao et al. 2008).

MSCs, with similar characteristics to bone marrow derived MSCs, have been isolated from different tissue sources including trabecular bone (Song, Young et al. 2005), periosteum (Choi, Noh et al. 2008), synovial membrane (De Bari, Dell'Accio et al. 2001), skeletal muscle (Dodson, Hausman et al. 2011), pericytes (Feng, Mantesso et al. 2010), peripheral blood (Shi, Ishikawa et al. 2009), deciduous teeth (Miura, Gronthos et al. 2003), periodontal ligament (Seo, Miura et al. 2004), and umbilical cord (Baksh, Yao et al. 2007). Although the stem cell populations derived from these sources are valuable, common problems include low number of harvested cells and limited amount of harvested tissues. Therefore, almost all adult-derived stem/progenitor cells require at least some degree of ex vivo expansion or further manipulation before they are used pre-clinically or clinically to satisfy efficacy and safety requirements.

In contrast, the multipotent stem cells within adipose tissue, termed adipose-derived stem cells (ADSCs) (Zuk, Zhu et al. 2001), are one of the most promising stem cell population identified thus far, since human adipose tissue is ubiquitous and easily obtained in large quantities with little donor site morbidity or patient discomfort. Therefore, the use of autologous ADSCs as both research tools and as cellular therapeutics is feasible and has been shown to be both safe and efficacious in preclinical and clinical studies of injury and disease (Gimble, Katz et al. 2007; Tobita, Orbay et al. 2011).

2. Mitochondrial biogenesis and upregulation of antioxidant enzymes during MSCs differentiation

Mitochondria produce the majority of ATP through respiration and oxidative phosphorylation (OXPHOS). The electron transport chain (ETC) is composed of NADH-coenzyme Q oxidoreductase (Complex I), succinate-coenzyme Q oxidoreductase (Complex II), ubiquinol-cytochrome c oxidoreductase (ComplexIII), and cytochrome c oxidase (COX, Complex IV). The electron flow through the ETC establishes a proton gradient across the inner membrane, which is utilized to drive ATP synthesis by the FoF1ATPase (Complex V) (Senior, Nadanaciva et al. 2002). Upregulation of mitochondrial biogenesis (Chen, Shih et al. 2008) and aerobic metabolism (Zhang, Marsboom et al. 2013) are the hallmarks of the differentiation of MSCs.

Mitochondrial biogenesis is regulated by extracellular stimuli such as cold exposure, fasting, exercise, oxidative stress and cell differentiation. It is established that proliferator activated receptor gamma coactivator-1α (PGC-1α) regulates mitochondrial biogenesis by increasing the expressionof mitochondrial biogenesis-associated genes, such as nuclear respiratory factors (NRFs) (Zhang, Marsboom et al. 2013). NRF-1 and NRF-2 are transcription factors, which regulate nuclear DNA-encoded proteins involved in mitochondrial respiration and OXPHOS. In addition, NRF-1 can activate the expression of mitochondrial transcription factor A (mtTFA), which binds to the D-loop of mtDNA and coordinates with DNA polymerase γ to replicate mtDNA (Ekstrand, Falkenberg et al. 2004). Many studies have revealed that defects in mitochondrial biogenesis or OXPHOS are involved in the pathophysiology of mitochondrial disease, metabolic syndrome, heart disease, and type 2 diabetes (Ren, Pulakat et al. 2010). It was demonstrated that upon osteogenic induction of MSCs, proteins involved in mitochondrial biogenesis are all increased, which include mtTFA, DNA polymerase γ and PGC-1α, and some of the enzymes of TCA cycle and protein subunits of respiratory enzymes (Chen, Shih et al. 2008). Furthermore, it was reported that osteogenic differentiation of MSCs is accompanied by cristae development and increase in the expression levels of the constituent subunits and activity of respiratory enzyme complexes (Sanchez-Arago, Garcia-Bermudez et al. 2013; Pietila, Palomaki et al. 2012). Moreover, the respiration rate, mitochondrial membrane potential and intracellular ATP content were also increased, indicating an upregulation of oxidative metabolism in mitochondria during the differentiation of MSCs (Chen, Shih et al. 2008). ATP synthesis is coupled with respiration in normal mitochondria, which also produces a certain amount of reactive oxygen species (ROS) as byproducts. During respiration of mitochondria, the electrons may leak out from Complex I and Complex III to react with O_2 to generate the superoxide anion ($O_2^{-\bullet}$) (Murphy 2009), which can be converted to hydrogen peroxide (H_2O_2) by superoxide dismutase (SOD) and further decomposed to O_2 and H_2O by catalase or glutathione peroxidase. Excess ROS can cause DNA damage, lipid peroxidation and oxidative modification of proteins, which are detrimental to cell function (Adam-Vizi and Starkov 2010). Accumulated evidence has substantiated the notion that oxidative stress can lead to a wide spectrum of human diseases such as cardiovascular disease, neurological disorders, diabetes and cancers (Turrens 2003). Therefore, the intracellular levels of ROS should be effectively controlled by the antioxidant defense system. MSCs express significant levels of active forms of catalase, glutathione peroxidase and superoxide dismutase, which confers the differentiating cells with the ability to cope with ROS-mediated oxidative stress

and avoid damages (Valle-Prieto and Conget 2010). It was reported that the mitochondrial ROS generated from Complex III during respiration is also involved in the regulation of adipogenic differentiation (Tormos, Anso et al. 2011). Recently was found that MnSOD, CAT, GPx and glutathione reductase are up-regulated during adipogenic differentiation of human MSCs. Furthermore, forkheadbox O 3a (FOXO3a), an upstream factor that regulates MnSOD transcription, is involved in the upregulation of antioxidant enzymes at the early stage of adipogenic differentiation of MSCs. It has been shown that adipogenic differentiation is associated with the up-regulation of FOXO1 to counteract the increase in the ROS production, which has a pivotal role in maintaining cellular redox homeostasis and regulating the expression of antioxidant enzymes (Higuchi, Dusting et al. 2013).

3. Metabolic switch during MSCs differentiation

Several studies demonstrated that oxidative metabolismis activated by induction of the expression of respiratory enzymes and increase of the OXPHOS of mitochondria during osteogenic differentiation of MSCs (Chen, Shih et al. 2008). In addition, glycolysis is reduced during osteogenic differentiation of MSCs as revealed by a dramatic decrease in the production of lactate (Chen, Hsu et al. 2010), (Figure 23).

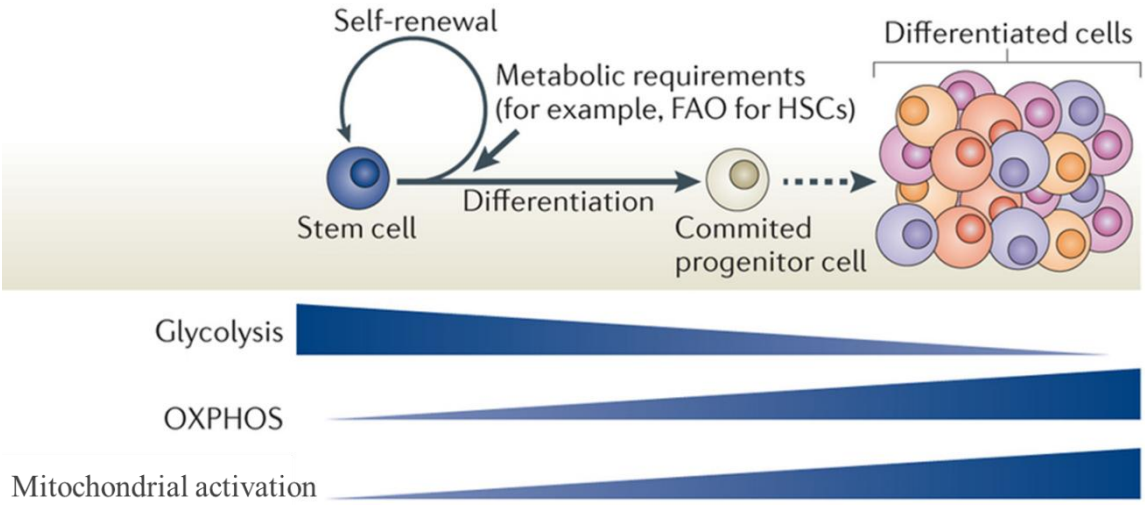

Figure 23. Stem cell equilibrium is bioenergetically and biosynthetically balanced through proper regulation of the flux of pathways that metabolize glucose, Mitochondria in stem cells are relatively inactive and stem cells heavily rely on anaerobic glycolysis, whereas oxidative phosphorylation (OXPHOS) is associated with differentiation. Figure modified from "Itp K, 2014. Metabolic requirements for the maintenance of self-renewing stem cells. Nature reviews molecular cell biology"

These findings suggest a metabolic switch upon the osteogenic differentiation of MSCs. A similar change in metabolic profile was also observed during adipogenic differentiation. A remarkable increase in mitochondrial respiration and decrease in glycolytic flux were observed in adipocytes differentiated form MSCs. In particular, the metabolic state of stem

cells may depend on their niche. Most differentiated cells are located around the blood vessels for ample supply of oxygen to support oxidative metabolism. By contrast, the stem cells or transplanted MSCs in the injured tissues are usually exposed to low oxygen tension or hypoxic stress that disturbs aerobic metabolism. Under such conditions, cells utilize anaerobic glycolysis to supply the majority of energy needed for the execution of cellular functions. It was demonstrated that hypoxia inducible factor-1α (HIF-1 α) can suppress oxidative metabolism through inhibition of pyruvate dehydrogenase (PDH) by PDH kinase (PDK) and activate the expression of glycolytic enzymes (Semenza 1998). Further, hypoxia could increase HIF-1α expression and inhibit osteogenic differentiation by blocking the metabolic switch of MSCs (Hsu, Chen et al. 2013; Yang, Yang et al. 2011). In addition, it was observed that adipogenic differentiation of MSCs was inhibited by HIF-1α and enhanced by knockdown of HIF-1α under both normoxia and hypoxia (Wagegg, Gaber et al. 2012).

4. Molecular mechanisms that link metabolism to regulation of differentiation

Metabolic networks are controlled by signaling pathways. However, the converse is also true, and often the same pathways that influence metabolism are themselves regulated by metabolic products (Agathocleous and Harris 2013). Metabolic function might therefore regulate epigenetic marks and gene expression through multiple mechanisms (Figure 24).

AMPK is activated by energetic stress through binding of ADP and AMP, and by phosphorylation by LKB1 (Mihaylova and Shaw 2011), and promotes catabolic while inhibiting anabolic reactions. In response to glucose restriction in cultured myoblasts, AMPK activation promotes NAD^+ biosynthesis, which results in activation of the NAD^+-dependent histone deacetylase Sirt1 and inhibition of differentiation (Fulco, Cen et al. 2008). AMPK also phosphorylates other components of the epigenetic machinery, providing additional mechanisms for influencing differentiation. The mTOR pathway, a negative target of AMPK, is activated by amino acids, promotes anabolic reactions (Zoncu, Efeyan et al. 2011), and has several roles in cell differentiation, as discussed above. HIF-1α and HIF-2α are transcriptional activators whose degradation is dependenton O_2. In hypoxia they are stabilized and activate several targets, most prominently glycolytic genes, switching the energy production of the cell from oxidative phosphorylation to glycolysis, thereby maintaining ATP production and avoiding ROS generation from the electron transport chain (Semenza 2012).

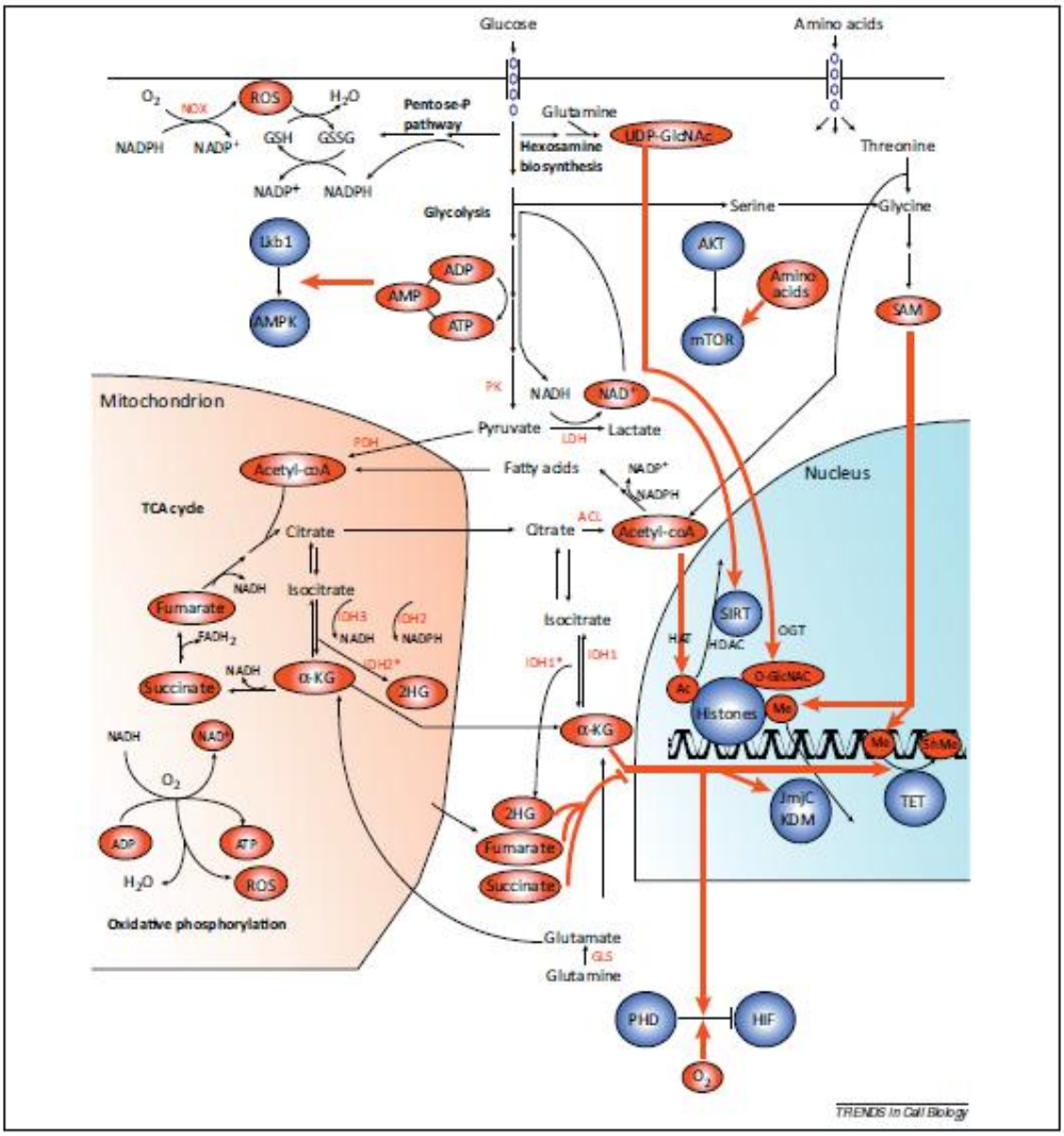

Figure 24. Summary of how metabolism can control cellular signals that regulate cell differentiation. Red circles show metabolites that directly affect signaling, blue circlestheir target proteins, and red lines their interactions. Metabolic enzymes are in red type. Blue signals affect differentiation, or control metabolism itself, as described in the text. Abbreviations not mentioned in the text: GLS, glutaminase; HAT, histone acetyltransferases; HDAC, histone deacetylases; IDH*, mutant form of isocitratedehydrogenase; JmjC KDM, JmjC domain-containing histone demethylases; LDH, lactate dehydrogenase; PDH, pyruvate dehydrogenase; PK, pyruvate kinase.

Genetic studies have pointed to multiple developmental roles for HIF factors, including the regulation of differentiation. For example, they inhibit adipocyte differentiation under hypoxia (Yun, Maecker et al. 2002), and changes in HIF-1a levels impair HSC function (Takubo, Goda et al. 2010). During hypoxia HIF-1 activates Notch targets and inhibits neural and myogenic differentiation (Gustafsson, Zheng et al. 2005), and might even stabilize and activate Notch in a ligand-independent manner during normoxia (Mukherjee, Kim et al. 2011). The AMPK, TOR, HIF, and Sirtuin pathways reciprocally interact with metabolic pathways and also cross-regulate each other inintricate ways.

Extensive epigenetic remodeling is necessary for differentiation. Histones or DNA are covalently modified by methylation, acetylation and glycosylation to regulate transcription. Recent evidence suggests that availability of the necessary metabolites affects epigenetic modifications, providing a direct link between nutritional changes, metabolic output, and gene expression (Kaelin and McKnight 2013).

Acetyl-CoA is a central metabolite in energy metabolism and biosynthesis. High levels of acetyl-CoA during periods of exponential growth in yeast promote histone acetylation and the activation of genes involved in cell growth, including ribosomal genes (Cai, Sutter et al. 2011; Cai and Tu 2012). In mammalian cells in vitro, ATP-citrate lyase (ACL), which produces cytoplasmic acetyl-CoA for fatty acid synthesis from citrate, mediates changes in histone acetylation downstream of glucose availability or growth factor stimulation. ACL knockdown inhibits expression of glycolytic genes during adipocyte differentiation (Wellen, Hatzivassiliou et al. 2009) and in cultured myoblasts it reduces histone acetylation and promotes myogenic differentiation (Bracha, Ramanathan et al. 2010).

DNA and histone methylation uses S-adenosyl-methionine (SAM), which in the process is converted to S-adenosyl-homocysteine (SAH). Carbons to generate SAM are supplied by the amino acids threonine, glycine, and serine through folate metabolism. Mouse ESCs (mESCs) are uniquely dependent on extracellular threonine (Wang, Alexander et al. 2009). Threonine deprivation leads to a decrease in the SAM:SAH ratio and histone H3K4 trimethylation levels, and promotes ESC differentiation (Shyh-Chang, Locasale et al. 2013). Threonine might also supply mESCs with the acetyl-CoA needed for the high biosynthetic needs of these rapidly proliferating cells. Therefore threonine catabolism in mESCs might be important both for the anabolic need of fast proliferationand for epigenetic regulation of differentiation by providing acetyl and methyl groups to regulate gene expression.

High NAD^+ levels may be an indication of energetic stress, and NAD^+ promotes the activity of the sirtuin family of histone deacetylases. Sirtuins deacetylate several proteins, including histones, therefore regulating gene activity, and have widespread effects on metabolism (Imai and Guarente 2010). Recent evidence implicates sirtuins in differentiation, particularly in relation to Notch signaling. In responseto oxidative stress, Sirt1 inhibits neurogenesis by blocking expression of the proneural transcription factor Mash1 (Prozorovski, Schulze-Topphoff et al. 2008), although another study found that Sirt1 promotes neural differentiation and represses the Notch target Hes1 (Hisahara, Chiba et al. 2008). During endothelial cell differentiation, Sirt1 deacetylates the Notch1 intracellular domain, destabilize lingand inhibiting Notch (Guarani, Deflorian et al. 2011).

Strong evidence for direct regulation of cell differentiation by metabolites in cancers comes from studies of neomorphic point mutations in the $NADP^+$- dependent isocitrate dehydrogenases IDH1 and IDH2 in gliomasand leukemias. IDH1/2 normally catalyzes the conversionof isocitrate to α-ketoglutarate but the mutant enzymes instead produce 2-hydroxyglutarate (2HG) (Dang, White et al. 2009). Overexpressionof the mutant IDH1/2, producing 2-hydroxyglutarate, blocks differentiation of hematopoietic cells (Figueroa, Abdel-Wahab et al. 2010; Sasaki, Knobbe et al. 2012) and conversely inhibition of mutant IDH1 promotes astrocytic differentiation in gliomas harboring this mutation (Rohle, Popovici-Muller et al. 2013). 2HG and the TCA cycle intermediates fumarate and succinate are thought to interfere with several α-ketoglutarate-dependent dioxygenases, including JmjC domain-containing histone demethylases, TETdioxygenases, which convert 5-methylcytosine to 5-hydroxymethylcytosine, and prolyl hydroxylases (PHD), which promote HIF degradation (Kaelin and McKnight 2013). These enzymes have widespread epigenetic and transcriptional effects. Inhibition ofTet2 affects hematopoietic differentiation and increases HSC self-renewal (Moran-Crusio, Reavie et al. 2011; Quivoron, Couronne et al. 2011) and Tet genes are involved in ESC differentiation (Ito, D'Alessio et al. 2010). It is therefore possible that fluctuations in the concentration of α-ketoglutarate, succinate and fumarate in normal cells modulate dioxygenaseactivity, thereby affecting gene expression and cell fate. Nuclear and cytoplasmic proteins are also modified by O-linked b-N-acetylglucosamine (O-GlcNAc) and the donor for this modification, UDP-GlcNAc, is synthesized from glucose and glutamine via the hexosamine biosynthesis pathway (Hanover, Krause et al. 2012). O-GlcNAc transferase (OGT) interacts with polycomb group members on chromatin and associates with TET2/3, promoting histone O-GlcNAcylation, and regulating transcription (Chen, Chen et al. 2013). O-GlcNAcylation on the promoters of key self-renewal genes such as Oct4 and Sox2 is necessary for ESC maintenance (Jang, Kim et al. 2012).

Results

1. Mitochondrial mass rise accompanied ADSCs differentiation

The multipotent stem cells within adipose tissue, termed adipose-derived stem cells (ADSCs) (Zuk, Zhu et al. 2001), are one of the most promising stem cell population identified thus far, since human adipose tissue is ubiquitous and easily obtained in large quantities with little donor site morbidity or patient discomfort. After isolation ADSCs were cultured in DMEM Low glucose to maintain their ability to self-renewal or were differentiated in adipocytes and osteocytes adding the specific differentiation medium (a schematic representation of the experimental workflow used in all the experiments of the paper is shown in Figure 25).

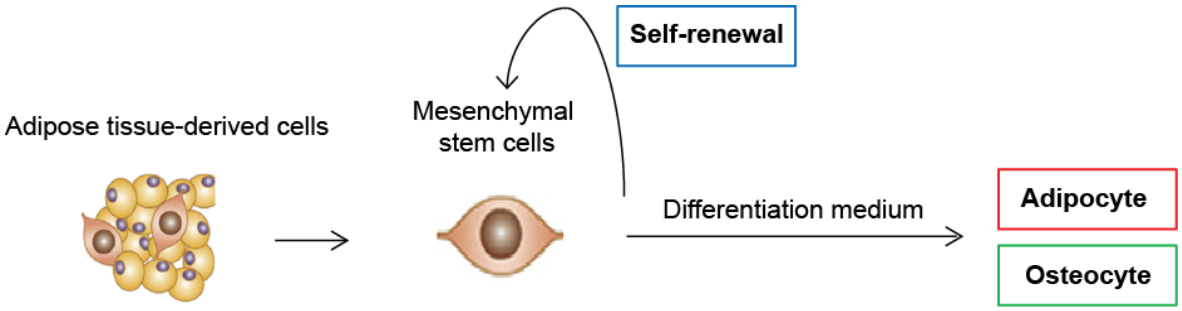

Figure 25. Experimental workflow
Adipose tissue was processed and mesenchymal stem cells were isolated; that cells are named adipose derived stem cell (ADSCs). ADSCs was maintained in DMEM Lg or differentiated in adipocyte and osteocyte. The adipogenic medium was composed by DMEM High Glucose plus 10 µg/mL insulin, 0.5 mM IBMX, 0.1 mM indomethacin and 1 µM dexamethasone. The osteogenic medium was composed by DMEM High Glucose plus10 nM dexamethasone, 10 ng/mL FGF-β and 10 mMβ-glycerophosphate.

The transcriptional factors involved in ADSC, and in general MSCs, differentiation process were extensively studied (see review (Almalki and Agrawal 2016)), while how metabolism could influence this process remains largely unknown.

Mitochondria are intracellular organelles that function as the cellular power station, with the central role of mediating aerobic respiration by oxidizing metabolic substrates to yield energy.

As discussed in "Introduction" section MSCs differentiation is characterized by two particular events: upregulation of mitochondrial biogenesis (Chen, Shih et al. 2008) and the switch to aerobic metabolism (Zhang, Marsboom et al. 2013).

To investigate the mitochondria contribution in differentiation process we analyzed mitochondrial mass in ADSCs differentiated towards adipogenic and osteogenic lineages for 7 and 21 days. HSP60, TOM20, VDAC and TIM23 were chosen as mitochondria markers.

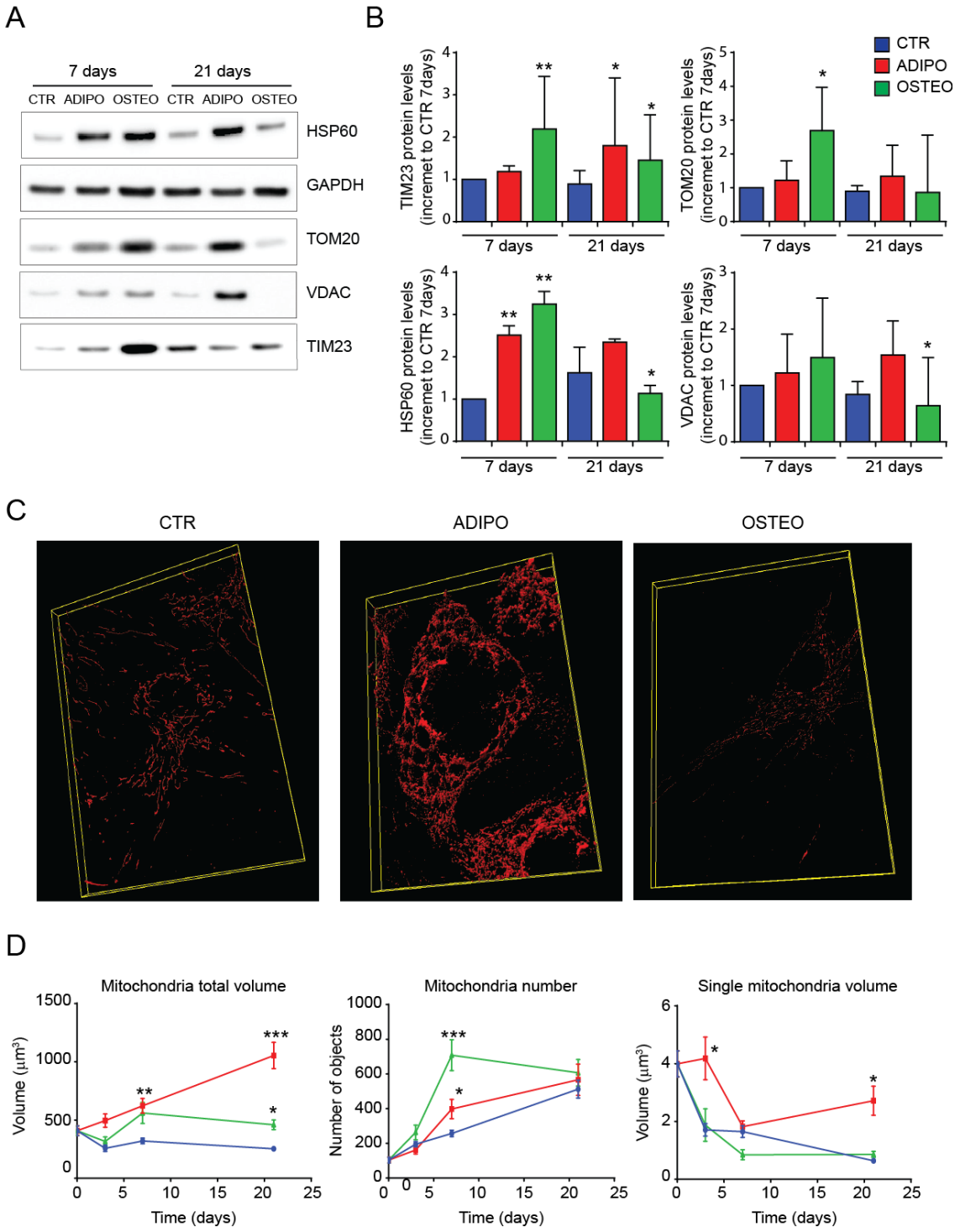

Figure 26. Mitochondrial mass increase during differentiation process
(**A**) Representative immunoblot and (**B**) quantification of HSP60, GAPDH, TOM20, VDAC, TIM23 protein levels in ADSCs cultured in Lg (CTR), adipogenic medium (ADIPO) and osteogenic medium (OSTEO) for 7 and 21 days. Mitochondrial morphology was detected by immunofluorescence using Ab anti-TOM20, (**C**) representative 3D images of mitochondria morphology in ADSCs cultured in Lg (CTR), adipogenic medium (ADIPO) and osteogenic medium (OSTEO) for 21 days. (**D**) Quantification of mitochondrial total volume, mitochondria number and single mitochondria volume in ADSCs cultured in Lg (CTR), adipogenic medium (ADIPO) and osteogenic medium (OSTEO) for 3, 7 and 21 days. Magnifications 60X. Data were shown as % mean ± stdev. ANOVA-test.

During adipogenesis the mitochondria mass increased progressively, while, interestingly, during osteogenesis an increment pick in mitochondrial mass was revealed after 7 days, followed by a reduction of mitochondria at 21 days (Fig 26A and 26B).

Moreover we analyzed mitochondrial morphology in single cell; ADSCs were fixed ad different time point (0, 3, 7 and 21 days) after induction of adipogenic (ADIPO) and osteogenic (OSTEO) and compared with ADSC maintained in DMEM Lg (CTR). Samples were stained for Ab anti-TOM20 following immunofluorescence standard protocol, and the mitochondrial structure was evaluated by confocal microscopy. After deconvolution and 3D reconstitution, the images were analyzed, evaluating three main aspects: the overall volume, the number and the size of individual mitochondrial objects.

During adipogenesis mitochondrial total volume progressively increased, as already suggested by immunoblot, and after 21 days of differentiation a marked difference between CTR and ADIPO was showed (Fig 26C and 26D). The number of mitochondria increased especially in early differentiation.

During early osteogenesis (7 days), mitochondrial total volume increased, followed by a prominent increase in number of mitochondria (Fig 26D). This considerable increment in number of mitochondria which were very small, as demonstrated by single mitochondrial volume that decreased respect initial points, suggested that mitochondrial biogenesis was triggered.

Unlike in adipogenesis, mitochondria seem to have a non-progressive accumulation during osteogenesis, proposing a more complex regulation of mitochondria involvement in differentiation process.

2. Mitochondria respiration increase during early phase of ADSCs differentiation

Mitochondria play central roles in cell metabolism by producing energy through oxidative phosphorylation. Complexes I–IV of the respiratory chain build up the proton gradient across the inner mitochondrial membrane that is required for oxidative phosphorylation and that forms mitochondrial membrane potential.

So, to assess ADSC bioenergetics, we analyzed mitochondrial membrane potential in ADSC cultured in DMEM Lg (CTR), adipogenic medium (ADIPO) and osteogenic medium (OSTEO) for 3, 7 and 21 days, using JC1 dye. JC-1 is a cationic carbocyanine dye that accumulates in mitochondria. The dye exists as a monomer at low concentrations and yields green fluorescence.

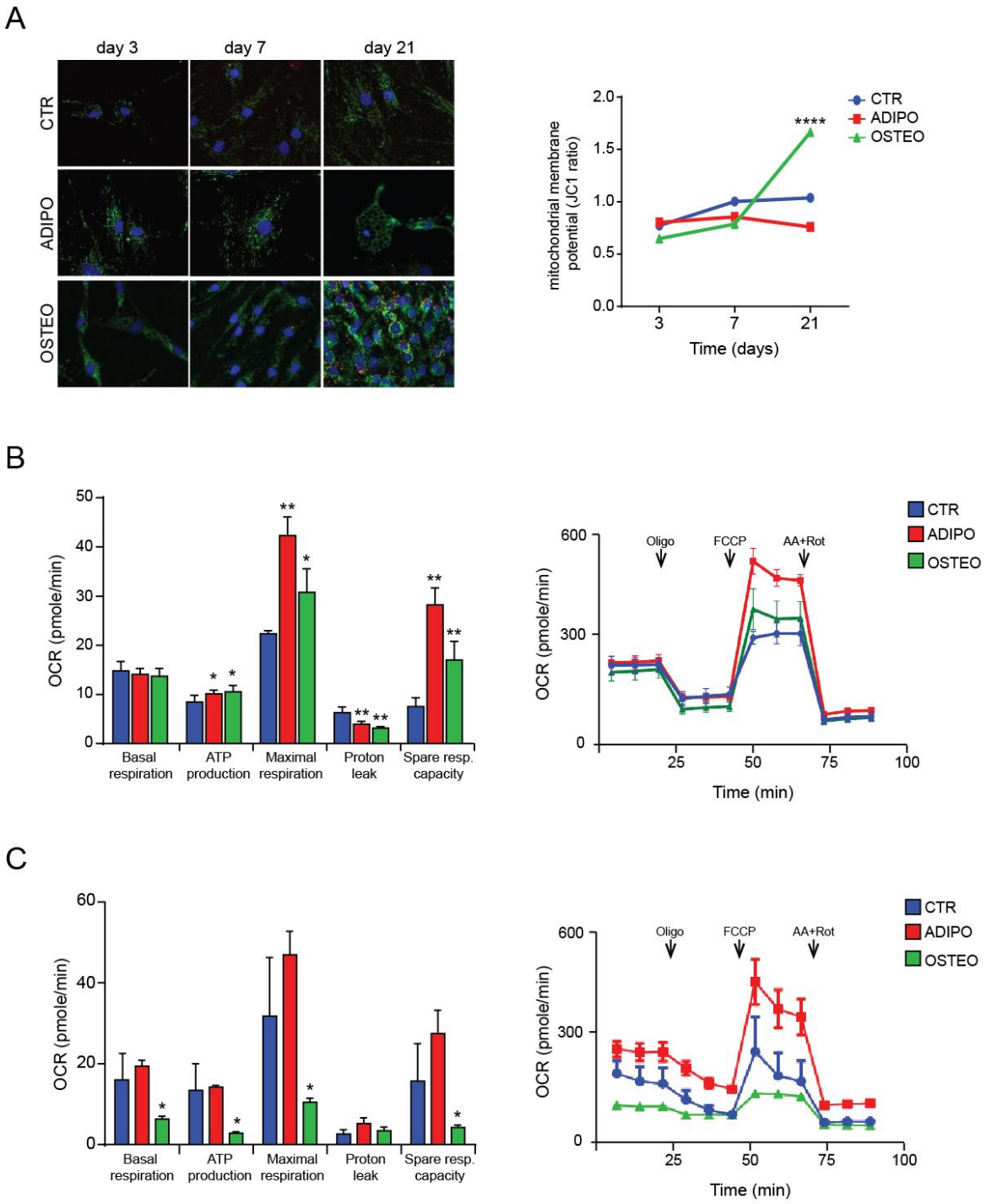

Figure27. Mitochondrial physiology during differentiation process

Mitochondrial membrane potential was detected by JC1 probe. (**A**) Representative composite images (JC1 in green/red fluorescence and nucleus in blue fluorescence) and quantification of JC1 ratio (red/green) of ADSCscultured in Lg (CTR), adipogenic medium (ADIPO) and osteogenic medium (OSTEO) for 3, 7 and 21 days. (**B**) Oxygen consumption rate (OCR) of ADSC after 7 days and (**C**) 21 daysof differentiationdetermined using the Extracellular Flux Analyzer (Seahorse Bioscience). Magnifications 40X. Data were shown as % mean ± stdev. ANOVA-test.

At higher concentrations, the dye forms J-aggregates that exhibit a broad excitation spectrum and an emission maximum at ~590 nm (red). These characteristics make JC-1 a sensitive marker for mitochondrial membrane potential.

As shown in Figure 27A, a significant increment in mitochondrial membrane potential was shown in the late phase of osteogenic differentiation (21 days), while no difference were detected during adipogenic differentiation.

The mitochondrial oxygen consumption rate (OCR) is a key metric of mitochondrial function, which can be determined using the Extracellular Flux Analyzer (Seahorse Bioscience).

By directly measuring the oxygen consumption rate (OCR), the Seahorse XF Cell Mito Stress Test provides a standard and comprehensive method to assess the key parameters of mitochondrial function in live cells: Basal respiration, ATP production, Proton Leak, Maximal Respiration and Spare Respiratory Capacity.

The Seahorse XF Cell Mito Stress Test Kit uses modulators of cellular respiration that specifically target components of the electron transport chain (ETC) to reveal key parameters of metabolic function. The compounds, oligomycin, FCCP, and a mix of rotenone and antimycin A, are serially injected to measure ATP production, maximal respiration, and non-mitochondrial respiration (used as experimental background), respectively. Proton leak and spare respiratory capacity are then calculated using basal respiration and these parameters.

Seahorse XF Cell Mito Stress Test Kit was performed in ADSCs after 7 days (Fig 27B) and after 21 days (Fig 27C) of differentiation.

After 7 days of both adipogenic and osteogenic differentiation an increment in ATP production, maximal respiration and spare respiratory capacity was observed, followed by a decrease in proton leak. Differently, after 21 days of differentiation adipocytes and osteocytes showed different behavior; adipogenesis was followed by an increment, even if non-significantly, in all the parameters analyzed, while during last phase of osteogenesis all the parameters drastically decrease.

3. Mitochondria-nucleus contact sites identification

The dynamic rearrangement of mitochondrial mass and the difference in mitochondrial physiology suggested that mitochondria could be directly involved in differentiation process. During differentiation the mainly difference are in nuclear reprogramming, so we hypothesis that mitochondria could communicates with nucleus to cooperate in this process.

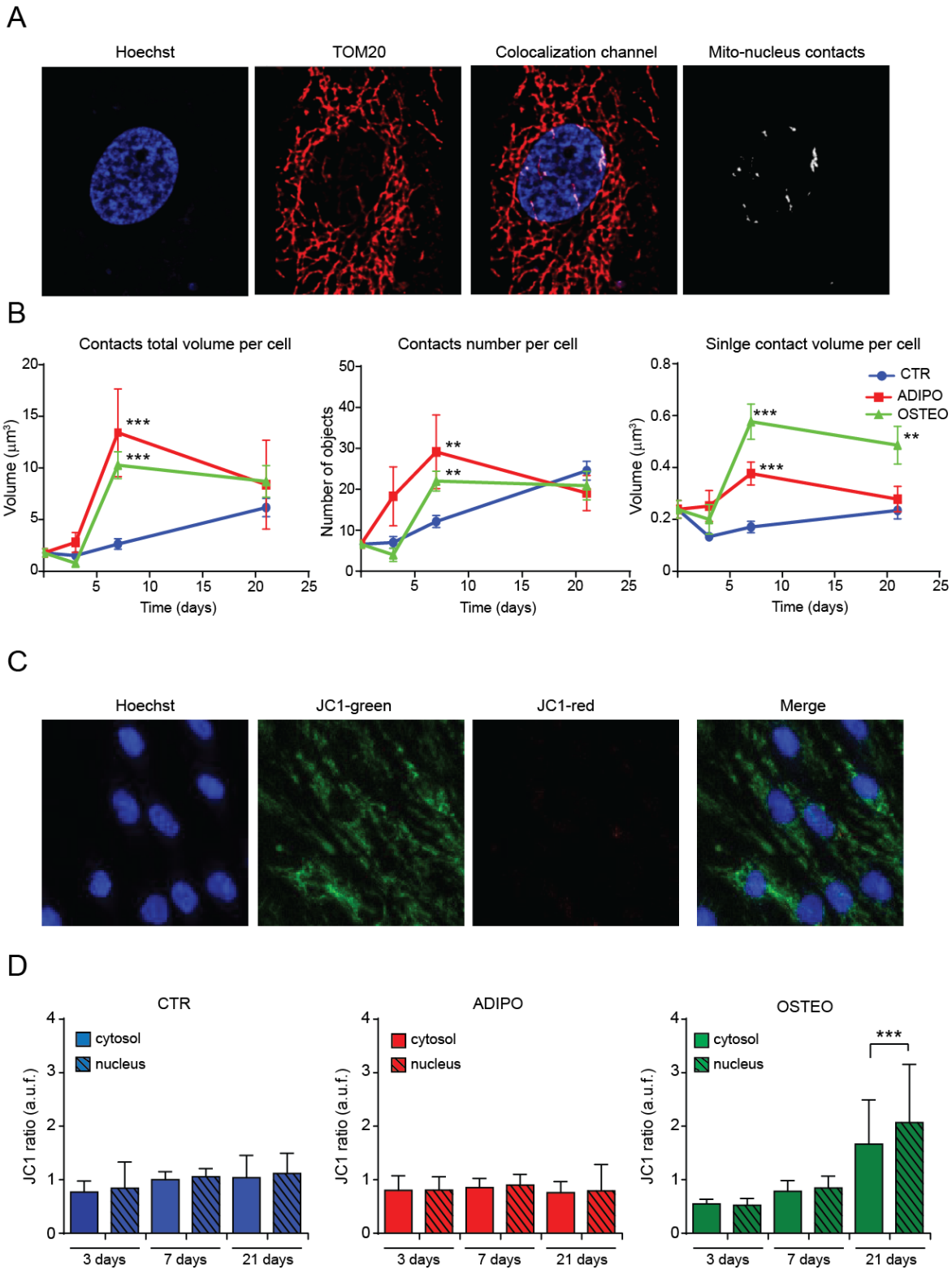

Figure 28. Mitochondria-nucleus contact sites.
(**A**) Mitochondria nucleus contact sites were detected by co-localization of nucleus staining (Hoechst) and mitochondrial staining (TOM20). After creation of co-localization channel (**B**) total volume, number and single volume of contacts was analyzed inADSCscultured in Lg (CTR), adipogenic medium (ADIPO) and osteogenic medium (OSTEO) for 3, 7 and 21 days. (**C-D**) The mitochondrial membrane potential of mitochondria in contact with nucleus was detected by analysis of JC1 ratio on mitochondria-nucleus contact sites. Data were shown as % mean ± stdev. ANOVA-test.

To verify this hypothesis, firstly, we identified site of contacts between nucleus and mitochondria. As shown in figure 28A, after cell fixing nucleus was stained by Hoechst and mitochondria by anti-TOMM20, following immunofluorescence standard protocol. The cells were acquired using confocal microscope, images were deconvolved and a 3D reconstitution was created. Using *Imaris* software the colocalization between the two fluorescent signals was analyzed and a colocalization-channel was created. In the end, a 3D reconstitution of the colocalization-channel was made and the total volume, the number of objects and the volume of single objects were analyzed.

Mitochondria-nucleus contacts were analyzed in ADSCs at different time points (0, 3, 7 and 21 days) of adipogenesis (ADIPO) and osteogenesis (OSTEO) and compared with ADSCs cultured in DMEM Lg (CTR).

The volume of mitochondria-nucleus contacts drastically increased after 7 days of differentiation due to the increase both of number and of volume of contact sites (Fig 28B). After 21 days of differentiation no difference in volume and number was showed, expect for the volume of single contacts in OSTEO.

Moreover we analyzed the mitochondrial membrane potential in mitochondria-nucleus contact sites, analyzing JC1 fluorescence signal only where it colocalized with Hoechst, used as nucleus staining (Fig 28C). In Figure 28D the JC1 ratio analysis was reported comparing cytosolic mitochondria and mitochondria in contacts sites. Interestingly we showed that, after 21 days of osteogenic differentiation, the mitochondria in close contact to nucleus had a higher mitochondrial membrane potential respect the cytosolic mitochondria.

Taken together, these data could suggest that mitochondria could play a key role during early differentiation toward both adipogenic and osteogenic lineages; in addition they could act and regulate the late differentiation stage of osteogenic commitment.

4. Acetyl-CoA transport inhibition impaired osteogenesis, but not adipogenesis

The factors that promote and regulate the differentiation process must also include the regulation of the stem cell's metabolic pathways. Mammalian cell intermediary energy metabolism is comprised of a collection of several major metabolic pathways that involve carbohydrate, lipid and protein metabolism, and terminal oxidation pathways. At some point in mammalian cell aerobic metabolism, essentially all of the pathways converge on and/or arise from the Krebs cycle. This highlighted the key role of mitochondria in metabolism and in the possible regulation of differentiation process.

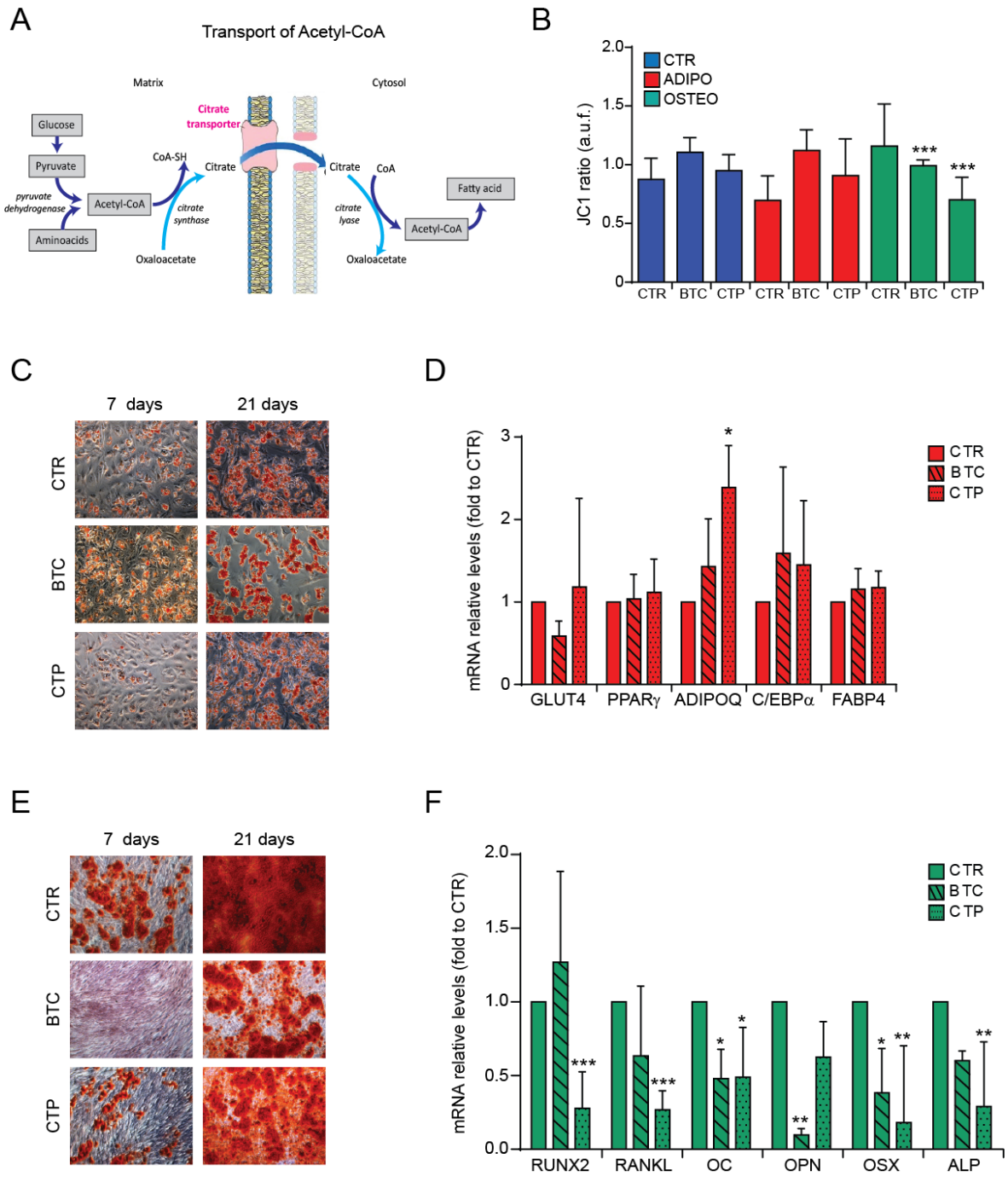

Figure29. Inhibition of Acetyl-CoA transport system impaired osteogenic, but not adipogenic differentiation (**A**) Schematic representation of acetyl-CoA transport system. In mitochondrial matrix Acetyl-CoA is converted in citrate by citrate synthase. Then citrate is transported by citrate transporterto cell cytosol, where it is reconverted in Acetyl-CoA by citrate lyase. (**B**) Effect of BTC and CTP (citrate transporter inhibitors) on mitochondrial membrane potential detected by JC1 probes in ADSCscultured in Lg (CTR), adipogenic medium (ADIPO) and osteogenic medium (OSTEO) plus, where indicated, BTC (5 mM) and CTP (500 µM) for 21 days. The effect of BTC and CTP on adipogenic differentiation was assessed by (**C**) Oil red O staining and by (**D**) analysis of mRNA relative levels of adipogenic markers (GLUT4, PPARγ, ADIPOQ, C/EBPα and FABP4). The effect of BTC and CTP on osteogenic differentiation was assessed by (**E**) Alizarin Red staining and by (**F**) analysis of mRNA relative levels of osteogenic markers (RUNX2, RANKL, osteocalcin (OC), osteopontin (OPN), osteix (OSX) and alkaline phosphatase (ALP)).

Acetyl-CoA is a key metabolite that links metabolism with signaling, chromatin structure, and transcription. Acetyl-CoA is produced by glycolysis as well as other catabolic pathways and used as a substrate for the citric acid cycle and as a precursor in synthesis of fatty acids and steroids and in other anabolic pathways (Galdieri, Zhang et al. 2014).

The acetyl-CoA is produced from pyruvate, which is generated from the glycolytic utilization of glucose. In the mitochondrial matrix the condensation of acetyl-CoA and oxaloacetate produce citrate. Citrate can enters the oxidative phase of the Krebs cycle or can be transported from the mitochondria to the cytosol where it can be reconverted in acetyl-CoA. The citrate exits from the mitochondria through the mitochondrial citrate transport protein (Scl25A1) (Figure 29A). Inhibition of mitochondrial citrate transport protein is obtained by the substrate analog 1,2,3-benzenetricarboxylate (BTC) and the CTP inhibitor (4-Chloro-3-[[(3-nitrophenyl)amino]sulfonyl]-benzoic acid). CTP inhibitor (referred in the text as CTP) is an inhibitor of mitochondrial citrate transport protein, which was the first purely competitive inhibitor to be discovered and is more potent than BTC. CTP inhibitor blocks the exchange of tricarboxylates the key intermediates in anabolism and catabolism by mitochondrial citrate transport protein (Sun, Aluvila et al. 2010).

Inhibition of mitochondrial citrate transport protein by BTC or CTP induced cytosolic acetyl-CoA depletion (Marino, Pietrocola et al. 2014). For that reason BTC and CTP were used to investigate the role of acetyl-CoA in differentiation process.

ADSCs were differentiated toward adipogenic and osteogenic lineage adding, where reported, 5 mM BTC or 500 µM CTP.

Analyzing the mitochondrial membrane potential by JC-1 probe, interestingly we showed that BTC and CTP were able to prevent the increment of mitochondrial membrane potential achieved during osteogenesis. Indeed, as reported in figure 29B, the JC1 ratio of OSTEO ADSCs treated both by BTC and CTP was significantly reduced compared to ADSCs cultured in CTR osteogenic medium.

The effects on adipogenic differentiation was assessed by staining of lipid drops accumulation (Oil Red O staining) at 7 and 21 days of differentiation and by the mRNA levels profile of adipogenic markers (GLUT4, PPARγ, ADIPOQ, C/EBPα and FABP4) at 21 days of differentiation. The data showed that BTC and CTP treatment did not affected ADSCs adipogenesis (Fig 29C and 29D).

By contrast, BTC and especially CTP, drastically inhibits osteogenic differentiation. The calcium deposits detected by Alizarin Red staining were reduced in ADSCs cultured in osteogenic medium plus BTC or CTP compared CTR condition both a 7 and 21 days (Fig 29E).

The osteogenesis process was evaluated also analyzing the mRNA levels profile of osteogenic markers (RUNX2, RANKL, osteocalcin, osteopontin, osterix and Alkaline phosphatase); from data of qRT-PCR (Fig 7F) we confirmed that inhibition of mitochondrial citrate transport strongly impaired ADSCs osteogenic differentiation.

5. H3K9 acetylation was reduced by mitochondrial citrate transport inhibitors

During the differentiation of stem cells, the relative abundance of epigenetic marks usually reflects the activation or repression of genes which further guide cells development toward a particular cell lineage. Modified histone domains such as acetylated histone H3 lysine 9 (H3K9ac) are considered as key epigenetic signatures as indicative of transcriptional activation (Zheng, He et al. 2013). In particular it was reported that HDAC8 functioned as a transcriptional repressor via regulating the level of H3K9ac and interacting with the osteogenic master transcriptional factor RUNX2 during the specification of BMSCs to the osteoblasts lineage in vitro (Fu, Zhang et al. 2014).

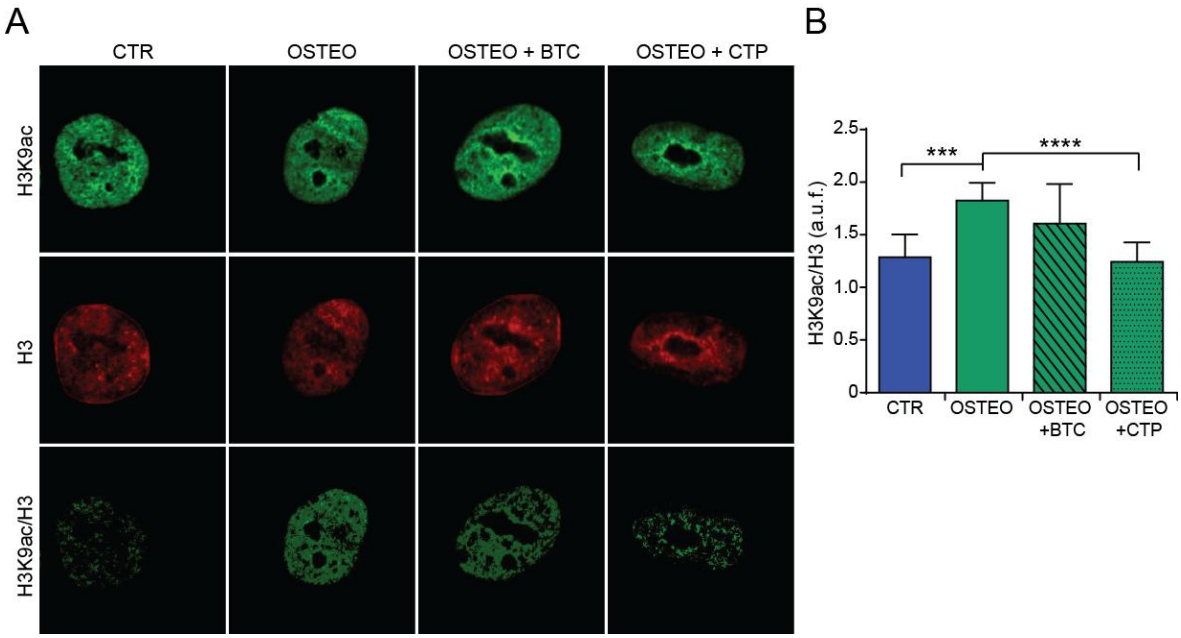

Figure 30. Inhibition of citrate transport affected H3K9 acetylation
(**A**) Representative images and (**B**) quantification of ratio between H3K9 acetylation (green) and H3 (red) in ADSC scultured in Lg (CTR), and osteogenic medium (OSTEO) plus, where indicated, BTC (5 mM) and CTP (500 µM) for 21 days.

In order to investigate the H3K9ac levels, ADSCs, after 21 days of differentiation, were fixed and stained for Ab anti-H3K9ac (green) and Ab anti-H3 (red) following immunofluorescence standard protocol. Green and red confocal images were acquired; the ratio images of H3K9ac/H3 were created and calculated using ImageJ software (Fig 30A and 30B).

Here we confirmed that during osteogenesis the levels of H3K9ac increased compared to ADSCs maintained in DMEM Lg (CTR). More interestingly we showed that mitochondrial citrate transport inhibition was related to a decrease in H3K9 acetylation, suggesting that histone acetylation was closely related to acetyl-group derived from mitochondria.

Discussion

Stem cells differentiation process was largely investigated from the transcriptional factors point of view, whereas little is known concerning how metabolism could regulate this complex process. However, understanding exactly why this metabolic switch occurs and how metabolism is linked to pluripotency and differentiation process has become a research topic of considerable recent interest. Pluripotent embryonic stem cells (ESCs), the master progenitors of all cells in an organism, possess immature mitochondria with poorly developed cristae, which mature into a densely tubular network only upon differentiation. Consistent with these observations, ESCs prefer high rates of glycolysis even when cultured outside the hypoxic blastocyst in atmospheric oxygen. Upon differentiation, ESCs down-regulate glycolysis and oxidize most of the glycolysis-derived pyruvate in mitochondria via oxidative phosphorylation (OXPHOS) (Shyh-Chang and Daley 2015).

In this study we investigated the possible contribution of mitochondria in stem cells differentiation process. Our cellular model was represented by multipotent stem cells within adipose tissue, termed adipose-derived stem cells (ADSCs). ADSCs are one of the most promising stem cell population identified thus far, since human adipose tissue is ubiquitous and easily obtained in large quantities with little donor site morbidity or patient discomfort. Therefore, the use of autologous ADSCs as both research tools and as cellular therapeutics is feasible and has been shown to be both safe and efficacious in preclinical and clinical studies of injury and disease (Gimble, Katz et al. 2007; Tobita, Orbay et al. 2011).

We showed that, during adipogenic and osteogenic differentiation, mitochondria volume and mitochondrial respiration drastically increasedin the early phase of both the lineage commitments. Interestingly, in the late phase of differentiation process, adipogenic cells showed conspicuous amount of mitochondria, whereas osteogenic cells had few mitochondria. However the mitochondria in the late phase of osteogenesis showed higher mitochondrial membrane potential, suggesting an active role of mitochondrial metabolism.

Suggesting a crucial implication of communication between mitochondria and nucleus, we identified site of tight contacts between the two organelles. From the analysis of mitochondria-nucleus contact sites emerged that, during differentiation process, the volume of nucleus close to mitochondria increased, creating micro-domains in which the exchange of metabolites could be advanced.

From this data we should hypothesize that (i) initially mitochondria could cooperate with cell in order to provide energy and metabolites to induce early differentiation, (ii) than mitochondria could participate in regulation of specific lineage commitment. In particular,

we supposed that, during osteogenesis, mitochondria could provide metabolites (such as acetyl-CoA) to nucleus in order to orchestrate the epigenetic regulation of the process.

In multiple cell types, histone acetylation is highly sensitive to the availability of acetyl-CoA (Cai, Sutter et al. 2011; Donohoe, Collins et al. 2012; Moussaieff, Rouleau et al. 2015). Acetyl-CoA is indeed the obligate cofactor for histone acetyltransferases (HATs), meaning that the abundance of the nucleus-cytosolic pool may have a direct impact on the enzymatic activity of HATs, especially those with a relatively high KD for acetyl-CoA. Thus, drops in nucleus-cytosolic acetyl-CoA levels below the KD of specific HATs may directly reduce their activity. This establishes a direct link between the nucleus-cytosolic abundance of acetyl-CoA and the epigenetic control of gene expression (Pietrocola, Galluzzi et al. 2015).

Recent studies have implicated distinct aspects of ESCs metabolism in regulating histone modifications and pluripotency, for instance, S-adenosylmethionine for histone methylation, and ascorbate and α-ketoglutarate for histone demethylation (Wang, Chen et al. 2011; Shyh-Chang, Daley et al. 2013; Carey, Finley et al. 2015). Moreover, the recent paper by Moussaieff et al. showed that glycolysis-derived acetyl-CoA is also important for maintaining histone acetylation in ESCs, further extending the connection between metabolic intermediates and the regulation of open chromatin that is essential to the unique capacities of pluripotent stem cells (Moussaieff, Rouleau et al. 2015).

Here, we demonstrated that acetyl-CoA transport system from mitochondria to cytosol is fundamental for ADSCs osteogenesis; indeed, the pharmacological inhibition of citrate transporter by BTC and CTP impaired calcium deposits and mRNA expression profile of master regulator genes involved in osteogenesis.

Several reviews reported the effect of epigenetic modifications on MSC multipotency and differentiation (Teven, Liu et al. 2011; Eslaminejad, Fani et al. 2013; Avgustinova and Benitah 2016); among which modified histone domains acetylated histone H3 lysine 9 (H3K9ac) is considered as key epigenetic signatures as indicative of transcriptional activation (Zheng, He et al. 2013) interacting with the osteogenic master transcriptional factor RUNX2 during osteogenesis (Fu, Zhang et al. 2014).

We demonstrated that H3K9ac levels increased during osteogenesis, but the inhibition of citrate transporter decreased thelevels of H3K9ac.

Taken together these data, we could conclude that during osteogenic differentiation mitochondria arrange close to nucleus to create micro-domains in order to facilitate exchange of metabolites from mitochondrial matrix to nucleus. Metabolites, in particular acetyl-CoA, exit from the mitochondria and enter in nucleus, where could provide acetyl

groups to histone modification, leading transcriptional activation of osteogenic-related genes.

These finding highlighted that mitochondria metabolites could play a key regulatory role in differentiation process which have to be deeply investigated and could suggest novel therapeutic strategies in field of regenerative medicine.

Materials and Methods

Cell culture

Adipose-derived stem cells (ADSCs) were extracted from human adipose tissues of healthy female patients undergoing cosmeticsurgery procedures, following guidelines from the Clinic of Plastic Surgery, Universityof Padova. Adipose tissues were digested with 0.075% collagenase (type 1A; Sigma–Aldrich) in Krebs–Ringer buffer (modified KRB) (125 mM NaCl, 5 mM KCl,1 mM Na_3PO_4, 1 mM $MgSO_4$, 5.5 mM glucose, and 20 mM Hepes (pH 7.4)) for 60 min at 37°C followed by 10 min with 0.25% trypsin. Floating adipocytes werediscarded, and cells from the stromal-vascular fraction were pelleted, rinsed withmedia, and centrifuged, and a red cell lysis step in NH_4Cl was done for 10 min atroom temperature. Obtained ADSCs were grown in Dulbecco's modified Eagle's Medium (DMEM) low-glucose, supplemented with 10% fetal bovine serum (EurocloneS.p.A. Milan, Italy), 2mM L-glutamine, antibiotics (penicillin 100 µg/mL and streptomycin 10 µg/ml), at 37 °C in a humidified atmosphere of 5 % CO_2.

Adipogenic and osteogenic differentiation

For adipogenic differentiation DMEM Lg (5mM) was replaced with DMEM Hg (25 mM) plus 10 µg/mL insulin, 0,5 mM IBMX, 0,1 mM indomethacin, 1 µM dexamethasonefor 3, 7 and 21 days. For osteogenic differentiation DMEM Lg (5mM) was replaced with DMEM Hg (25mM) plus 10 nM dexamethasone, 10 ng/mL FGF-β and 10 mM β-glycerophosphate for 3, 7 and 21 days.

Immunoblotting

For immunoblotting, cells were scraped into ice-cold, phosphate buffered saline (PBS) and lysed in a buffer containing 50 mM Tris-HCl pH 7.4, 150 mM NaCl, 1% Triton X-100, 0.2% SDS, protease, and phosphates inhibitor cocktail. After 30 min of incubation on ice and centrifugation at 2,500 rpm 4°C for 5 min, proteins were quantifiedby the Lowry method and 15 µg of each sample were loaded on an acrilamide gel and transferred to nitrocellulose membranes. After incubation with TBS–Tween-20 (0.05%) supplemented with 5% non-fat powdered milk for 1 h to saturate unspecific binding sites, membranes were incubated overnight with primary antibodies. Finally, membranes were incubated with appropriate horseradish peroxidase (HRP)-labeled secondary antibodies (Thermo Fischer Scientific), followed by detection by chemiluminescence (ThermoScientific), using ImageQuant LAS4000 (GE Healthcare).

Antibodies

For immunoblotting, the following primary antibodies were used: rabbit anti-GAPDH [2118] (1:5000) from Cell Signaling; rabbit anti-TOM20 [sc-11415] (1:1000) and mouse anti-HSP60 [sc-13115] (1:1000) from S.Cruz; anti-VDAC [ab-15895] (1:1000) from Abcam; anti-TIM23 [611222] (1:1000) from BD Bioscience.

Immunofluorescence microscopy

Immunofluorescence microscopy was performed according to standard procedures. Briefly, cells were fixed in 4% PFA for 20 min at room temperature, washed three times in PBS and permeabilized with 0.1% Triton X-100 for 5 min at room temperature. Thereafter, unspecific binding sites were blocked by incubating cells in PBS supplemented with 2% BSA (blocking buffer) for 1 h at room temperature. Cells were then incubated overnight at 4°C with primary antibodies specific for TOM20 (1:100 in blocking buffer, from Santa Cruz SC-11415), H3 (1:100 in blocking buffer, from Cell Signaling 14269), H3K9ac (1:100 in blocking buffer, from Cell Signaling 9649). Finally, primary antibodies were revealed by means of appropriate AlexaFluor 488® or AlexaFluor 594® conjugates (Thermo Fischer Scientific). Nucleus was stained by Hoechst probe. Images were acquired with a LSM 510 confocal microscope (Carl Zeiss Microscopy, LLC) through a Plan-Apochromat 63x/1.4 oil objective (Carl Zeiss Microscopy, LLC).

Mitochondrial membrane potential

Mitochondrial membrane potential was assayed by JC-1 probe. ADSCs were loaded with 1 µM JC-1 (Thermo Fischer Scientific) in Krebs-Ringer buffer, then placed in a humidified chamber at 37°C and imaged with a LiveScan Swept Field Confocal Microscope (Nikon Instruments, Inc.) equipped with a 40× oil immersion (N.A. 1.4, from Nikon Instruments, Inc.).

XF bioenergetic analysis

Oxygen consumption rates were measured using the SeahorseXF96 instrument (Seahorse Biosciences, North Billerica, MA) according to the manufacturer's protocols. After differentiation, ADSC were seeded in a poly-lysine coated XF96 microplate at the density of 50000 cells per well in 175 µl unbuffered XF assay media at pH 7.4 supplemented with 5.5 mM glucose (Sigma), 1 mM sodium pyruvate and 1 mM glutamine, for 60 minutes in a 37°C non-CO_2 incubator, while sensor cartridges were calibrated prior to the start of an assay.

Respiration was measured in four blocks of three for 3 min. The first block measured the basal respiration rate. Next 1 μM oligomycin was added toinhibit complex V (second block). Then 1 μM carbonylcyanide 4-(trifluoromethoxy)-phenylhydrazone (FCCP) was added touncouple respiration (third block). Finally, 1 μM antimycin A and 1 μM rotenone was added to inhibit complex III (forth block). All reagents are from Seahorse Biosciences, North Billerica, MA. Immediately after finishing themeasurements, cells were washed with phosphate-buffered saline, fixed with 4% paraphormaldehyde and stained with 0.1% crystal violet (1 mol/l acetic acid) and absorbance at 595 nm was measured as index of cell amount.

Oil Red O staining

Oil red (Sigma-Aldrich) staining of the cytoplasmic droplets of neutral lipids was performed according to the standard procedure. Monolayer cultures were fixed by 10% paraformaldehyde for 10 min, washed with PBS, permeabilized by isopropanol for 5 min and let dry. Then Oil Red working solution was added to well for 10 min at room temperature. After washing, stained cells were acquired by light microscopy.

Alizarin Red staining

For Alizarin Red S (ARS) staining, the cells were fixed with 70% ethanol for 1 hour and then stained with 40 mM Alizarin Red S solution (pH 4.2) at room temperature for 10 min. After washing, stained cells were acquired by light microscopy.

RNA extraction and Quantitative RT-PCR

Total RNA was extracted with TRIzol Reagent (Invitrogen, Carlsbad, CA, USA). RNAs were purified with RNeasy Mini Kit (Qiagen GmbH, Hilden, Germany), and DNase digestion was performed with RNase-Free DNase Set (Qiagen). The RNA quality and concentrationwere measured using the NanoDropTM ND-1000 (Thermo Scientific). For the first-strand cDNA synthesis, 1,000 ng of total RNA ofeach sample was reverse-transcribed with M-MLV Reverse Transcriptase (Invitrogen), following the manufacturers protocol.

Real-time PCRs were carried out using the designedprimers at a concentration of 300 nM and FastStart SYBR GreenMaster (Roche Diagnostics, Mannheim, Germany) on a Rotor-Gene3000 (Corbett Research, Sydney, Australia). Thermal cycling conditions were as follows: 10 min denaturation at 95°C, followed by 40 cycles of denaturation for 10 s at 95°C; annealing for 20 s at 60°C; and elongation for 30 s at 72°C. Values were normalized

to the expression of the glyceraldehyde-3-phosphate dehydrogenase (GAPDH) internal reference.

Statistical analysis

The results were expressed as the mean ± SD. The probability of statistical differences between experimental groups was determined by the ANOVA test, results from treatments showing significant overall changes were subjected to post hoc Bonferroni tests. The Student's t-test was used to determine statistical significance between two groups.*p* values <0.05 were considered statistically significant. Different labels indicate *p<0.05, ** p<0.001, *** p<0.0001 and ****p< 0.00001.

References

Chapter 1. Mitochondrial permeability transition involves dissociation of F_1F_O ATP synthase dimers and C-ring conformation

Alavian, K. N., G. Beutner, et al. (2014). "An uncoupling channel within the c-subunit ring of the F1FO ATP synthase is the mitochondrial permeability transition pore." Proc Natl Acad Sci U S A **111**(29): 10580-10585.

Alcala, S., M. Klee, et al. (2008). "A high-throughput screening for mammalian cell death effectors identifies the mitochondrial phosphate carrier as a regulator of cytochrome c release." Oncogene **27**(1): 44-54.

Allegretti, M., N. Klusch, et al. (2015). "Horizontal membrane-intrinsic alpha-helices in the stator a-subunit of an F-type ATP synthase." Nature **521**(7551): 237-240.

Arnold, I., M. F. Bauer, et al. (1997). "Yeast mitochondrial F1F0-ATPase: the novel subunit e is identical to Tim11." FEBS Lett **411**(2-3): 195-200.

Arselin, G., M. F. Giraud, et al. (2003). "The GxxxG motif of the transmembrane domain of subunit e is involved in the dimerization/oligomerization of the yeast ATP synthase complex in the mitochondrial membrane." Eur J Biochem **270**(8): 1875-1884.

Azarashvili, T., D. Grachev, et al. (2007). "The peripheral-type benzodiazepine receptor is involved in control of Ca2+-induced permeability transition pore opening in rat brain mitochondria." Cell Calcium **42**(1): 27-39.

Azarashvili, T., I. Odinokova, et al. (2014). "Potential role of subunit c of F0F1-ATPase and subunit c of storage body in the mitochondrial permeability transition. Effect of the phosphorylation status of subunit c on pore opening." Cell Calcium **55**(2): 69-77.

Baines, C. P., R. A. Kaiser, et al. (2007). "Voltage-dependent anion channels are dispensable for mitochondrial-dependent cell death." Nat Cell Biol **9**(5): 550-555.

Baines, C. P., C. X. Song, et al. (2003). "Protein kinase Cepsilon interacts with and inhibits the permeability transition pore in cardiac mitochondria." Circ Res **92**(8): 873-880.

Basso, E., L. Fante, et al. (2005). "Properties of the permeability transition pore in mitochondria devoid of Cyclophilin D." J Biol Chem **280**(19): 18558-18561.

Beutner, G., A. Ruck, et al. (1998). "Complexes between porin, hexokinase, mitochondrial creatine kinase and adenylate translocator display properties of the permeability transition pore. Implication for regulation of permeability transition by the kinases." Biochim Biophys Acta **1368**(1): 7-18.

Beutner, G., A. Ruck, et al. (1996). "Complexes between kinases, mitochondrial porin and adenylate translocator in rat brain resemble the permeability transition pore." FEBS Lett **396**(2-3): 189-195.

Bonora, M., A. Bononi, et al. (2013). "Role of the c subunit of the FO ATP synthase in mitochondrial permeability transition." Cell Cycle **12**(4): 674-683.

Bonora, M., C. Morganti, et al. (2016). "Comprehensive analysis of mitochondrial permeability transition pore activity in living cells using fluorescence-imaging-based techniques." Nat Protoc **11**(6): 1067-1080.

Campanella, M., G. Szabadkai, et al. (2008). "Modulation of intracellular Ca2+ signalling in HeLa cells by the apoptotic cell death enhancer PK11195." Biochem Pharmacol **76**(11): 1628-1636.

Carraro, M., V. Giorgio, et al. (2014). "Channel formation by yeast F-ATP synthase and the role of dimerization in the mitochondrial permeability transition." J Biol Chem **289**(23): 15980-15985.

Chelli, B., A. Falleni, et al. (2001). "Peripheral-type benzodiazepine receptor ligands: mitochondrial permeability transition induction in rat cardiac tissue." Biochem Pharmacol **61**(6): 695-705.

Cheng, E. H., T. V. Sheiko, et al. (2003). "VDAC2 inhibits BAK activation and mitochondrial apoptosis." Science **301**(5632): 513-517.

Chiara, F., D. Castellaro, et al. (2008). "Hexokinase II detachment from mitochondria triggers apoptosis through the permeability transition pore independent of voltage-dependent anion channels." PLoS One **3**(3): e1852.

Crompton, M., S. Virji, et al. (1998). "Cyclophilin-D binds strongly to complexes of the voltage-dependent anion channel and the adenine nucleotide translocase to form the permeability transition pore." Eur J Biochem **258**(2): 729-735.

Das, S., R. Wong, et al. (2008). "Glycogen synthase kinase 3 inhibition slows mitochondrial adenine nucleotide transport and regulates voltage-dependent anion channel phosphorylation." Circ Res **103**(9): 983-991.

Daum, B., A. Walter, et al. (2013). "Age-dependent dissociation of ATP synthase dimers and loss of inner-membrane cristae in mitochondria." Proc Natl Acad Sci U S A **110**(38): 15301-15306.

Desagher, S., A. Osen-Sand, et al. (1999). "Bid-induced conformational change of Bax is responsible for mitochondrial cytochrome c release during apoptosis." J Cell Biol **144**(5): 891-901.

Devenish, R. J., M. Prescott, et al. (2008). "The structure and function of mitochondrial F1F0-ATP synthases." Int Rev Cell Mol Biol **267**: 1-58.
Dolder, M., B. Walzel, et al. (2003). "Inhibition of the mitochondrial permeability transition by creatine kinase substrates. Requirement for microcompartmentation." J Biol Chem **278**(20): 17760-17766.
Fredriksson, S., M. Gullberg, et al. (2002). "Protein detection using proximity-dependent DNA ligation assays." Nat Biotechnol **20**(5): 473-477.
Fujikawa, M., S. Ohsakaya, et al. (2014). "Population of ATP synthase molecules in mitochondria is limited by available 6.8-kDa proteolipid protein (MLQ)." Genes Cells **19**(2): 153-160.
Galluzzi, L., K. Blomgren, et al. (2009). "Mitochondrial membrane permeabilization in neuronal injury." Nat Rev Neurosci **10**(7): 481-494.
Galluzzi, L., O. Kepp, et al. (2012). "Mitochondria: master regulators of danger signalling." Nat Rev Mol Cell Biol **13**(12): 780-788.
Galluzzi, L., O. Kepp, et al. (2008). "Disruption of the hexokinase-VDAC complex for tumor therapy." Oncogene **27**(34): 4633-4635.
Galluzzi, L., O. Kepp, et al. (2013). "Metabolic targets for cancer therapy." Nat Rev Drug Discov **12**(11): 829-846.
Galluzzi, L., I. Vitale, et al. (2012). "Molecular definitions of cell death subroutines: recommendations of the Nomenclature Committee on Cell Death 2012." Cell Death Differ **19**(1): 107-120.
Garcia, J. J., E. Morales-Rios, et al. (2006). "The inhibitor protein (IF1) promotes dimerization of the mitochondrial F1F0-ATP synthase." Biochemistry **45**(42): 12695-12703.
Gerle, C. (2016). "On the structural possibility of pore-forming mitochondrial FoF1 ATP synthase." Biochim Biophys Acta **1857**(8): 1191-1196.
Giorgio, V., E. Bisetto, et al. (2009). "Cyclophilin D modulates mitochondrial F0F1-ATP synthase by interacting with the lateral stalk of the complex." J Biol Chem **284**(49): 33982-33988.
Giorgio, V., S. von Stockum, et al. (2013). "Dimers of mitochondrial ATP synthase form the permeability transition pore." Proc Natl Acad Sci U S A **110**(15): 5887-5892.
Gonzalez-Polo, R. A., G. Carvalho, et al. (2005). "PK11195 potently sensitizes to apoptosis induction independently from the peripheral benzodiazepin receptor." Oncogene **24**(51): 7503-7513.
Green, D. R., L. Galluzzi, et al. (2011). "Mitochondria and the autophagy-inflammation-cell death axis in organismal aging." Science **333**(6046): 1109-1112.
Hagen, T., C. J. Lagace, et al. (2003). "Permeability transition in rat liver mitochondria is modulated by the ATP-Mg/Pi carrier." Am J Physiol Gastrointest Liver Physiol **285**(2): G274-281.
Huertas, V. E., R. M. Maletz, et al. (1976). "Derman necrosis due to thrombosis in severe secondary hyperparathyroidism." Arch Intern Med **136**(6): 712-716.
Hunter, D. R. and R. A. Haworth (1979). "The Ca2+-induced membrane transition in mitochondria. I. The protective mechanisms." Arch Biochem Biophys **195**(2): 453-459.
Izzo, V., J. M. Bravo-San Pedro, et al. (2016). "Mitochondrial permeability transition: new findings and persisting uncertainties." Trends Cell Biol.
Jiko, C., K. M. Davies, et al. (2015). "Bovine F1Fo ATP synthase monomers bend the lipid bilayer in 2D membrane crystals." Elife **4**: e06119.
Jonckheere, A. I., J. A. Smeitink, et al. (2012). "Mitochondrial ATP synthase: architecture, function and pathology." J Inherit Metab Dis **35**(2): 211-225.
Jouaville, L. S., P. Pinton, et al. (1999). "Regulation of mitochondrial ATP synthesis by calcium: evidence for a long-term metabolic priming." Proc Natl Acad Sci U S A 96(24): 13807-13812.
Juhaszova, M., D. B. Zorov, et al. (2004). "Glycogen synthase kinase-3beta mediates convergence of protection signaling to inhibit the mitochondrial permeability transition pore." J Clin Invest **113**(11): 1535-1549.
Kallberg, M., H. Wang, et al. (2012). "Template-based protein structure modeling using the RaptorX web server." Nat Protoc **7**(8): 1511-1522.
Karch, J., J. Q. Kwong, et al. (2013). "Bax and Bak function as the outer membrane component of the mitochondrial permeability pore in regulating necrotic cell death in mice." Elife **2**: e00772.
Kishikawa, J., T. Ibuki, et al. (2013). "Common evolutionary origin for the rotor domain of rotary ATPases and flagellar protein export apparatus." PLoS One **8**(5): e64695.
Klaffschenkel, R. A., M. Waidmann, et al. (2012). "PK11195, a specific ligand of the peripheral benzodiazepine receptor, may protect pancreatic beta-cells from cytokine-induced cell death." Artif Cells Blood Substit Immobil Biotechnol **40**(1-2): 56-61.
Kokoszka, J. E., K. G. Waymire, et al. (2004). "The ADP/ATP translocator is not essential for the mitochondrial permeability transition pore." Nature **427**(6973): 461-465.
Korzick, D. H., J. C. Kostyak, et al. (2007). "Local delivery of PKCepsilon-activating peptide mimics ischemic preconditioning in aged hearts through GSK-3beta but not F1-ATPase inactivation." Am J Physiol Heart Circ Physiol **293**(4): H2056-2063.

Krah, A., D. Pogoryelov, et al. (2010). "Structural and energetic basis for H+ versus Na+ binding selectivity in ATP synthase Fo rotors." Biochim Biophys Acta **1797**(6-7): 763-772.
Kroemer, G., L. Galluzzi, et al. (2007). "Mitochondrial membrane permeabilization in cell death." Physiol Rev **87**(1): 99-163.
Kroemer, G., L. Galluzzi, et al. (2009). "Classification of cell death: recommendations of the Nomenclature Committee on Cell Death 2009." Cell Death Differ **16**(1): 3-11.
Kuhlbrandt, W. and K. M. Davies (2016). "Rotary ATPases: A New Twist to an Ancient Machine." Trends Biochem Sci **41**(1): 106-116.
Leist, M., B. Single, et al. (1997). "Intracellular adenosine triphosphate (ATP) concentration: a switch in the decision between apoptosis and necrosis." J Exp Med **185**(8): 1481-1486.
Leung, A. W., P. Varanyuwatana, et al. (2008). "The mitochondrial phosphate carrier interacts with cyclophilin D and may play a key role in the permeability transition." J Biol Chem **283**(39): 26312-26323.
Lightowlers, R. N., S. M. Howitt, et al. (1988). "The proton pore in the Escherichia coli F0F1-ATPase: substitution of glutamate by glutamine at position 219 of the alpha-subunit prevents F0-mediated proton permeability." Biochim Biophys Acta **933**(2): 241-248.
Linkermann, A., F. De Zen, et al. (2012). "Programmed necrosis in acute kidney injury." Nephrol Dial Transplant **27**(9): 3412-3419.
Marchi, S., S. Patergnani, et al. (2014). "The endoplasmic reticulum-mitochondria connection: one touch, multiple functions." Biochim Biophys Acta **1837**(4): 461-469.
Marsh, G. V. (1977). "Hospital administration: the new order--problems of obesity." R Soc Health J **97**(2): 70-73, 84.
Marzo, I., C. Brenner, et al. (1998). "Bax and adenine nucleotide translocator cooperate in the mitochondrial control of apoptosis." Science **281**(5385): 2027-2031.
Masgras, I., A. Rasola, et al. (2012). "Induction of the permeability transition pore in cells depleted of mitochondrial DNA." Biochim Biophys Acta **1817**(10): 1860-1866.
Matthies, D., L. Preiss, et al. (2009). "The c13 ring from a thermoalkaliphilic ATP synthase reveals an extended diameter due to a special structural region." J Mol Biol **388**(3): 611-618.
McEnery, M. W., A. M. Snowman, et al. (1992). "Isolation of the mitochondrial benzodiazepine receptor: association with the voltage-dependent anion channel and the adenine nucleotide carrier." Proc Natl Acad Sci U S A **89**(8): 3170-3174.
McGeoch, J. E. and G. Guidotti (1997). "A 0.1-700 Hz current through a voltage-clamped pore: candidate protein for initiator of neural oscillations." Brain Res **766**(1-2): 188-194.
Meier, T., U. Matthey, et al. (2001). "The central plug in the reconstituted undecameric c cylinder of a bacterial ATP synthase consists of phospholipids." FEBS Lett **505**(3): 353-356.
Meyer, B., I. Wittig, et al. (2007). "Identification of two proteins associated with mammalian ATP synthase." Mol Cell Proteomics **6**(10): 1690-1699.
Minauro-Sanmiguel, F., S. Wilkens, et al. (2005). "Structure of dimeric mitochondrial ATP synthase: novel F0 bridging features and the structural basis of mitochondrial cristae biogenesis." Proc Natl Acad Sci U S A **102**(35): 12356-12358.
Mukhin, A. G., V. Papadopoulos, et al. (1989). "Mitochondrial benzodiazepine receptors regulate steroid biosynthesis." Proc Natl Acad Sci U S A **86**(24): 9813-9816.
Mulkidjanian, A. Y., K. S. Makarova, et al. (2007). "Inventing the dynamo machine: the evolution of the F-type and V-type ATPases." Nat Rev Microbiol **5**(11): 892-899.
Murata, T., I. Yamato, et al. (2005). "Structure of the rotor of the V-Type Na+-ATPase from Enterococcus hirae." Science **308**(5722): 654-659.
Narita, M., S. Shimizu, et al. (1998). "Bax interacts with the permeability transition pore to induce permeability transition and cytochrome c release in isolated mitochondria." Proc Natl Acad Sci U S A **95**(25): 14681-14686.
Nishihara, M., T. Miura, et al. (2007). "Modulation of the mitochondrial permeability transition pore complex in GSK-3beta-mediated myocardial protection." J Mol Cell Cardiol **43**(5): 564-570.
Oberfeld, B., J. Brunner, et al. (2006). "Phospholipids occupy the internal lumen of the c ring of the ATP synthase of Escherichia coli." Biochemistry **45**(6): 1841-1851.
Ohsakaya, S., M. Fujikawa, et al. (2011). "Knockdown of DAPIT (diabetes-associated protein in insulin-sensitive tissue) results in loss of ATP synthase in mitochondria." J Biol Chem **286**(23): 20292-20296.
Okuno, D., R. Iino, et al. (2011). "Rotation and structure of FoF1-ATP synthase." J Biochem **149**(6): 655-664.
Ong, S. B., P. Samangouei, et al. (2015). "The mitochondrial permeability transition pore and its role in myocardial ischemia reperfusion injury." J Mol Cell Cardiol **78**: 23-34.
Palmieri, F. (2004). "The mitochondrial transporter family (SLC25): physiological and pathological implications." Pflugers Arch **447**(5): 689-709.

Pandini, A., J. Kleinjung, et al. (2015). "The phylogenetic signature underlying ATP synthase c-ring compliance." Biophys J **109**(5): 975-987.
Pastorino, J. G. and J. B. Hoek (2003). "Hexokinase II: the integration of energy metabolism and control of apoptosis." Curr Med Chem **10**(16): 1535-1551.
Pastorino, J. G. and J. B. Hoek (2008). "Regulation of hexokinase binding to VDAC." J Bioenerg Biomembr **40**(3): 171-182.
Pastorino, J. G., J. B. Hoek, et al. (2005). "Activation of glycogen synthase kinase 3beta disrupts the binding of hexokinase II to mitochondria by phosphorylating voltage-dependent anion channel and potentiates chemotherapy-induced cytotoxicity." Cancer Res **65**(22): 10545-10554.
Pastorino, J. G., G. Simbula, et al. (1994). "Protoporphyrin IX, an endogenous ligand of the peripheral benzodiazepine receptor, potentiates induction of the mitochondrial permeability transition and the killing of cultured hepatocytes by rotenone." J Biol Chem **269**(49): 31041-31046.
Pauleau, A. L., L. Galluzzi, et al. (2008). "Unexpected role of the phosphate carrier in mitochondrial fragmentation." Cell Death Differ **15**(3): 616-618.
Pediaditakis, P., J. S. Kim, et al. (2010). "Inhibition of the mitochondrial permeability transition by protein kinase A in rat liver mitochondria and hepatocytes." Biochem J **431**(3): 411-421.
Pogoryelov, D., A. L. Klyszejko, et al. (2012). "Engineering rotor ring stoichiometries in the ATP synthase." Proc Natl Acad Sci U S A **109**(25): E1599-1608.
Pogoryelov, D., O. Yildiz, et al. (2009). "High-resolution structure of the rotor ring of a proton-dependent ATP synthase." Nat Struct Mol Biol **16**(10): 1068-1073.
Roy, S. S., M. Madesh, et al. (2009). "Bad targets the permeability transition pore independent of Bax or Bak to switch between Ca2+-dependent cell survival and death." Mol Cell **33**(3): 377-388.
Rubinstein, J. L., J. E. Walker, et al. (2003). "Structure of the mitochondrial ATP synthase by electron cryomicroscopy." EMBO J **22**(23): 6182-6192.
Ruck, A., M. Dolder, et al. (1998). "Reconstituted adenine nucleotide translocase forms a channel for small molecules comparable to the mitochondrial permeability transition pore." FEBS Lett **426**(1): 97-101.
Saroussi, S., M. Schushan, et al. (2012). "Structure and flexibility of the C-ring in the electromotor of rotary F(0)F(1)-ATPase of pea chloroplasts." PLoS One **7**(9): e43045.
Schindler, A. and E. Foley (2013). "Hexokinase 1 blocks apoptotic signals at the mitochondria." Cell Signal **25**(12): 2685-2692.
Schroers, A., R. Kramer, et al. (1997). "The reversible antiport-uniport conversion of the phosphate carrier from yeast mitochondria depends on the presence of a single cysteine." J Biol Chem **272**(16): 10558-10564.
Shimizu, S., M. Narita, et al. (1999). "Bcl-2 family proteins regulate the release of apoptogenic cytochrome c by the mitochondrial channel VDAC." Nature **399**(6735): 483-487.
Smeele, K. M., R. Southworth, et al. (2011). "Disruption of hexokinase II-mitochondrial binding blocks ischemic preconditioning and causes rapid cardiac necrosis." Circ Res **108**(10): 1165-1169.
Stock, D., A. G. Leslie, et al. (1999). "Molecular architecture of the rotary motor in ATP synthase." Science **286**(5445): 1700-1705.
Symersky, J., D. Osowski, et al. (2012). "Oligomycin frames a common drug-binding site in the ATP synthase." Proc Natl Acad Sci U S A **109**(35): 13961-13965.
Symersky, J., V. Pagadala, et al. (2012). "Structure of the c(10) ring of the yeast mitochondrial ATP synthase in the open conformation." Nat Struct Mol Biol **19**(5): 485-491, S481.
Szabo, I., P. Bernardi, et al. (1992). "Modulation of the mitochondrial megachannel by divalent cations and protons." J Biol Chem **267**(5): 2940-2946.
Szabo, I., V. De Pinto, et al. (1993). "The mitochondrial permeability transition pore may comprise VDAC molecules. II. The electrophysiological properties of VDAC are compatible with those of the mitochondrial megachannel." FEBS Lett **330**(2): 206-210.
Szabo, I. and M. Zoratti (1992). "The mitochondrial megachannel is the permeability transition pore." J Bioenerg Biomembr **24**(1): 111-117.
Szabo, I. and M. Zoratti (1993). "The mitochondrial permeability transition pore may comprise VDAC molecules. I. Binary structure and voltage dependence of the pore." FEBS Lett **330**(2): 201-205.
Tait, S. W. and D. R. Green (2010). "Mitochondria and cell death: outer membrane permeabilization and beyond." Nat Rev Mol Cell Biol **11**(9): 621-632.
Takuma, K., P. Phuagphong, et al. (2001). "Anti-apoptotic effect of cGMP in cultured astrocytes: inhibition by cGMP-dependent protein kinase of mitochondrial permeable transition pore." J Biol Chem **276**(51): 48093-48099.
Tani, K., T. Mitsuma, et al. (2009). "Mechanism of aquaporin-4's fast and highly selective water conduction and proton exclusion." J Mol Biol **389**(4): 694-706.
Tedeschi, H., H. J. Hegarty, et al. (1965). "Osmotic reversal of phosphate-induced mitochondrial swelling." Biochim Biophys Acta **104**(2): 612-615.

Traba, J., A. Del Arco, et al. (2012). "SCaMC-1 promotes cancer cell survival by desensitizing mitochondrial permeability transition via ATP/ADP-mediated matrix Ca(2+) buffering." Cell Death Differ **19**(4): 650-660.
Vandenabeele, P., L. Galluzzi, et al. (2010). "Molecular mechanisms of necroptosis: an ordered cellular explosion." Nat Rev Mol Cell Biol **11**(10): 700-714.
Vander Heiden, M. G., N. S. Chandel, et al. (1999). "Bcl-xL prevents cell death following growth factor withdrawal by facilitating mitochondrial ATP/ADP exchange." Mol Cell **3**(2): 159-167.
Varanyuwatana, P. and A. P. Halestrap (2012). "The roles of phosphate and the phosphate carrier in the mitochondrial permeability transition pore." Mitochondrion **12**(1): 120-125.
Vaseva, A. V., N. D. Marchenko, et al. (2012). "p53 opens the mitochondrial permeability transition pore to trigger necrosis." Cell **149**(7): 1536-1548.
Verrier, F., A. Deniaud, et al. (2004). "Dynamic evolution of the adenine nucleotide translocase interactome during chemotherapy-induced apoptosis." Oncogene **23**(49): 8049-8064.
von Stockum, S., V. Giorgio, et al. (2015). "F-ATPase of Drosophila melanogaster forms 53-picosiemen (53-pS) channels responsible for mitochondrial Ca2+-induced Ca2+ release." J Biol Chem **290**(8): 4537-4544.
Whitehead, T. R. and R. B. Hespell (1990). "Heterologous expression of the Bacteroides ruminicola xylanase gene in Bacteroides fragilis and Bacteroides uniformis." FEMS Microbiol Lett **54**(1-3): 61-65.
Wittig, I. and H. Schagger (2008). "Structural organization of mitochondrial ATP synthase." Biochim Biophys Acta **1777**(7-8): 592-598.
Yoshida, M., E. Muneyuki, et al. (2001). "ATP synthase--a marvellous rotary engine of the cell." Nat Rev Mol Cell Biol **2**(9): 669-677.
Zamzami, N., C. El Hamel, et al. (2000). "Bid acts on the permeability transition pore complex to induce apoptosis." Oncogene **19**(54): 6342-6350.
Zamzami, N., P. Marchetti, et al. (1995). "Sequential reduction of mitochondrial transmembrane potential and generation of reactive oxygen species in early programmed cell death." J Exp Med **182**(2): 367-377.
Zamzami, N., P. Marchetti, et al. (1995). "Reduction in mitochondrial potential constitutes an early irreversible step of programmed lymphocyte death in vivo." J Exp Med **181**(5): 1661-1672.
Zhou, M., N. Morgner, et al. (2011). "Mass spectrometry of intact V-type ATPases reveals bound lipids and the effects of nucleotide binding." Science **334**(6054): 380-385.

Chapter 2. Regulation of autophagy and PKCβ levels by PML is essential for MDSC high glucose-dependent adipogenesis

Aguiari, P., S. Leo, et al. (2008). "High glucose induces adipogenic differentiation of muscle-derived stem cells." Proc Natl Acad Sci U S A **105**(4): 1226-1231.
Aouadi, M., K. Laurent, et al. (2006). "Inhibition of p38MAPK increases adipogenesis from embryonic to adult stages." Diabetes **55**(2): 281-289.
Artemenko, Y., A. Gagnon, et al. (2005). "Anti-adipogenic effect of PDGF is reversed by PKC inhibition." J Cell Physiol **204**(2): 646-653.
Baerga, R., Y. Zhang, et al. (2009). "Targeted deletion of autophagy-related 5 (atg5) impairs adipogenesis in a cellular model and in mice." Autophagy **5**(8): 1118-1130.
Bansode, R. R., W. Huang, et al. (2008). "Protein kinase C deficiency increases fatty acid oxidation and reduces fat storage." J Biol Chem **283**(1): 231-236.
Behrends, C., M. E. Sowa, et al. (2010). "Network organization of the human autophagy system." Nature **466**(7302): 68-76.
Bernardi, R., I. Guernah, et al. (2006). "PML inhibits HIF-1alpha translation and neoangiogenesis through repression of mTOR." Nature **442**(7104): 779-785.
Bernardi, R. and P. P. Pandolfi (2007). "Structure, dynamics and functions of promyelocytic leukaemia nuclear bodies." Nat Rev Mol Cell Biol **8**(12): 1006-1016.
Bernardi, R., P. P. Scaglioni, et al. (2004). "PML regulates p53 stability by sequestering Mdm2 to the nucleolus." Nat Cell Biol **6**(7): 665-672.
Bernardo, M. E., D. Pagliara, et al. (2012). "Mesenchymal stromal cell therapy: a revolution in Regenerative Medicine?" Bone Marrow Transplant **47**(2): 164-171.
Bluher, M., M. D. Michael, et al. (2002). "Adipose tissue selective insulin receptor knockout protects against obesity and obesity-related glucose intolerance." Dev Cell **3**(1): 25-38.
Bohensky, J., I. M. Shapiro, et al. (2007). "HIF-1 regulation of chondrocyte apoptosis: induction of the autophagic pathway." Autophagy **3**(3): 207-214.

Bost, F., M. Aouadi, et al. (2005). "The role of MAPKs in adipocyte differentiation and obesity." Biochimie **87**(1): 51-56.
Brook, C. G., J. K. Lloyd, et al. (1972). "Relation between age of onset of obesity and size and number of adipose cells." Br Med J **2**(5804): 25-27.
Camp, H. S., O. Li, et al. (2000). "Differential activation of peroxisome proliferator-activated receptor-gamma by troglitazone and rosiglitazone." Diabetes **49**(4): 539-547.
Carames, B., N. Taniguchi, et al. (2010). "Autophagy is a protective mechanism in normal cartilage, and its aging-related loss is linked with cell death and osteoarthritis." Arthritis Rheum **62**(3): 791-801.
Carnevalli, L. S., K. Masuda, et al. (2010). "S6K1 plays a critical role in early adipocyte differentiation." Dev Cell **18**(5): 763-774.
Carracedo, A., D. Rousseau, et al. (2015). "The promyelocytic leukemia protein is upregulated in conditions of obesity and liver steatosis." Int J Biol Sci **11**(6): 629-632.
Carracedo, A., D. Weiss, et al. (2012). "A metabolic prosurvival role for PML in breast cancer." J Clin Invest **122**(9): 3088-3100.
Chen, B. Y., X. Wang, et al. (2012). "Molecular targeting regulation of proliferation and differentiation of the bone marrow-derived mesenchymal stem cells or mesenchymal stromal cells." Curr Drug Targets **13**(4): 561-571.
Cheng, H. C., S. W. Liu, et al. (2015). "Arsenic trioxide regulates adipogenic and osteogenic differentiation in bone marrow MSCs of aplastic anemia patients through BMP4 gene." Acta Biochim Biophys Sin (Shanghai) **47**(9): 673-679.
Cheng, X., S. Guo, et al. (2013). "Ablation of promyelocytic leukemia protein (PML) re-patterns energy balance and protects mice from obesity induced by a Western diet." J Biol Chem **288**(41): 29746-29759.
Choy, L. and R. Derynck (2003). "Transforming growth factor-beta inhibits adipocyte differentiation by Smad3 interacting with CCAAT/enhancer-binding protein (C/EBP) and repressing C/EBP transactivation function." J Biol Chem **278**(11): 9609-9619.
Chuang, C. C., R. S. Yang, et al. (2007). "Hyperglycemia enhances adipogenic induction of lipid accumulation: involvement of extracellular signal-regulated protein kinase 1/2, phosphoinositide 3-kinase/Akt, and peroxisome proliferator-activated receptor gamma signaling." Endocrinology **148**(9): 4267-4275.
Clemens, M. J., I. Trayner, et al. (1992). "The role of protein kinase C isoenzymes in the regulation of cell proliferation and differentiation." J Cell Sci **103 (Pt 4)**: 881-887.
Clouthier, D. E., S. A. Comerford, et al. (1997). "Hepatic fibrosis, glomerulosclerosis, and a lipodystrophy-like syndrome in PEPCK-TGF-beta1 transgenic mice." J Clin Invest **100**(11): 2697-2713.
Coller, H. A., L. Sang, et al. (2006). "A new description of cellular quiescence." PLoS Biol **4**(3): e83.
De Boer, J., H. J. Wang, et al. (2004). "Effects of Wnt signaling on proliferation and differentiation of human mesenchymal stem cells." Tissue Eng **10**(3-4): 393-401.
de The, H., C. Lavau, et al. (1991). "The PML-RAR alpha fusion mRNA generated by the t(15;17) translocation in acute promyelocytic leukemia encodes a functionally altered RAR." Cell **66**(4): 675-684.
Farmer, S. R. (2006). "Transcriptional control of adipocyte formation." Cell Metab **4**(4): 263-273.
Faust, I. M., P. R. Johnson, et al. (1978). "Diet-induced adipocyte number increase in adult rats: a new model of obesity." Am J Physiol **235**(3): E279-286.
Fleming, I., S. J. MacKenzie, et al. (1998). "Protein kinase C isoforms play differential roles in the regulation of adipocyte differentiation." Biochem J **333 (Pt 3)**: 719-727.
Fracanzani, A. L., L. Valenti, et al. (2011). "Risk of nonalcoholic steatohepatitis and fibrosis in patients with nonalcoholic fatty liver disease and low visceral adiposity." J Hepatol **54**(6): 1244-1249.
Freytag, S. O., D. L. Paielli, et al. (1994). "Ectopic expression of the CCAAT/enhancer-binding protein alpha promotes the adipogenic program in a variety of mouse fibroblastic cells." Genes Dev **8**(14): 1654-1663.
Gallicano, G. I., M. C. Yousef, et al. (1997). "PKC--a pivotal regulator of early development." Bioessays **19**(1): 29-36.
Garofalo, R. S., S. J. Orena, et al. (2003). "Severe diabetes, age-dependent loss of adipose tissue, and mild growth deficiency in mice lacking Akt2/PKB beta." J Clin Invest **112**(2): 197-208.
Giorgi, C., K. Ito, et al. (2010). "PML regulates apoptosis at endoplasmic reticulum by modulating calcium release." Science **330**(6008): 1247-1251.
Gray, S., M. W. Feinberg, et al. (2002). "The Kruppel-like factor KLF15 regulates the insulin-sensitive glucose transporter GLUT4." J Biol Chem **277**(37): 34322-34328.
Guan, J. L., A. K. Simon, et al. (2013). "Autophagy in stem cells." Autophagy **9**(6): 830-849.
Hale, A. N., D. J. Ledbetter, et al. (2013). "Autophagy: regulation and role in development." Autophagy **9**(7): 951-972.

He, C. and D. J. Klionsky (2009). "Regulation mechanisms and signaling pathways of autophagy." Annu Rev Genet **43**: 67-93.
Hirsch, J. and B. Batchelor (1976). "Adipose tissue cellularity in human obesity." Clin Endocrinol Metab **5**(2): 299-311.
Hu, Y., E. Kutscher, et al. (2010). "Berberine inhibits SREBP-1-related clozapine and risperidone induced adipogenesis in 3T3-L1 cells." Phytother Res **24**(12): 1831-1838.
Hutley, L., W. Shurety, et al. (2004). "Fibroblast growth factor 1: a key regulator of human adipogenesis." Diabetes **53**(12): 3097-3106.
Ito, K., R. Bernardi, et al. (2008). "PML targeting eradicates quiescent leukaemia-initiating cells." Nature **453**(7198): 1072-1078.
Jia, J., W. Yao, et al. (2011). "Glucocorticoid dose determines osteocyte cell fate." FASEB J **25**(10): 3366-3376.
Joyner, J. M., L. J. Hutley, et al. (2000). "Glucocorticoid receptors in human preadipocytes: regional and gender differences." J Endocrinol **166**(1): 145-152.
Kajimura, S., P. Seale, et al. (2008). "Regulation of the brown and white fat gene programs through a PRDM16/CtBP transcriptional complex." Genes Dev **22**(10): 1397-1409.
Kakizuka, A., W. H. Miller, Jr., et al. (1991). "Chromosomal translocation t(15;17) in human acute promyelocytic leukemia fuses RAR alpha with a novel putative transcription factor, PML." Cell **66**(4): 663-674.
Kanazawa, A., S. Tsukada, et al. (2005). "Wnt5b partially inhibits canonical Wnt/beta-catenin signaling pathway and promotes adipogenesis in 3T3-L1 preadipocytes." Biochem Biophys Res Commun **330**(2): 505-510.
Kim, J. B., P. Sarraf, et al. (1998). "Nutritional and insulin regulation of fatty acid synthetase and leptin gene expression through ADD1/SREBP1." J Clin Invest **101**(1): 1-9.
Kim, J. B., H. M. Wright, et al. (1998). "ADD1/SREBP1 activates PPARgamma through the production of endogenous ligand." Proc Natl Acad Sci U S A **95**(8): 4333-4337.
Kim, J. E. and J. Chen (2004). "regulation of peroxisome proliferator-activated receptor-gamma activity by mammalian target of rapamycin and amino acids in adipogenesis." Diabetes **53**(11): 2748-2756.
Kim, M. K., S. Yang, et al. (2011). "Promyelocytic leukemia inhibits adipogenesis, and loss of promyelocytic leukemia results in fat accumulation in mice." Am J Physiol Endocrinol Metab **301**(6): E1130-1142.
Kimmelman, A. C. (2011). "The dynamic nature of autophagy in cancer." Genes Dev **25**(19): 1999-2010.
Komatsu, M., S. Waguri, et al. (2007). "Homeostatic levels of p62 control cytoplasmic inclusion body formation in autophagy-deficient mice." Cell **131**(6): 1149-1163.
Lallemand-Breitenbach, V. and H. de The (2010). "PML nuclear bodies." Cold Spring Harb Perspect Biol **2**(5): a000661.
Lallemand-Breitenbach, V., J. Zhu, et al. (2001). "Role of promyelocytic leukemia (PML) sumolation in nuclear body formation, 11S proteasome recruitment, and As2O3-induced PML or PML/retinoic acid receptor alpha degradation." J Exp Med **193**(12): 1361-1371.
Lavasani, M., A. Lu, et al. (2013). "Isolation of muscle-derived stem/progenitor cells based on adhesion characteristics to collagen-coated surfaces." Methods Mol Biol **976**: 53-65.
Le Bacquer, O., E. Petroulakis, et al. (2007). "Elevated sensitivity to diet-induced obesity and insulin resistance in mice lacking 4E-BP1 and 4E-BP2." J Clin Invest **117**(2): 387-396.
Lee, K., J. A. Villena, et al. (2003). "Inhibition of adipogenesis and development of glucose intolerance by soluble preadipocyte factor-1 (Pref-1)." J Clin Invest **111**(4): 453-461.
Lee, S. W., H. B. Kwak, et al. (2003). "Participation of protein kinase C beta in osteoclast differentiation and function." Bone **32**(3): 217-227.
Li, D., S. Yea, et al. (2005). "Kruppel-like factor-6 promotes preadipocyte differentiation through histone deacetylase 3-dependent repression of DLK1." J Biol Chem **280**(29): 26941-26952.
Ling, L., V. Nurcombe, et al. (2009). "Wnt signaling controls the fate of mesenchymal stem cells." Gene **433**(1-2): 1-7.
Liu, F., F. Fang, et al. (2013). "Suppression of autophagy by FIP200 deletion leads to osteopenia in mice through the inhibition of osteoblast terminal differentiation." J Bone Miner Res **28**(11): 2414-2430.
Longo, K. A., W. S. Wright, et al. (2004). "Wnt10b inhibits development of white and brown adipose tissues." J Biol Chem **279**(34): 35503-35509.
Mathew, R., V. Karantza-Wadsworth, et al. (2007). "Role of autophagy in cancer." Nat Rev Cancer **7**(12): 961-967.
Matsushita, K. (2016). "Mesenchymal Stem Cells and Metabolic Syndrome: Current Understanding and Potential Clinical Implications." Stem Cells Int **2016**: 2892840.
McGowan, K., J. DeVente, et al. (1996). "Protein kinase C isoform expression during the differentiation of 3T3-L1 preadipocytes: loss of protein kinase C-alpha isoform correlates with loss of phorbol 12-myristate 13-acetate activation of nuclear factor kappaB and acquisition of the adipocyte phenotype." J Cell Physiol **167**(1): 113-120.

Missiroli, S., M. Bonora, et al. (2016). "PML at Mitochondria-Associated Membranes Is Critical for the Repression of Autophagy and Cancer Development." Cell Rep **16**(9): 2415-2427.
Mizushima, N. and D. J. Klionsky (2007). "Protein turnover via autophagy: implications for metabolism." Annu Rev Nutr **27**: 19-40.
Mizushima, N. and M. Komatsu (2011). "Autophagy: renovation of cells and tissues." Cell **147**(4): 728-741.
Mizushima, N. and B. Levine (2010). "Autophagy in mammalian development and differentiation." Nat Cell Biol **12**(9): 823-830.
Mori, T., H. Sakaue, et al. (2005). "Role of Kruppel-like factor 15 (KLF15) in transcriptional regulation of adipogenesis." J Biol Chem **280**(13): 12867-12875.
Nuschke, A., M. Rodrigues, et al. (2014). "Human mesenchymal stem cells/multipotent stromal cells consume accumulated autophagosomes early in differentiation." Stem Cell Res Ther **5**(6): 140.
Oliver, L., E. Hue, et al. (2012). "Basal autophagy decreased during the differentiation of human adult mesenchymal stem cells." Stem Cells Dev **21**(15): 2779-2788.
Ortega, F. J., J. M. Moreno-Navarrete, et al. (2009). "Subcutaneous fat shows higher thyroid hormone receptor-alpha1 gene expression than omental fat." Obesity (Silver Spring) **17**(12): 2134-2141.
Park, J., S. Chung, et al. (2012). "Haloperidol and clozapine block formation of autophagolysosomes in rat primary neurons." Neuroscience **209**: 64-73.
Patergnani, S., S. Marchi, et al. (2013). "PRKCB/protein kinase C, beta and the mitochondrial axis as key regulators of autophagy." Autophagy **9**(9): 1367-1385.
Pei, H., Y. Yao, et al. (2011). "Kruppel-like factor KLF9 regulates PPARgamma transactivation at the middle stage of adipogenesis." Cell Death Differ **18**(2): 315-327.
Phadwal, K., A. S. Watson, et al. (2013). "Tightrope act: autophagy in stem cell renewal, differentiation, proliferation, and aging." Cell Mol Life Sci **70**(1): 89-103.
Pittenger, M. F., A. M. Mackay, et al. (1999). "Multilineage potential of adult human mesenchymal stem cells." Science **284**(5411): 143-147.
Polak, P., N. Cybulski, et al. (2008). "Adipose-specific knockout of raptor results in lean mice with enhanced mitochondrial respiration." Cell Metab **8**(5): 399-410.
Prusty, D., B. H. Park, et al. (2002). "Activation of MEK/ERK signaling promotes adipogenesis by enhancing peroxisome proliferator-activated receptor gamma (PPARgamma) and C/EBPalpha gene expression during the differentiation of 3T3-L1 preadipocytes." J Biol Chem **277**(48): 46226-46232.
Ramji, D. P. and P. Foka (2002). "CCAAT/enhancer-binding proteins: structure, function and regulation." Biochem J **365**(Pt 3): 561-575.
Rebbapragada, A., H. Benchabane, et al. (2003). "Myostatin signals through a transforming growth factor beta-like signaling pathway to block adipogenesis." Mol Cell Biol **23**(20): 7230-7242.
Regad, T., C. Bellodi, et al. (2009). "The tumor suppressor Pml regulates cell fate in the developing neocortex." Nat Neurosci **12**(2): 132-140.
Ren, Y., Y. Xie, et al. (2011). "Autophagy modification augmented the treatment effects initiated by arsenic trioxide in NB4 cells." Med Oncol **28**(1): 231-236.
Reusch, J. E., L. A. Colton, et al. (2000). "CREB activation induces adipogenesis in 3T3-L1 cells." Mol Cell Biol **20**(3): 1008-1020.
Rosen, E. D., C. H. Hsu, et al. (2002). "C/EBPalpha induces adipogenesis through PPARgamma: a unified pathway." Genes Dev **16**(1): 22-26.
Ross, S. E., N. Hemati, et al. (2000). "Inhibition of adipogenesis by Wnt signaling." Science **289**(5481): 950-953.
Rowley, J. D. (1982). "Identification of the constant chromosome regions involved in human hematologic malignant disease." Science **216**(4547): 749-751.
Rubinsztein, D. C. (2006). "The roles of intracellular protein-degradation pathways in neurodegeneration." Nature **443**(7113): 780-786.
Rubinsztein, D. C., G. Marino, et al. (2011). "Autophagy and aging." Cell **146**(5): 682-695.
Satija, N. K., G. U. Gurudutta, et al. (2007). "Mesenchymal stem cells: molecular targets for tissue engineering." Stem Cells Dev **16**(1): 7-23.
Shtutman, M., J. Zhurinsky, et al. (2002). "PML is a target gene of beta-catenin and plakoglobin, and coactivates beta-catenin-mediated transcription." Cancer Res **62**(20): 5947-5954.
Singh, R., J. N. Artaza, et al. (2006). "Testosterone inhibits adipogenic differentiation in 3T3-L1 cells: nuclear translocation of androgen receptor complex with beta-catenin and T-cell factor 4 may bypass canonical Wnt signaling to down-regulate adipogenic transcription factors." Endocrinology **147**(1): 141-154.
Singh, R., Y. Xiang, et al. (2009). "Autophagy regulates adipose mass and differentiation in mice." J Clin Invest **119**(11): 3329-3339.
Smas, C. M. and H. S. Sul (1995). "Control of adipocyte differentiation." Biochem J **309 (Pt 3)**: 697-710.
Smith, P. J., L. S. Wise, et al. (1988). "Insulin-like growth factor-I is an essential regulator of the differentiation of 3T3-L1 adipocytes." J Biol Chem **263**(19): 9402-9408.

Spalding, K. L., E. Arner, et al. (2008). "Dynamics of fat cell turnover in humans." Nature **453**(7196): 783-787.
Spiegelman, B. M., L. Choy, et al. (1993). "Regulation of adipocyte gene expression in differentiation and syndromes of obesity/diabetes." J Biol Chem **268**(10): 6823-6826.
Sun, J., S. Fu, et al. (2013). "PML overexpression inhibits proliferation and promotes the osteogenic differentiation of human mesenchymal stem cells." Oncol Rep **30**(6): 2785-2794.
Tang, Q. Q., M. Gronborg, et al. (2005). "Sequential phosphorylation of CCAAT enhancer-binding protein beta by MAPK and glycogen synthase kinase 3beta is required for adipogenesis." Proc Natl Acad Sci U S A **102**(28): 9766-9771.
Tang, Q. Q., T. C. Otto, et al. (2003). "CCAAT/enhancer-binding protein beta is required for mitotic clonal expansion during adipogenesis." Proc Natl Acad Sci U S A **100**(3): 850-855.
Tolar, J., K. Le Blanc, et al. (2010). "Concise review: hitting the right spot with mesenchymal stromal cells." Stem Cells **28**(8): 1446-1455.
Tong, Q., G. Dalgin, et al. (2000). "Function of GATA transcription factors in preadipocyte-adipocyte transition." Science **290**(5489): 134-138.
Tong, Q., J. Tsai, et al. (2005). "Interaction between GATA and the C/EBP family of transcription factors is critical in GATA-mediated suppression of adipocyte differentiation." Mol Cell Biol **25**(2): 706-715.
Tontonoz, P., E. Hu, et al. (1994). "mPPAR gamma 2: tissue-specific regulator of an adipocyte enhancer." Genes Dev **8**(10): 1224-1234.
Trotman, L. C., A. Alimonti, et al. (2006). "Identification of a tumour suppressor network opposing nuclear Akt function." Nature **441**(7092): 523-527.
Um, S. H., F. Frigerio, et al. (2004). "Absence of S6K1 protects against age- and diet-induced obesity while enhancing insulin sensitivity." Nature **431**(7005): 200-205.
Vessoni, A. T., A. R. Muotri, et al. (2012). "Autophagy in stem cell maintenance and differentiation." Stem Cells Dev **21**(4): 513-520.
Villena, J. A., K. H. Kim, et al. (2002). "Pref-1 and ADSF/resistin: two secreted factors inhibiting adipose tissue development." Horm Metab Res **34**(11-12): 664-670.
Wang, G. L., X. Shi, et al. (2006). "Cyclin D3 maintains growth-inhibitory activity of C/EBPalpha by stabilizing C/EBPalpha-cdk2 and C/EBPalpha-Brm complexes." Mol Cell Biol **26**(7): 2570-2582.
Wei, H., S. Wei, et al. (2011). "Suppression of autophagy by FIP200 deletion inhibits mammary tumorigenesis." Genes Dev **25**(14): 1510-1527.
Wolfrum, C., D. Q. Shih, et al. (2003). "Role of Foxa-2 in adipocyte metabolism and differentiation." J Clin Invest **112**(3): 345-356.
Wu, J. and J. B. Lingrel (2005). "Kruppel-like factor 2, a novel immediate-early transcriptional factor, regulates IL-2 expression in T lymphocyte activation." J Immunol **175**(5): 3060-3066.
Wu, J., S. V. Srinivasan, et al. (2005). "The KLF2 transcription factor does not affect the formation of preadipocytes but inhibits their differentiation into adipocytes." Biochemistry **44**(33): 11098-11105.
Wu, Z., N. L. Bucher, et al. (1996). "Induction of peroxisome proliferator-activated receptor gamma during the conversion of 3T3 fibroblasts into adipocytes is mediated by C/EBPbeta, C/EBPdelta, and glucocorticoids." Mol Cell Biol **16**(8): 4128-4136.
Xie, Z. and D. J. Klionsky (2007). "Autophagosome formation: core machinery and adaptations." Nat Cell Biol **9**(10): 1102-1109.
Yoon, M. S., C. Zhang, et al. (2013). "Mechanistic target of rapamycin controls homeostasis of adipogenesis." J Lipid Res **54**(8): 2166-2173.
Zeng, M. and J. N. Zhou (2008). "Roles of autophagy and mTOR signaling in neuronal differentiation of mouse neuroblastoma cells." Cell Signal **20**(4): 659-665.
Zhang, J. W., D. J. Klemm, et al. (2004). "Role of CREB in transcriptional regulation of CCAAT/enhancer-binding protein beta gene during adipogenesis." J Biol Chem **279**(6): 4471-4478.
Zhang, Y., S. Goldman, et al. (2009). "Adipose-specific deletion of autophagy-related gene 7 (atg7) in mice reveals a role in adipogenesis." Proc Natl Acad Sci U S A **106**(47): 19860-19865.
Zheng, Y., C. J. Hu, et al. (2014). "Inhibition of autophagy alleviates the senescent state of rat mesenchymal stem cells during long-term culture." Mol Med Rep **10**(6): 3003-3008.
Zhou, Y., D. Wang, et al. (2006). "Different roles of protein kinase C-betaI and -delta in the regulation of adipocyte differentiation." Int J Biochem Cell Biol **38**(12): 2151-2163.

Chapter 3. Mitochondria-nucleus communication in mesenchymal stem cell differentiation: key role of acetyl-CoA transport system

Adam-Vizi, V. and A. A. Starkov (2010). "Calcium and mitochondrial reactive oxygen species generation: how to read the facts." J Alzheimers Dis **20 Suppl 2**: S413-426.
Agathocleous, M. and W. A. Harris (2013). "Metabolism in physiological cell proliferation and differentiation." Trends Cell Biol **23**(10): 484-492.

Almalki, S. G. and D. K. Agrawal (2016). "Key transcription factors in the differentiation of mesenchymal stem cells." Differentiation **92**(1-2): 41-51.
Avgustinova, A. and S. A. Benitah (2016). "Epigenetic control of adult stem cell function." Nat Rev Mol Cell Biol **17**(10): 643-658.
Baksh, D., R. Yao, et al. (2007). "Comparison of proliferative and multilineage differentiation potential of human mesenchymal stem cells derived from umbilical cord and bone marrow." Stem Cells **25**(6): 1384-1392.
Bauer, G., M. A. Dao, et al. (2008). "In vivo biosafety model to assess the risk of adverse events from retroviral and lentiviral vectors." Mol Ther **16**(7): 1308-1315.
Ben-David, U. and N. Benvenisty (2011). "The tumorigenicity of human embryonic and induced pluripotent stem cells." Nat Rev Cancer **11**(4): 268-277.
Bracha, A. L., A. Ramanathan, et al. (2010). "Carbon metabolism-mediated myogenic differentiation." Nat Chem Biol **6**(3): 202-204.
Cai, L., B. M. Sutter, et al. (2011). "Acetyl-CoA induces cell growth and proliferation by promoting the acetylation of histones at growth genes." Mol Cell **42**(4): 426-437.
Cai, L. and B. P. Tu (2012). "Driving the cell cycle through metabolism." Annu Rev Cell Dev Biol **28**: 59-87.
Carey, B. W., L. W. Finley, et al. (2015). "Intracellular alpha-ketoglutarate maintains the pluripotency of embryonic stem cells." Nature **518**(7539): 413-416.
Chen, C. T., S. H. Hsu, et al. (2010). "Upregulation of mitochondrial function and antioxidant defense in the differentiation of stem cells." Biochim Biophys Acta **1800**(3): 257-263.
Chen, C. T., Y. R. Shih, et al. (2008). "Coordinated changes of mitochondrial biogenesis and antioxidant enzymes during osteogenic differentiation of human mesenchymal stem cells." Stem Cells **26**(4): 960-968.
Chen, Q., Y. Chen, et al. (2013). "TET2 promotes histone O-GlcNAcylation during gene transcription." Nature **493**(7433): 561-564.
Choi, Y. S., S. E. Noh, et al. (2008). "Multipotency and growth characteristic of periosteum-derived progenitor cells for chondrogenic, osteogenic, and adipogenic differentiation." Biotechnol Lett **30**(4): 593-601.
Dang, L., D. W. White, et al. (2009). "Cancer-associated IDH1 mutations produce 2-hydroxyglutarate." Nature **462**(7274): 739-744.
De Bari, C., F. Dell'Accio, et al. (2001). "Multipotent mesenchymal stem cells from adult human synovial membrane." Arthritis Rheum **44**(8): 1928-1942.
Dezawa, M., H. Kanno, et al. (2004). "Specific induction of neuronal cells from bone marrow stromal cells and application for autologous transplantation." J Clin Invest **113**(12): 1701-1710.
Dodson, M. V., G. J. Hausman, et al. (2011). "Potential impact of mature adipocyte dedifferentiation in terms of cell numbers." Int J Stem Cells **4**(1): 76-78.
Dominici, M., K. Le Blanc, et al. (2006). "Minimal criteria for defining multipotent mesenchymal stromal cells. The International Society for Cellular Therapy position statement." Cytotherapy **8**(4): 315-317.
Donohoe, D. R., L. B. Collins, et al. (2012). "The Warburg effect dictates the mechanism of butyrate-mediated histone acetylation and cell proliferation." Mol Cell **48**(4): 612-626.
Ekstrand, M. I., M. Falkenberg, et al. (2004). "Mitochondrial transcription factor A regulates mtDNA copy number in mammals." Hum Mol Genet **13**(9): 935-944.
Eslaminejad, M. B., N. Fani, et al. (2013). "Epigenetic regulation of osteogenic and chondrogenic differentiation of mesenchymal stem cells in culture." Cell J **15**(1): 1-10.
Feng, J., A. Mantesso, et al. (2010). "Perivascular cells as mesenchymal stem cells." Expert Opin Biol Ther **10**(10): 1441-1451.
Figueroa, M. E., O. Abdel-Wahab, et al. (2010). "Leukemic IDH1 and IDH2 mutations result in a hypermethylation phenotype, disrupt TET2 function, and impair hematopoietic differentiation." Cancer Cell **18**(6): 553-567.
Fu, Y., P. Zhang, et al. (2014). "Histone deacetylase 8 suppresses osteogenic differentiation of bone marrow stromal cells by inhibiting histone H3K9 acetylation and RUNX2 activity." Int J Biochem Cell Biol **54**: 68-77.
Fulco, M., Y. Cen, et al. (2008). "Glucose restriction inhibits skeletal myoblast differentiation by activating SIRT1 through AMPK-mediated regulation of Nampt." Dev Cell **14**(5): 661-673.
Galdieri, L., T. Zhang, et al. (2014). "Protein acetylation and acetyl coenzyme a metabolism in budding yeast." Eukaryot Cell **13**(12): 1472-1483.
Gimble, J. M., A. J. Katz, et al. (2007). "Adipose-derived stem cells for regenerative medicine." Circ Res **100**(9): 1249-1260.
Guarani, V., G. Deflorian, et al. (2011). "Acetylation-dependent regulation of endothelial Notch signalling by the SIRT1 deacetylase." Nature **473**(7346): 234-238.

Gustafsson, M. V., X. Zheng, et al. (2005). "Hypoxia requires notch signaling to maintain the undifferentiated cell state." Dev Cell **9**(5): 617-628.
Hanover, J. A., M. W. Krause, et al. (2012). "Bittersweet memories: linking metabolism to epigenetics through O-GlcNAcylation." Nat Rev Mol Cell Biol **13**(5): 312-321.
Higuchi, M., G. J. Dusting, et al. (2013). "Differentiation of human adipose-derived stem cells into fat involves reactive oxygen species and Forkhead box O1 mediated upregulation of antioxidant enzymes." Stem Cells Dev **22**(6): 878-888.
Hisahara, S., S. Chiba, et al. (2008). "Histone deacetylase SIRT1 modulates neuronal differentiation by its nuclear translocation." Proc Natl Acad Sci U S A **105**(40): 15599-15604.
Hsu, S. H., C. T. Chen, et al. (2013). "Inhibitory effects of hypoxia on metabolic switch and osteogenic differentiation of human mesenchymal stem cells." Stem Cells **31**(12): 2779-2788.
Imai, S. and L. Guarente (2010). "Ten years of NAD-dependent SIR2 family deacetylases: implications for metabolic diseases." Trends Pharmacol Sci **31**(5): 212-220.
Ito, S., A. C. D'Alessio, et al. (2010). "Role of Tet proteins in 5mC to 5hmC conversion, ES-cell self-renewal and inner cell mass specification." Nature **466**(7310): 1129-1133.
Jang, H., T. W. Kim, et al. (2012). "O-GlcNAc regulates pluripotency and reprogramming by directly acting on core components of the pluripotency network." Cell Stem Cell **11**(1): 62-74.
Kaelin, W. G., Jr. and S. L. McKnight (2013). "Influence of metabolism on epigenetics and disease." Cell **153**(1): 56-69.
Kassem, M. and B. M. Abdallah (2008). "Human bone-marrow-derived mesenchymal stem cells: biological characteristics and potential role in therapy of degenerative diseases." Cell Tissue Res **331**(1): 157-163.
Lenoir, N. (2000). "Europe confronts the embryonic stem cell research challenge." Science **287**(5457): 1425-1427.
Marino, G., F. Pietrocola, et al. (2014). "Regulation of autophagy by cytosolic acetyl-coenzyme A." Mol Cell **53**(5): 710-725.
Mihaylova, M. M. and R. J. Shaw (2011). "The AMPK signalling pathway coordinates cell growth, autophagy and metabolism." Nat Cell Biol **13**(9): 1016-1023.
Miura, M., S. Gronthos, et al. (2003). "SHED: stem cells from human exfoliated deciduous teeth." Proc Natl Acad Sci U S A **100**(10): 5807-5812.
Mizuno, H., M. Tobita, et al. (2012). "Concise review: Adipose-derived stem cells as a novel tool for future regenerative medicine." Stem Cells **30**(5): 804-810.
Moran-Crusio, K., L. Reavie, et al. (2011). "Tet2 loss leads to increased hematopoietic stem cell self-renewal and myeloid transformation." Cancer Cell **20**(1): 11-24.
Moussaieff, A., M. Rouleau, et al. (2015). "Glycolysis-mediated changes in acetyl-CoA and histone acetylation control the early differentiation of embryonic stem cells." Cell Metab **21**(3): 392-402.
Mukherjee, T., W. S. Kim, et al. (2011). "Interaction between Notch and Hif-alpha in development and survival of Drosophila blood cells." Science **332**(6034): 1210-1213.
Murphy, M. P. (2009). "How mitochondria produce reactive oxygen species." Biochem J **417**(1): 1-13.
Pietila, M., S. Palomaki, et al. (2012). "Mitochondrial function and energy metabolism in umbilical cord blood- and bone marrow-derived mesenchymal stem cells." Stem Cells Dev **21**(4): 575-588.
Pietrocola, F., L. Galluzzi, et al. (2015). "Acetyl coenzyme A: a central metabolite and second messenger." Cell Metab **21**(6): 805-821.
Pittenger, M. F., A. M. Mackay, et al. (1999). "Multilineage potential of adult human mesenchymal stem cells." Science **284**(5411): 143-147.
Prozorovski, T., U. Schulze-Topphoff, et al. (2008). "Sirt1 contributes critically to the redox-dependent fate of neural progenitors." Nat Cell Biol **10**(4): 385-394.
Quivoron, C., L. Couronne, et al. (2011). "TET2 inactivation results in pleiotropic hematopoietic abnormalities in mouse and is a recurrent event during human lymphomagenesis." Cancer Cell **20**(1): 25-38.
Ren, J., L. Pulakat, et al. (2010). "Mitochondrial biogenesis in the metabolic syndrome and cardiovascular disease." J Mol Med (Berl) **88**(10): 993-1001.
Rohle, D., J. Popovici-Muller, et al. (2013). "An inhibitor of mutant IDH1 delays growth and promotes differentiation of glioma cells." Science **340**(6132): 626-630.
Sanchez-Arago, M., J. Garcia-Bermudez, et al. (2013). "Degradation of IF1 controls energy metabolism during osteogenic differentiation of stem cells." EMBO Rep **14**(7): 638-644.
Sasaki, M., C. B. Knobbe, et al. (2012). "IDH1(R132H) mutation increases murine haematopoietic progenitors and alters epigenetics." Nature **488**(7413): 656-659.
Semenza, G. L. (1998). "Hypoxia-inducible factor 1: master regulator of O2 homeostasis." Curr Opin Genet Dev **8**(5): 588-594.
Semenza, G. L. (2012). "Hypoxia-inducible factors in physiology and medicine." Cell **148**(3): 399-408.

Senior, A. E., S. Nadanaciva, et al. (2002). "The molecular mechanism of ATP synthesis by F1F0-ATP synthase." Biochim Biophys Acta **1553**(3): 188-211.
Seo, B. M., M. Miura, et al. (2004). "Investigation of multipotent postnatal stem cells from human periodontal ligament." Lancet **364**(9429): 149-155.
Shi, M., M. Ishikawa, et al. (2009). "Acceleration of skeletal muscle regeneration in a rat skeletal muscle injury model by local injection of human peripheral blood-derived CD133-positive cells." Stem Cells **27**(4): 949-960.
Shyh-Chang, N. and G. Q. Daley (2015). "Metabolic switches linked to pluripotency and embryonic stem cell differentiation." Cell Metab **21**(3): 349-350.
Shyh-Chang, N., G. Q. Daley, et al. (2013). "Stem cell metabolism in tissue development and aging." Development **140**(12): 2535-2547.
Shyh-Chang, N., J. W. Locasale, et al. (2013). "Influence of threonine metabolism on S-adenosylmethionine and histone methylation." Science **339**(6116): 222-226.
Song, L., N. J. Young, et al. (2005). "Origin and characterization of multipotential mesenchymal stem cells derived from adult human trabecular bone." Stem Cells Dev **14**(6): 712-721.
Sun, J., S. Aluvila, et al. (2010). "Mitochondrial and Plasma Membrane Citrate Transporters: Discovery of Selective Inhibitors and Application to Structure/Function Analysis." Mol Cell Pharmacol **2**(3): 101-110.
Takahashi, K. and S. Yamanaka (2006). "Induction of pluripotent stem cells from mouse embryonic and adult fibroblast cultures by defined factors." Cell **126**(4): 663-676.
Takubo, K., N. Goda, et al. (2010). "Regulation of the HIF-1alpha level is essential for hematopoietic stem cells." Cell Stem Cell **7**(3): 391-402.
Teven, C. M., X. Liu, et al. (2011). "Epigenetic regulation of mesenchymal stem cells: a focus on osteogenic and adipogenic differentiation." Stem Cells Int **2011**: 201371.
Tobita, M., H. Orbay, et al. (2011). "Adipose-derived stem cells: current findings and future perspectives." Discov Med **11**(57): 160-170.
Tormos, K. V., E. Anso, et al. (2011). "Mitochondrial complex III ROS regulate adipocyte differentiation." Cell Metab **14**(4): 537-544.
Turrens, J. F. (2003). "Mitochondrial formation of reactive oxygen species." J Physiol **552**(Pt 2): 335-344.
Valle-Prieto, A. and P. A. Conget (2010). "Human mesenchymal stem cells efficiently manage oxidative stress." Stem Cells Dev **19**(12): 1885-1893.
Wagegg, M., T. Gaber, et al. (2012). "Hypoxia promotes osteogenesis but suppresses adipogenesis of human mesenchymal stromal cells in a hypoxia-inducible factor-1 dependent manner." PLoS One **7**(9): e46483.
Wang, J., P. Alexander, et al. (2009). "Dependence of mouse embryonic stem cells on threonine catabolism." Science **325**(5939): 435-439.
Wang, T., K. Chen, et al. (2011). "The histone demethylases Jhdm1a/1b enhance somatic cell reprogramming in a vitamin-C-dependent manner." Cell Stem Cell **9**(6): 575-587.
Wellen, K. E., G. Hatzivassiliou, et al. (2009). "ATP-citrate lyase links cellular metabolism to histone acetylation." Science **324**(5930): 1076-1080.
Yang, D. C., M. H. Yang, et al. (2011). "Hypoxia inhibits osteogenesis in human mesenchymal stem cells through direct regulation of RUNX2 by TWIST." PLoS One **6**(9): e23965.
Yun, Z., H. L. Maecker, et al. (2002). "Inhibition of PPAR gamma 2 gene expression by the HIF-1-regulated gene DEC1/Stra13: a mechanism for regulation of adipogenesis by hypoxia." Dev Cell **2**(3): 331-341.
Zhang, Y., G. Marsboom, et al. (2013). "Mitochondrial respiration regulates adipogenic differentiation of human mesenchymal stem cells." PLoS One **8**(10): e77077.
Zheng, Y., L. He, et al. (2013). "H3K9me-enhanced DNA hypermethylation of the p16INK4a gene: an epigenetic signature for spontaneous transformation of rat mesenchymal stem cells." Stem Cells Dev **22**(2): 256-267.
Zoncu, R., A. Efeyan, et al. (2011). "mTOR: from growth signal integration to cancer, diabetes and ageing." Nat Rev Mol Cell Biol **12**(1): 21-35.
Zuk, P. A., M. Zhu, et al. (2001). "Multilineage cells from human adipose tissue: implications for cell-based therapies." Tissue Eng **7**(2): 211-228.

PROTOCOL

Comprehensive analysis of mitochondrial permeability transition pore activity in living cells using fluorescence-imaging-based techniques

Massimo Bonora[1,3], Claudia Morganti[1,3], Giampaolo Morciano[1,3], Carlotta Giorgi[1], Mariusz R Wieckowski[2] & Paolo Pinton[1]

[1]Department of Morphology, Surgery and Experimental Medicine, Section of Pathology, Oncology and Experimental Biology, Laboratory for Technologies of Advanced Therapies (LTTA), University of Ferrara, Ferrara, Italy. [2]Department of Biochemistry, Nencki Institute of Experimental Biology, Warsaw, Poland. [3]These authors contributed equally to this work. Correspondence should be addressed to P.P. (pnp@unife.it).

Published online 12 May 2016; doi:10.1038/nprot.2016.064

Mitochondrial permeability transition (mPT) refers to a sudden increase in the permeability of the inner mitochondrial membrane. Long-term studies of mPT revealed that this phenomenon has a critical role in multiple pathophysiological processes. mPT is mediated by the opening of a complex termed the mPT pore (mPTP), which is responsible for the osmotic influx of water into the mitochondrial matrix, resulting in swelling of mitochondria and dissipation of the mitochondrial membrane potential. Here we provide three independent optimized protocols for monitoring mPT in living cells: (i) measurement using a calcein–cobalt technique, (ii) measurement of the mPTP-dependent alteration of the mitochondrial membrane potential, and (iii) measurement of mitochondrial swelling. These procedures can easily be modified and adapted to different cell types. Cell culture and preparation of the samples are estimated to take ~1 d for methods (i) and (ii), and ~3 d for method (iii). The entire experiment, including analyses, takes ~2 h.

INTRODUCTION

mPT is believed to occur as a result of the opening of a nonspecific high-conductance channel in the inner mitochondrial membrane, which has become known as the mPTP. The mPTP may exist in low- and high-conductance modes[1]. Its low-conductance state is characterized by very limited permeability (cutoff, <300 Da), which permits the diffusion of small ions such as H^+, Ca^{2+}, and K^+ but does not trigger detectable mitochondrial swelling. Alternatively, its high-conductance state (1–1.3 nS) allows the free movement of molecules with a molecular mass up to 1.5 kDa across the inner mitochondrial membrane and results in mitochondrial matrix swelling[2].

Accumulating evidence supports the speculation that the mPTP is related to mitochondrial ATP synthase[3–7]. Our hypothesis, which was validated using the protocol described herein, indicates that a key element of the mPTP core is the c-subunit of mitochondrial ATP synthase[8,9]. This conclusion was further supported by the observations of other groups[10,11]. Interestingly, this model does not exclude the dependence and regulation of mPT by regulatory proteins previously associated with the mPTP.

Advantages and disadvantages of monitoring mPT in isolated mitochondria or intact cells

Numerous methods are available to monitor mPTP opening, which enables the study of various aspects of mPT in either isolated mitochondria or intact cells. The most popular mPT monitoring method using isolated mitochondria is based on measuring an increase in mitochondrial matrix volume with a mitochondrial swelling assay (usually detecting changes in the diffraction/absorption of light measured at 540 nm)[12,13]. mPTP opening can also be measured indirectly as, for example, the dissipation of mitochondrial membrane potential ($\Delta\psi m$)[8,14,15], elevated mitochondrial oxygen consumption (increased respiration)[16], and the capture of radioactive compounds (such as C^{14}-sucrose) in the mitochondrial matrix[17] in response to activators of mPTP opening. Another extensively used procedure is the so-called calcium-retention capacity method[18]. This technique is based on the ability of mitochondria to accumulate Ca^{2+} in the matrix ($[Ca^{2+}]_m$) before triggering mPT. To exclude mPTP-independent factors, a specific amount of Ca^{2+}, mitochondrial substrate, Pi, and adenine nucleotides has to be provided. This again implies the use of isolated mitochondria or (at least) permeabilized cells[19,20] measured by spectrofluorometry. In all cases, it is necessary to confirm that the observed changes in the aforementioned measurement parameters are directly caused by mPTP opening. For this reason, as a 'gold standard' to confirm mPT, cyclosporine A (CsA) is used to inhibit mPTP opening. CsA inhibition provides the most convincing evidence for mPT occurrence, as described in the literature. mPTP opening can also be monitored *in vivo* using radioactive deoxyglucose[21]. However, for estimation of the entrance of this compound into the mitochondrial matrix, isolation of mitochondria or at least plasma membrane permeabilization should be performed to eliminate the accumulation of radioactivity in the cytosol. This method has been used successfully to monitor mPTP opening during ischemia/reperfusion of the heart[22].

As described in detail in the present paper, assays of mPTP opening can be performed in living cells. These techniques avoid many of the artifacts (nonphysiological conditions) that accompany experiments using isolated mitochondria, and they offer the advantage of increased physiological relevance.

Overview of the protocol

mPT is a fascinating but quite obscure phenomenon that requires careful investigation in living cells. For this reason, we describe three different methods that can be used to monitor mPTP activity: the Co^{2+}–calcein assay, mitochondrial membrane depolarization, and the swelling technique.

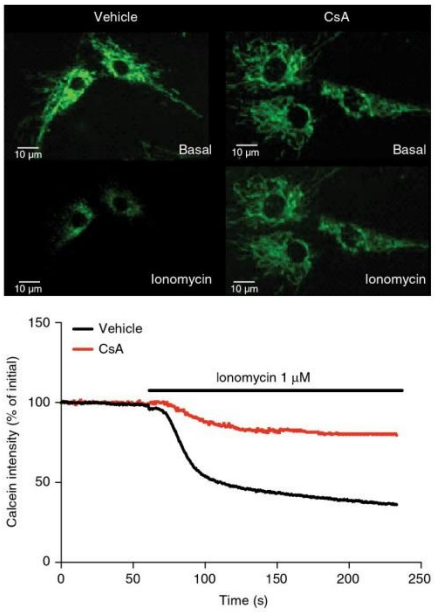

Figure 1 | Representative images and kinetics of HeLa cells stained using the Co^{2+}–calcein technique. Challenging cells with the ionophore ionomycin induced mPTP opening and quenching of the calcein signal. This event was inhibited by pretreatment with the mPTP-desensitizing agent CsA.

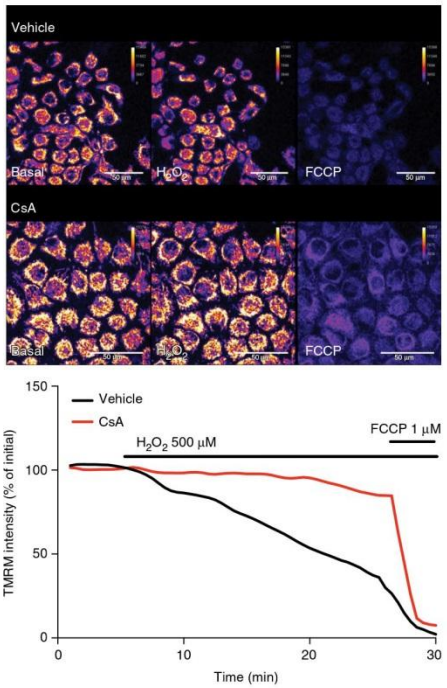

Figure 2 | Representative images and kinetics of HeLa cells stained with TMRM (Fire LUT was applied). Challenging the cells with the pro-oxidant H_2O_2 induced mPTP opening, mitochondrial depolarization, and reduced TMRM signal intensity. This was inhibited by pretreatment with the mPTP-desensitizing agent CsA. Scale bars, 50 µm.

The Co^{2+}–calcein assay is a direct and efficient method for measuring mPTP opening in living cells that has been in use since the 1990s. This method can be used in a wide range of cell types and under many pathological conditions related to the mitochondria[8,23–26]. Cells are loaded with calcein dye (excitation/emmission: 494/517 nm), which can passively diffuse into the cells and collect in cytosolic compartments including the mitochondria. Once the dye is inside cells, esterases cleave the acetoxymethyl esters, trapping the dye in intracellular compartments. At this point, the living cells become fluorescently labeled, with fluorescence spread throughout all subcellular compartments. The utility of the method originates from the ability of cobalt to quench calcein fluorescence in the cytosol but not in mitochondria. Thus, in the case of healthy cells, calcein is able to reveal the mitochondrial matrix network with good localization (**Fig. 1**). Opening of the mPTP leads to both the exit of calcein from the mitochondrial matrix and entry of Co^{2+} into the mitochondrial matrix, resulting in quenching of calcein stored in the mitochondria. This event manifests as a reduction of calcein fluorescence intensity and is easily measurable by fluorescence microscopy[27].

As mPTP opening leads to the loss of the proton gradient across membranes, the second assay measures this gradient using the Nernstian dye tetramethylrhodamine methyl ester (TMRM). TMRM is a cell-permeable, cationic, red-orange fluorescent dye. TMRM freely passes through cellular and mitochondrial membranes and, because of the large electrochemical H^+ gradient across the mitochondrial inner membrane, accumulates in the mitochondrial matrix according to $\Delta\psi m$. Opening of mPTP causes an efflux of TMRM from the mitochondria that manifests as a reduction of fluorescence intensity that is easily measurable by fluorescence microscopy (**Fig. 2**).

The final assay to verify mPTP activity is the measurement of mitochondrial network integrity. Osmotic shock induced by mPTP opening allows for the uptake of H_2O into the mitochondrial matrix and concomitant swelling of the inner mitochondrial membrane. This swelling causes mitochondria matrix expansion, which results in rupture of the outer mitochondrial membrane with loss of mitochondrial network integrity[28–30]. Overall *in vivo* mitochondrial swelling appears as a transformation of the mitochondrial network to a disorganized group of sphere-shaped structures. This can be quantified by counting the amount of objects composing the mitochondrial network when mitochondria are stained with specific fluorescent probes[8,31–33] (**Fig. 3**).

The procedure can be divided into four main and distinct sections. In the first section, seeded cells are stained to properly label mitochondria depending on the assay of interest (e.g., Co^{2+}–calcein quenching, mitochondrial depolarization, or swelling). In the second step, it is essential to set up the imaging protocol to perform basal acquisitions that are necessary before treatment with chemical compounds to modulate inhibition or induction of the mPTP. Third, challenging the mPTP opening is the aim of the protocol, so a Ca^{2+}- or reactive oxygen species (ROS)-dependent stimulus is added to the ongoing experiment. Finally, image processing and data analysis are performed to obtain a numeric index that describes mPTP activity and can be used for statistical data analysis.

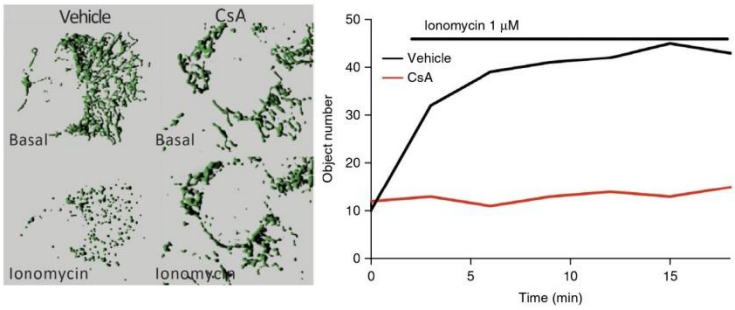

Figure 3 | Representative images and kinetics of HeLa cells expressing mitochondrially targeted GFP. Challenging the cells with the ionophore ionomycin induced mPTP opening, mitochondrial swelling, and mitochondrial network fragmentation, as represented by the increase in object count. This was inhibited by pretreatment with the mPTP-desensitizing agent CsA.

Potential applications of the protocol

The different methods described in this protocol can be used to measure mPTP opening in a wide range of intact cells. The use of the described fluorescent dyes, a controlled temperature, and the experimental setup allows for mitochondria to be present in their physiological environment. Under these conditions, the mPTP is regulated by the relevant mix of endogenous inhibitors and mPT activators in a manner that corresponds to *in vivo* conditions.

Two major advantages are obvious when considering the use of intact cells compared with isolated mitochondria or permeabilized cells. First, the system is much more physiological. Given that the mPTP interfaces with different signaling pathways, these protocols allow investigations of signaling pathways afferent to the mPTP, putative mPTP components or regulators, or novel stimulators or inhibitors of the mPT. This could be easily achieved by exposure to medium enriched with compounds of interest, or by the use of molecular biology tools such as siRNA, shRNA, cDNA overexpression of wild-type or mutant proteins, Cas9 knockout, and mutant knock-in, among many other approaches. Second, live-cell imaging requires far fewer cells than mitochondrial isolation procedures or spectrofluorimetric techniques, which extends the field of application to cells that are not easily cultured.

In our laboratory, this protocol has been successfully tested in HeLa cells, PC3 cells, HEK293T cells, SH-SY5Y cells, myoblasts, mouse embryonic fibroblasts, human adult fibroblasts, epithelial cells, HL-1 cells, rat neonatal cardiomyocytes, and CHO cells. Finally, these protocols are not time-consuming, the microscope setup is easy, and acquisition is fast. All methods apply different techniques to achieve the same purpose, so that a positive (or negative) result that is confirmed by all methods provides a high degree of statistical power and reproducibility.

Limitations of the protocol

The protocol is not feasible in cells cultured in suspension or for intact tissues. This is because of difficulties in focusing a stable sample in the former case and the thickness or degradation of the tissue slice in the latter. In addition, even if intact cells are best for testing these methods, the mPTP is not directly accessible to the full range of activators and mPT inhibitors mentioned above. Moreover, the presence of separate pools of adenine nucleotides and Ca^{2+}, and of other modulators in the cytoplasm and the mitochondrial matrix, should also be considered as a factor influencing mPT. Alternatively, studying mPTP function using isolated mitochondria simplifies the model and enables investigation of several plasma-membrane-impermeable compounds on mPT opening/closure, as well as direct control of the experimental environment by modulating, for example, the redox state and the concentrations of different ions.

Experimental design

Analysis of mPTP activity in living cells requires comparison of the results among the three imaging techniques described in this protocol. Each assay challenges mPTP in a specific manner to verify a particular aspect of its activity, and global interpretation and integration of the data are necessary in order for the results of the experiments to be fully understood. The protocol is divided into the following main sections: sample preparation, fluorescence measurements, and analysis.

Sample preparation. The first phase is relatively flexible, and it allows researchers to optimize the protocol to their own experimental situations with respect to the following specifications. Concerning cell

Box 1 | Alternative mitochondrial membrane potential probes

In addition to TMRM, several fluorescent lipophilic cationic dyes, such as tetramethylrhodamine ethyl (TMRE) ester, Rhodamine 123 (RH-123), 3,3′-dihexyloxacarbocyanine iodide (DiOC6(3)), and JC-1 (5,5′,6,6′-tetrachloro-1,1′,3,3′-tetraethylbenzimidazolylcarbocyanine iodide), are able to directly measure the mitochondrial membrane potential. As positively charged molecules, these dyes accumulate within mitochondria in inverse proportion to $\Delta\psi m$ according to the Nernst equation.

Different probes can be used for mPTP-induced mitochondrial depolarization; here, a brief description of each probe is provided, along with the modifications that researchers should make to the protocol.

TMRE is a cell-permeant, cationic, red-orange fluorescent dye that is readily sequestered by active mitochondria as TMRM. TMRM and TMRE are both quickly equilibrating dyes, but TMRM inhibits the electron-transport chain less, and it is recommended for this reason. TMRE application does not require modification of the protocol[63].

RH-123 is lipophilic in nature, which allows it to diffuse through the mitochondrial membrane in response to potential and concentration gradients. Mitochondrial energization induces the quenching of RH-123 fluorescence, and the rate of fluorescence decay is proportional to the mitochondrial membrane potential. The application of RH-123 is suggested for short-time-scale (min) studies to monitor rapid step changes in $\Delta\psi m$ (ref. 63).

(continued)

Box 1 | Alternative mitochondrial membrane potential probes (continued)

DiOC6(3) is a cell-permeant, green-fluorescent, lipophilic dye that, when used at low concentrations, is selective for the mitochondria of live cells. At higher concentrations, the dye may be used to stain other internal membranes, such as the endoplasmic reticulum. However, the use of DiOC6(3) is not recommended because of its higher toxicity toward mitochondrial respiration[64].

JC-1 is used as an indicator of mitochondrial potential in a variety of cell types. JC-1 exists as either a green-fluorescent monomer at depolarizing membrane potentials or a red-fluorescent aggregate at hyperpolarizing membrane potentials. The ratio of red to green fluorescence depends only on the membrane potential and not on other factors such as mitochondrial size, shape, and density, which may influence single-component fluorescence signals.

All these mitochondrial probes are differentially permeable according to their distinct molecular structure, and JC-1 is the least permeable. More specifically, whereas the monomer form of JC-1 has been reported to equilibrate on a time scale similar to that of TMRM/TMRE (~15 min), the aggregate form of the dye takes ~90 min to equilibrate[65]. For this reason, the use of TMRM is suggested for this particular protocol.

Additional reagents

- TMRE (Thermo Fisher Scientific, cat. no. T-669)
- RH-123 (Thermo Fisher Scientific, cat. no. R-302)
- DiOC6(3) (Thermo Fisher Scientific, cat. no. D-273)
- JC-1 dye (mitochondrial membrane potential probe; Thermo Fisher Scientific, cat. no. T-3168)

Additional procedures

For the use of RH-123 in place of TMRM, the following step should be performed instead of that in the original PROCEDURE:

- Step 2B(ii)—Cell staining: add RH-123 working solution (10 µM diluted in modified KRB) and incubate the cells for 20 min at 37 °C in a 5% CO_2 atmosphere.
- Anticipated results: using RH-123 to probe mPTP opening results in increased fluorescence, so pay particular attention to the interpretation of the data; the slope values are positive and increase in proportion to mPTP opening.

For the use of DiOC6 in place of TMRM, the following step should be performed instead of that in the original PROCEDURE:

- Step 2B(ii)—Cell staining: add DiOC6(3) working solution (<1 nM diluted in modified KRB) and incubate the cells for 20 min at 37 °C in a 5% CO_2 atmosphere.
- Step 3B—Imaging setup:

Menu	Settings
Excitation filter	Select the dedicated FITC filter set to detect DiOC6(3).
Experiment manager	Set the FITC wavelength to detect DiOC6(3) fluorescence.

Set the acquisition frequency as indicated for TMRM in **Table 3**.

For the use of JC-1 in place of TMRM, the following step should be performed instead of that in the original PROCEDURE:

- Step 2B(ii)—Cell staining: add JC-1 working solution (5 µM diluted in modified KRB) and incubate the cells for 30 min at 37 °C in a 5% CO_2 atmosphere. Remove the cells from the incubator and rinse them twice with 1 ml of modified KRB to remove the unbound dye; then, add 900 µl of modified KRB.
- Step 3B(iii)—Imaging setup and basal acquisition:

Menu	Settings
Excitation filter	Select the dedicated FITC filter set and the TRITC filter set to detect JC-1 fluorescence.
Experiment manager	Set the FITC and the TRITC wavelengths to detect both red and green dyes. Acquire two images (one red and one green) at the frequency indicated for TMRM in **Table 3**.

- Step 4B(ii)—Challenging mPTP opening: after H_2O_2 addition, acquire images for at least 40 min.
- Step 5B(i)—Image processing: open the two time-lapse images obtained (one for red and one for green fluorescence) in the Fiji software. Create a time-lapse ratio image using the process 'image calculator' and by dividing the intensity values for the red images by those for the green images. Then, using this time-lapse ratio image, proceed with the remaining image processing steps in the protocol.
- Step 5B(ii)—Image processing: on the FITC channel, draw an ROI; using freehand selections, encircle each mitochondrion, excluding the nucleus, and draw an ROI of a background region in an empty corner of the field.
- Step 5B(iii)—Image processing: for FITC and TRITC channels, estimate a global threshold to restrict the analysis to the pixels displaying intensity values greater than the threshold value.
  ▲ **CRITICAL STEP** Estimate the threshold on the final image of the time-lapse.
- Step 5B(iv)—Image processing: for FITC and TRITC channels, use the multimeasure tool to calculate the mean gray values limited by the threshold for the selected ROI (including the background ROI) in each time-lapse image.
- Step 5B(vii)—Image processing: normalize the values. Generate a new column representing the 'Ratio' value; for each timepoint, divide the TRITC intensity by the FITC intensity. Then divide each timepoint value by the initial value, considering the first value as 100%.
- Step 5B(viii)—Image processing: using the normalized 'Ratio' column, calculate the slope from minute 15 to minute 25, for instance, using the function 'SLOPE' in Microsoft Office Excel.

TABLE 1 | Genetically encoded fluorescent probes to visualize mitochondria.

Name	Fluorescent rotein	Excitation (nm)	Emission (nm)	Refs.	Distributor, code
Turquoise2-Mito	Turquoise2	425	475	53	Addgene plasmid, 36208
MtGFP	GFP10	488	515	47	NA
EYFP-Mito	EYFP	513	527	54	Clonetech, 6115-1
mtDsRed1	DsRed1	558	583	55	NA
mKate2-mito	mKate2	588	633	55	Evrogene, cat. no. FP187

NA, not applicable

seeding, it is necessary that cells reach 50–70% confluence as a monolayer on the day of the experiment. Indeed, excessive cell density can interfere with stimulus delivery and weaken mPTP activity, leading to misunderstanding of the phenomena. Moreover, the choice of a suitable imaging coverslip for individual imaging setups and cell lines is important; for instance, glass coverslips with a suitable coating should be chosen on the basis of the cell adhesion.

Cell staining and mitochondrial-labeling optimization should be specific for each of the three methods. We have found that problems may occur when calcein–cobalt formation is incomplete, leaving a large amount of cytoplasmic calcein visible (see TROUBLESHOOTING). This should be verified by microscopic examination of the coverslip before the acquisition procedure is started. A mitochondrial counterstain may be particularly helpful, and in this procedure we suggest the use of Mitotracker Red. The mitochondrial accumulation of Mitotracker is dependent on $\Delta\psi m$, and it can be partially quenched by calcein; indeed, this counterstaining is not intended for quantitative measurement and should not be included in the time-lapse acquisition.

For potentiometric measurements, TMRM is suggested, as it is probably one of the most common potentiometric dyes used. Nevertheless, alternative staining procedures that can lead to the same conclusion are described in **Box 1**.

Finally, the use of fluorescent reporters targeted to the mitochondrial matrix is strongly recommended for morphometric measurements because of their selective localization and resistance to photobleaching. The present procedures describe the use of mitochondrial GFP (mtGFP), but examples of alternatives that provide the same information are indicated in **Table 1**.

Fluorescence measurement. Imaging setup is the most critical step of the procedure; this protocol describes the most common problems that may occur at this step. Particular attention should be paid to the exposure time and light intensity to avoid artifacts due to, for instance, photobleaching of the fluorescent probe. A correct setup allows the user to obtain optimal basal measurements that are fundamental to later challenges to mPTP opening. A variety of different mPT-inducing stimuli can be used; here we describe the use of two stimuli, $[Ca^{2+}]_m$ (by means of the ionophore ionomycin) and ROS (by means of H_2O_2), that exert their effects in the range of seconds to tens of minutes, respectively. Nevertheless, alternative stimuli can be chosen depending on the experimental goals of the researcher; a list of potential alternatives is reported in **Table 2**. The time of sample acquisition varies depending on the stability of the reagents used, especially the probes. TMRM and mitochondrial fluorescent proteins are quite stable and can be monitored for up to 48–72 h. Conversely, calcein is somewhat rapidly extruded by the cell. In our hands, calcein signals display stable intensity for up to 46–60 min; indeed, for longer recording times, the user should set up the best conditions for the experimental situation. We also hasten to add that ionophores that can alter the plasma membrane potential[34] can lead to mPT-independent TMRM re-distribution. Even if the combined use of a dye for plasma membrane potential allows for the correction of this artifact, the induced mitochondrial Ca^{2+} uptake generates an mPTP-independent mitochondrial depolarization[35] that can produce experimental artifacts. Thus, even though several studies have successfully combined potentiometric dyes with ionophores to challenge mPTP opening, we recommend following this procedure, carefully evaluating the results, and considering different challenge methods (**Table 2**).

Induction and inhibition of the mPTP. Modulators of the mammalian mPTP can be divided into two classes: activators and inhibitors of mPT. mPT can be stimulated by several conditions and chemical compounds, such as accumulation of mitochondrial Ca^{2+} (ref. 36), ROS (superoxide) and pro-oxidative agents[37,38], oxidized thiols[39], P_i[40,41], long-chain free fatty acids[42], atractyloside[43],

TABLE 2 | Inducers of mPTP opening.

Stimulus	Ca^{2+} signaling	ROS signaling	Co^{2+}–calcein (refs.)	Ψm (refs.)	Mitochondrial swelling (refs.)
Ionomycin	X		8		8
A23187	X		27		56
H_2O_2		X	57	8	8
Thapsigargin	X	X	26	58	26
Menadione	X		59	59	60
Ceramide	X	X		61	62

mastoparan[44], and 1-(2-chlorophenyl)-*N*-methyl-*N*-(1-methylpropyl)-3-isoquinoline-carboxamide (PK11195)[45]. In turn, mPT can be inhibited by high $\Delta\psi m$; CsA; sanglifehrin A; bongkrekic acid; antamanide; 5-isothiocyanato-2-[2-(4-isothiocyanato-2-sulfophenyl)ethenyl]benzene-1-sulfonic acid; adenine nucleotides (ATP and ADP); creatine; cyclocreatine; glucose; König's polyanion; NADH; NADPH; UTP; ubiquinone; decylubiquinone; antioxidants; calcium chelators; and divalent cations such as Ba^{2+}, Mg^{2+}, Mn^{2+}, and Sr^{2+}. However, the conditions and compounds listed above can have no, or even opposing, effects on eukaryotic cells of different taxa (for further details, see ref. 46).

Data analysis. In this section, guidelines for image and data processing are comprehensively described to allow researchers who are not familiar with microscopy to perform the experiment. Specialists can optimize the analyses according to their own needs, but we recommend meticulously following the critical steps of the procedure.

Experimental controls. As described before, CsA is a well-known inhibitor of mPT, and its activity is reported to prevent mPTP opening. Hence, we suggest including CsA treatment as a negative control in each experiment.

MATERIALS

REAGENTS

- Sodium chloride (NaCl; Sigma-Aldrich, cat. no. S7653)
- Potassium chloride (KCl; Fluka, cat. no. 60128)
- Potassium phosphate monobasic (KH_2PO_4; Sigma-Aldrich, cat. no. P0662)
- Magnesium sulfate heptahydrate ($MgSO_4{\cdot}7H_2O$; Sigma-Aldrich, cat. no. M5921)
- $CaCl_2$, 1 M (Fluka, cat. no. 10043-52-4)
- Glucose (Sigma-Aldrich, cat. no. G7528)
- HEPES (Sigma-Aldrich, cat. no. H3375)
- Ionomycin calcium salt (Sigma-Aldrich, cat. no. I0634) **! CAUTION** Ionomycin can cause skin and eye irritation.
- MitoTracker Red CMXRos (Thermo Fisher Scientific, cat. no. M-7510)
- Cobalt(II) chloride hexahydrate ($CoCl_2$; Sigma-Aldrich, cat. no. 20 2185) **! CAUTION** $CoCl_2$ is dangerous for health and is potentially carcinogenic.
- Calcein, acetoxymethyl ester (Thermo Fisher Scientific, cat. no. C310)
- Sulfinpyrazone (Sigma-Aldrich, cat. no. S9509)
- DMSO (Sigma-Aldrich, cat. no. 154938)
- Sodium hydroxide (NaOH; Fluka, cat. no. 71691)
- Tetramethylrhodamine methyl ester (TMRM; Invitrogen, cat. no. T668)
- Hydrogen peroxide, 10 M (H_2O_2; Sigma-Aldrich, cat. no. H-1009)
- Carbonyl cyanide 4-(trifluoromethoxy)phenylhydrazone (FCCP; Sigma-Aldrich, cat. no. C2920)
- Milli-Q water (Millipore)
- Ethanol (Sigma-Aldrich, cat. no. 02860)
- Adherent cultured cell lines. The anticipated results described in this protocol have been obtained using HeLa cells (ATCC CCL-2). However, the procedure has been successfully tested in HeLa cells, PC3 cells, HEK293T cells, SH-SY5Y cells, myoblasts, mouse embryonic fibroblasts, human adult fibroblasts, epithelial cells, HL-1 cells, rat neonatal cardiomyocytes, and CHO cells **! CAUTION** Cell lines should be regularly checked to ensure that they are authentic and not infected with *Mycoplasma*.
- Mammalian expression plasmid containing the mitochondrially targeted fluorescent reporter. This protocol is performed using the plasmid encoding mtGFP, which was described by Rizzuto *et al.*[47]. However, equivalent results can be obtained using other mitochondrially targeted fluorescent proteins, as listed in **Table 1**.

EQUIPMENT

- Parafilm (Sigma-Aldrich, cat. no. P7793)
- 0.5-ml Microcentrifuge tubes
- Aluminum foil
- 35 mm #1.5 glass-bottom Petri dish (CellVis, cat. no. D35-14-1.5-N)
- Inverted wide-field fluorescence microscope
- Image analysis software. The procedure describes the use of FIJI (http://fiji.sc/Fiji)[48]; however, similar results can be obtained using equivalent competitors (i.e., PerkinElmer Volocity, Bitplane Imaris, 3i Slidebook, and Bioimageanalysis Icy)

REAGENT SETUP

Kreb's Ringer buffer Kreb's ringer buffer (KRB) is 135 mM NaCl, 5 mM KCl, 0.4 mM KH_2PO_4, 1 mM $MgSO_4{\cdot}7H_2O$, 20 mM HEPES, and 5.5 mM glucose, pH 7.4. Dissolve 7.89 g of NaCl, 0.373 g of KCl, 0.054 g of KH_2PO_4, 0.247 g of $MgSO_4{\cdot}7H_2O$, 4.76 g of HEPES, and 1 g of glucose in <1,000 ml of Milli-Q water. Adjust the pH to 7.4 with NaOH, and then bring the final volume to 1,000 ml. Store it at 4 °C for up to 3 d.

Modified KRB Add 0.5 ml of 1 M $CaCl_2$ to 500 ml of KRB. Store it at 4 °C for up to 3 d. ▲ **CRITICAL** This solution should be prepared in a polypropylene cylinder, as glass containers can bind Ca^{2+}, and this can produce imprecise experimental conditions.

Calcein, 1 mM stock solution Prepare 1 mM calcein stock solution by dissolving 50 µg of calcein in 50 µl of DMSO. Divide the stock solution into aliquots. This solution can be stored at 20 °C for 3 months. ▲ **CRITICAL** Avoid multiple freeze–thaw cycles, and protect the solution from light.

200 µM MitoTracker Red CMXRos stock solution Prepare 200 µM MitoTracker Red stock solution by dissolving 50 µg of MitoTracker Red CMXRos in 470 µl of DMSO. Divide the stock solution into aliquots. This solution can be stored at −20 °C for 3 months. ▲ **CRITICAL** Avoid multiple freeze–thaw cycles, and protect the solution from light.

1 M $CoCl_2$ stock solution Prepare 1 M $CoCl_2$ stock solution by dissolving 0.238 g of $CoCl_2$ in 1 ml of Milli-Q water. This solution can be stored at 4 °C for 3 months.

10 mM Sulfinpyrazone stock solution Prepare 10 mM sulfinpyrazone stock solution by dissolving 0.04 g of sulfinpyrazone in 10 ml of Milli-Q water. Divide the stock solution into aliquots. This solution can be stored at 4 °C for 6 months. ▲ **CRITICAL** Add NaOH to alkalinize the solution until the drug dissolves.

1 mM Ionomycin stock solution Dissolve 1 mg of ionomycin in 1.34 ml of DMSO. Divide the stock solution into aliquots. Store the aliquots at 20 °C for 6 months. ▲ **CRITICAL** Avoid multiple freeze–thaw cycles of the stock solution.

10 µM Ionomycin solution Dissolve 3 µl of 1 mM ionomycin stock solution in 300 µl of modified KRB. The solution can be stored on ice until use. At the end of the experiment, this solution should be discarded.

Calcein loading solution Prepare 1 ml of calcein loading solution by adding 1 µl of 1 mM calcein stock solution (final concentration: 1 µM), 1 µl of 200 µM MitoTracker Red CMXRos stock solution (final concentration: 200 nM), 2 µl of 1 M $CoCl_2$ stock solution (final concentration: 2 mM), and 20 µl of 10 mM sulfinpyrazone stock solution (final concentration: 200 µM) to 1 ml of KRB. ▲ **CRITICAL** Protect the solution from light and use it within 1 h of preparation. ▲ **CRITICAL** Sulfinpyrazone is recommended to inhibit organic anion transport, which can induce leakage of de-esterified acetoxymethyl (AM) indicators[49].

100 µM TMRM stock solution Dissolve 0.5 mg of TMRM powder in 10 ml of ethanol. We recommend splitting the solution into aliquots, wrapping the tubes with aluminum foil, and freezing the aliquots until use. The aliquots can be stored for 6 months at −20 °C.

10 mM FCCP stock solution Dissolve 0.025 g of FCCP powder in 10 ml of ethanol. We recommend splitting the solution into aliquots, wrapping the tubes with aluminum foil, and freezing the aliquots until use. The aliquots can be stored for 6 months at −20 °C.

10 µM TMRM loading solution Prepare the loading solution by adding 1 µl of 100 µM TMRM stock solution to 10 ml of modified KRB. The solution can be stored on ice until use. At the end of the experiment, this solution should be discarded. ▲ **CRITICAL** TMRM is sensitive to light, so avoid light exposure by handling this solution in a low-light environment and by wrapping the tubes in aluminum foil.

5 mM H_2O_2 solution Prepare H_2O_2 solution by adding 0.5 µl of 10 M H_2O_2 to 1 ml of TMRM loading solution. Because H_2O_2 is not stable, we recommend splitting the solution into aliquots of 100 µl each, wrapping the tubes with aluminum foil, and freezing the aliquots at −20 °C until use. At the end of the experiment, these aliquots should be discarded.

10 μM FCCP solution Prepare FCCP solution by adding 1 μl of 10 mM FCCP to 1 ml of TMRM loading solution. We recommend splitting the solution into aliquots of 100 μl, wrapping the tubes with aluminum foil, and freezing the aliquots at −20 °C until use. At the end of the experiment, these aliquots should be discarded.

EQUIPMENT SETUP

Microscope setup A motorized inverted fluorescence microscope equipped with high-numerical-aperture lenses, a fluorescein isothiocyanate (FITC)/tetramethylrhodamine isothiocyanate (TRIC) filter set, and environmental control is required to complete this procedure. In this protocol, the instrument described is provided by Olympus. However, similar performance can be achieved using imaging setups distributed by all the major brands in the field (e.g., Zeiss, Nikon, Leica, Crisel Instruments, and Intelligent Imaging Innovations (3i)) or using custom-built equipment. Essential components are as follows:

- Motorized Olympus IX81-ZDC inverted microscope. At a minimum, the microscope has to be motorized to allow 3D image acquisition. Equivalent equipment is available from competitors (e.g., Zeiss Axio Observer, Nikon Eclipse Ti-E, Leica DMi8).
- 40×/1.30-N.A. UPlanFLN oil-immersion objective or equivalent (e.g., Zeiss Plan-Apochromat 40×/1.3 Oil, Nikon CFI Plan Fluor 40× Oil, and Leica HC PL APO 40×/1.30 Oil CS2).
- 60×/1.35-N.A. UPlanFLN oil-immersion objective or equivalent (e.g., Zeiss Plan-Apochromat 63×/1.4 Oil, Nikon CFI Plan Apo Lambda 60× Oil, Leica HC PL APO 63×/1.40 Oil CS2).
- Cell MT20E xenon lamp. The use of an illuminating device equipped with a fast shutter is recommended to reduce photobleaching. Xenon- or light-emitting-diode-based light sources are suggested but are not mandatory (examples of equivalent competitors are Sutter Instruments Lambda DG-4 and EXCELITAS Technologies X-Cite).
- HAMAMATSU ORCA RG. The CCD camera should have a 6.45-μm pixel size to ensure the highest resolution, and it should be cooled to −30 °C for noise reduction (examples of equivalent competitors are Photometrics CoolSNAP HQ2 CCD and Andor Clara Interline CCD).
- Okolab environmental control. Optimal performance is obtained by fixing the temperature at 37 °C, setting the CO_2 level to 5%, and using a humidified environment. At a minimum, temperature control is mandatory (examples of equivalent competitors are provided by Bioscience Tools, Harvard Apparatus, and Warner Instruments).
- Xcellence rt software equipped with a 3D deconvolution module. The image acquisition software should be able to control the hardware and perform 3D reconstruction of point spread function (PSF)-degraded images. Examples of equivalent competitors are Universal Imaging Metamorph, Nikon NIS elements, Zeiss ZEN, and LEICA LAS X. High-performance 3D digital deconvolution can be performed by additional software such as PerkinElmer Volocity, Bitplane Imaris, 3i Slidebook, and Media Cybernetics Autoquant.

PROCEDURE

Cell preparation ● TIMING 1 h

1| Seed cells onto a circular imaging dish, and allow the cells to grow until they reach 50% confluence. The researcher must optimize the seeding density for the given cell line. After seeding cells, wait for at least 24 h.

Cell staining and mitochondrial labeling

2| The following section describes how to perform sample staining. Please proceed to option A for Co^{2+}–calcein, to option B for the TMRM method, and to option C for the mitochondrial morphology assay.

(A) *In vivo* measurement of mPTP-induced Co^{2+}–calcein quenching ● TIMING 20 min

(i) Remove the cells from the incubator, and wash them once with 1 ml of modified KRB to remove residual cellular debris and medium.
? TROUBLESHOOTING

(ii) Add 1 ml of calcein loading solution, and incubate the cells for 15 min at 37 °C in a 5% CO_2 atmosphere.
▲ CRITICAL STEP Calcein is sensitive to light. Avoid exposure to light by handling the staining solution in low-light conditions and by protecting the sample with aluminum foil during the incubation step.
? TROUBLESHOOTING

(iii) Remove the cells from the incubator and wash them twice with 1 ml of modified KRB to remove the unbound dye; then, add 900 μl of modified KRB.
▲ CRITICAL STEP Washing must be performed carefully. Avoid the use of automatic aspiration tools.

(B) *In vivo* measurement of mPTP-induced mitochondrial depolarization ● TIMING 40 min

(i) Remove cells from the incubator, and wash them once with 1 ml of modified KRB to remove residual cellular debris and medium.
? TROUBLESHOOTING

(ii) Add 900 μl of TMRM loading solution, and incubate the cells for 30 min at 37 °C in a 5% CO_2 atmosphere.
▲ CRITICAL STEP TMRM is sensitive to light. Avoid exposure to light by handling the solution in low-light conditions and by protecting the sample with aluminum foil during the incubation step.
? TROUBLESHOOTING

(C) Measurement of *in vivo* mPTP-induced mitochondrial swelling ● TIMING 90 min

(i) Once the cells have reached 40–60% confluence, transfect them with 1–2 μg of mitochondrially targeted GFP per coverslip (for equivalent reporters, see **Table 1**). The amount used for transfection depends on the chosen transfection method (usually 1 $\mu g/cm^2$ for liposome- or polyethylenimine-based transfection and 2 $\mu g/cm^2$ for Ca^{2+} phosphate–based transfection). After transfection, wait for 36–48 h.
▲ CRITICAL STEP Each researcher should choose the appropriate transfection reagent and optimize the transfection protocol for the particular cell line being used. Alternatively, a stable cell line can be created using standard protocols.

Imaging setup and basal acquisition

3| The following section describes how to set up for image acquisition. Please proceed to option A for Co^{2+}–calcein, to option B for the TMRM method, and to option C for the mitochondrial morphology assay.

(A) *In vivo* measurement of mPTP-induced Co^{2+}–calcein quenching ● TIMING 1–5 min

(i) Place the imaging coverslip inside the temperature-controlled (37 °C) microscope stage.

▲ **CRITICAL STEP** Living cells are sensitive to high and low temperatures. Be sure to maintain the temperature constant at 37 °C.

(ii) Start the Xcellence Olympus software, and select the following specifications, which provide optimal image acquisition under standard conditions:

Menu	Settings
Illumination settings	Switch on the illumination system and wait for ~10 min before starting
Excitation filter	Select the dedicated FITC or TRITC filter set to detect calcein or MitoTracker fluorescence, respectively
Camera control	Set the binning at 2 × 2
Microscope control	Select the 40× oil-immersion objective from the list
Experiment manager	Set the wavelength, the exposure time, and the lamp power according to **Table 3**

▲ **CRITICAL STEP** Avoid extended and intense excitation of the sample.

(iii) Focus on the sample and acquire a snapshot of a field containing cells that display a well-localized FITC signal in the mitochondrial compartment.

▲ **CRITICAL STEP** Calcein localization must overlap with the MitoTracker signal. Be sure to validate this result before the experiment.

? TROUBLESHOOTING

(iv) Strictly draw the regions of interest (ROIs) near the mitochondria of the selected cells for analysis of kinetic trends.

▲ **CRITICAL STEP** One ROI should always be dedicated to the background.

(v) Start image acquisition at the frequency indicated in **Table 3**, and perform basal recording for 1 min.

? TROUBLESHOOTING

(B) *In vivo* measurement of mPTP-induced mitochondrial depolarization ● TIMING 1–5 min

(i) Remove cells from the incubator.

▲ **CRITICAL STEP** Do not wash away the TMRM to avoid dye re-distribution.

(ii) Place the imaging dish inside the temperature-controlled (37 °C) microscope stage.

▲ **CRITICAL STEP** Living cells are sensitive to high and low temperatures. Be sure to maintain the temperature constant at 37 °C.

(iii) Start Xcellence Olympus software, and select the following specifications, which provide optimal image acquisition under standard conditions:

Menu	Settings
Illumination settings	Switch on the illumination system and wait for ~10 min before starting
Excitation filter	Select the dedicated Rhodamine filter set to detect TMRM fluorescence
Camera control	Set the binning at 2 × 2
Microscope control	Select the 40× oil-immersion objective from the list
Experiment manager	Set the wavelength, the exposure time, and the lamp power according to **Table 3**

▲ **CRITICAL STEP** Avoid extended and intense excitation of the sample.

(iv) Select suitable field: we recommend selecting a field that displays no more than 70% confluence of cells and that contains an empty corner.

? TROUBLESHOOTING

(v) Strictly draw the ROIs near the mitochondria of the selected cells for analysis of kinetic trends.

(vi) Start image acquisition at the frequency indicated in **Table 3**, and perform basal recording for 5 min.

? TROUBLESHOOTING

(C) Measurement of *in vivo* mPTP-induced mitochondrial swelling ● TIMING 1–5 min

(i) Remove the cells from the incubator, and extensively wash the cells with modified KRB.

(ii) Cover the cells with 900 µl of modified KRB.

TABLE 3 | Image acquisition settings.

Staining method	Excitation filter (nm)	Emission filter (nm)	Exposure time (ms)	Lamp power (%)	Time delay (ms)	Experiment duration (min)
Calcein	494	520	30	3	500	10
TMRM	549	573	80	15	1,800	30
mtGFP	488	535	50	10	3,600	10

(iii) Place the imaging coverslip inside the temperature-controlled (37 °C) microscope stage.
▲ CRITICAL STEP Living cells are sensitive to high and low temperatures. Be sure to maintain the temperature constant at 37 °C.

(iv) Start the Xcellence Olympus software, and select the following specifications, which provide optimal image acquisition under standard conditions:

Menu	Settings
Illumination settings	Switch on the illumination system and wait for ~10 min before starting
Excitation filter	Select the dedicated GFP filter set to detect mtGFP
Camera control	Set the binning at 1 × 1
Microscope control	Select the 60× oil-immersion objective from the list
Experiment manager	Set the wavelength, the exposure time, and the lamp power according to **Table 3**
	Set *Z* stack acquisition of 51 planes spaced at 200-nm intervals

▲ CRITICAL STEP Avoid extended and intense excitation of the sample.

(v) Focus on the sample and identify a field in which the cells display a well-localized mitochondrially targeted GFP signal in the mitochondrial compartment.
▲ CRITICAL STEP Be sure to select the central *Z* plane of the cell to enable acquisition of the entire cell volume.

(vi) Start image acquisition at the frequency indicated in **Table 3**, and perform basal recording for 3 min.

Challenging mPTP opening

4| The following section describes how to stimulate mPT during image acquisition. Please proceed to option A for Co^{2+}–calcein, to option B for the TMRM method, and to option C for the mitochondrial morphology assay.

(A) *In vivo* measurement of mPTP-induced Co^{2+}–calcein quenching ● TIMING 10 min

(i) Add 100 µl of 10 µM ionomycin solution and mix it carefully.
▲ CRITICAL STEP Add the solution without touching the coverslip to avoid shifting the selected field.

(ii) Perform acquisition for 9 min to ensure measurement of a response to the stimulus.
? TROUBLESHOOTING

(B) *In vivo* measurement of mPTP-induced mitochondrial depolarization ● TIMING 30 min

(i) Add 100 µl of 5 mM H_2O_2 solution and mix it carefully.
▲ CRITICAL STEP Add the solution without touching the coverslip to avoid shifting the selected field.

(ii) Perform acquisition for 20 min to ensure measurement of a response to the stimulus.
? TROUBLESHOOTING

(iii) Add 100 µl of 10 µM FCCP solution and mix it carefully.
▲ CRITICAL STEP Add the solution without touching the coverslip to avoid shifting the selected field.

(iv) Perform acquisition for 5 min to ensure measurement of a response to the stimulus.
? TROUBLESHOOTING

(C) Measurement of *in vivo* mPTP-induced mitochondrial swelling ● TIMING 10 min

(i) Add 100 µl of 10 µM ionomycin solution and mix carefully.
▲ CRITICAL STEP Add the solution without touching the coverslip to avoid shifting the selected field.

(ii) Perform acquisition for 15 min to ensure measurement of a response to the stimulus.
? TROUBLESHOOTING

Image processing and data analysis

5| The following section describes how to perform image correction, data extraction, and analysis. Please proceed to option A for Co^{2+}–calcein, to option B for the TMRM method, and to option C for mitochondria morphology assay.

(A) *In vivo* measurement of mPTP-induced Co^{2+}-calcein quenching ● TIMING 10 min

(i) Export the results as a spreadsheet by clicking "Save As" on the kinetic graph.

(ii) Open the exported files using spreadsheet software, and subtract the background trace from each ROI arranged in a column.

(iii) Calculate the slope of the curves for the first minute after ionomycin stimulation, for instance, using the function 'SLOPE' in Microsoft Office Excel.

(iv) Input the slope values in a single column, and proceed with statistical analysis.

▲ CRITICAL STEP Slope calculation for periods of >1 min may underestimate the final results.

▲ CRITICAL STEP See **Supplementary Video 1** for a video tutorial on this section (step 5A).

(B) *In vivo* measurement of mPTP-induced mitochondrial depolarization ● TIMING 10 min

(i) Open time-lapse image using the Fiji software.

(ii) Draw an ROI; using freehand selections, encircle each mitochondrion, excluding the nucleus, and draw an ROI of a background region in an empty corner of the field.

(iii) Estimate a global threshold to restrict the analysis to the pixels displaying intensity values greater than the threshold value.

▲ CRITICAL STEP Estimate the threshold on the final image of the time-lapse.

(iv) Use the multimeasure tool to calculate the mean gray values limited by the threshold for the selected ROI (including the background ROI) in each time-lapse image.

(v) Export the data in a spreadsheet-compatible format (i.e., Microsoft Office Excel) and arrange the data for each ROI in a single column.

(vi) For every column, subtract the background value at the sampling time.

(vii) Normalize the values, considering the first value as 100%.

(viii) Calculate the slope from minute 15 to minute 25, for instance, using the function 'SLOPE' in Microsoft Office Excel.

▲ CRITICAL STEP Every trace must be analyzed using the same parameters, especially in the time-lapse slope calculation.

(ix) Use the slope values to perform statistical analysis, and compare the results under different experimental conditions.

▲ CRITICAL STEP See **Supplementary Video 2** for a video tutorial on this section (step 5B).

(C) Measurement of *in vivo* mPTP-induced mitochondrial swelling ● TIMING 30 min

(i) Select the last acquired time-lapse image and apply 3D digital deconvolution. Ensure that *XY* and *Z* calibration and the refraction index of the lens are properly set. Be sure to perform automated spherical aberration detection.

(ii) Export the deconvolved time-lapse image as multiple TIFF or Image Cytometry Standard files.

(iii) Open Fiji software and load the generated files.

? TROUBLESHOOTING

(iv) Split different time points using the tool 'Stack Splitter'; set the number of substacks as the number of time points (Menu Image → Stack → Tools).

(v) Select time point 1 and open the 3D object counter tool (Menu Analyze).

(vi) Set the threshold to include all mitochondria and to exclude the background. Set the minimum object size to ten pixels to avoid noise contamination.

(vii) Record the number of objects counted.

(viii) Repeat this procedure for all time points.

(ix) Collect all object counts in a spreadsheet file, arranging the data by row or column.

▲ CRITICAL STEP See **Supplementary Video 3** for a video tutorial on this section (step 5C).

? TROUBLESHOOTING

? TROUBLESHOOTING

Troubleshooting advice can be found in **Table 4**.

TABLE 4 | Troubleshooting table.

Step	Problem	Possible reason	Solution
2A(i), 2B(i)	Cells detach from the coverslip	Low adhesion of cells	Prepare a selective coating (depending on the cell type)
2A(ii), 2B(ii)	Cells detach from the coverslip	Cells are lost during the staining phase	Replace KRB solution with HBSS or phenol-red-free DMEM supplemented with 10% FBS

(continued)

TABLE 4 | Troubleshooting table (continued).

Step	Problem	Possible reason	Solution
3A(iii)	Nonspecific staining	Presence of cellular debris	Increase the number of washes before and after the staining phase
	Calcein fluorescence is not localized to mitochondria	Cytosolic calcein is not quenched during basal acquisition	Increase the $CoCl_2$ concentration in the staining solution (from 1 to 2 mM)
3A(v), 3B(vi)	Progressive reduction in basal fluorescence	Fluorophore bleaching	Decrease the light source power and/or the exposure time
3B(vi)	Signal is unstable during the first 5 min	TMRM loading solution is not equilibrated because of a difference in the temperature between the incubator and the microscope stage	Keep the sample on the stage until the dye reaches equilibrium (it could take up to 30 min)
	Progressive reduction in basal fluorescence intensity	TMRM is extruded from the cells by the drug delivery system	Add 250 μM sulfinpyrazone to the loading solution
3B(iv)	Very weak signal	TMRM loading solution was washed away	Replace the TMRM loading solution
3A(iii), 3B(iv)	Very weak signal	Stock solution was exposed to light	Use a fresh aliquot of stock solution
4A(ii), 4B(ii), 4B(iv), 4C(ii)	Delayed or absent response to stimuli	Improper stimulus concentration	Increase the stimulus concentration
		Degraded stimulus solution	Prepare fresh stimulus solution
		Stimulus does not reach the selected cells	Mix the solution more extensively in the imaging chamber
		Excessive cell density hampers stimulus distribution or reduces the stimulus strength	Reduce the density of cells in the seeding phase
4A(ii), 4B(ii), 4C(ii)	Delayed or absent response to stimuli	Cells withstand mPTP opening	Elongate the length of time-lapse imaging
4A(ii)	Cytosolic fluorescence quenching is not maintained during stimulus-induced mPTP opening	Extrusion of cytosolic $CoCl_2$	Increase $CoCl_2$ concentration in the medium
5C(iii)	The 3D time-lapse acquisition appears as a single stack; there is no separation between time points	The software could not differentiate between *Z* and *t* dimensions	Manually define the *Z* and *t* dimensions (Menu Image → Hyperstack → Stack to Hyperstack)
5C(ix)	Object number progressively increases independently of mPTP challenging	Signal photobleaching causes reduction of the optimal thresholding value, with consequent artificial object fragmentation	Decrease the light source power and/or the exposure time

● TIMING

Experiment and reagent setup: ~1 week
Step 1, cell preparation: 1 h
Step 2, cell staining and mitochondrial labeling
Step 2A, *in vivo* measurement of mPTP-induced Co^{2+}-calcein quenching: 20 min
Step 2B, *in vivo* measurement of mPTP-induced mitochondrial depolarization: 40 min
Step 2C, measurement of *in vivo* mPTP-induced mitochondrial swelling: 90 min

Step 3, imaging setup and basal acquisition
Step 3A, *in vivo* measurement of mPTP-induced Co^{2+}–calcein quenching: 1–5 min
Step 3B, *in vivo* measurement of mPTP-induced mitochondrial depolarization: 1–5 min
Step 3C, measurement of *in vivo* mPTP-induced mitochondrial swelling: 1–5 min
Step 4, challenging mPTP opening
Step 4A, *in vivo* measurement of mPTP-induced Co^{2+}–calcein quenching: 10 min
Step 4B, *in vivo* measurement of mPTP-induced mitochondrial depolarization: 30 min
Step 4C, measurement of *in vivo* mPTP-induced mitochondrial swelling: 10 min
Step 5, image processing and data analysis
Step 5A, *in vivo* measurement of mPTP-induced Co^{2+}–calcein quenching: 10 min
Step 5B, *in vivo* measurement of mPTP-induced mitochondrial depolarization: 10 min
Step 5C, measurement of *in vivo* mPTP-induced mitochondrial swelling: 30 min
Box 1, alternative mitochondrial membrane potential probes: 80–85 min

ANTICIPATED RESULTS

During analysis of mPTP activity by the calcein–Co^{2+} technique, basal measurements should produce a stable signal. If the signal does not seem stable or if calcein displays a localization pattern that is different from that of MitoTracker (or another counterstain, if used), please refer to Table 4 for Troubleshooting guidelines (**Supplementary Fig. 1**).

Stimulating cells with ionomycin facilitates the entry of excess Ca^{2+} into cells to trigger mPTP opening. This event causes Co^{2+} entry into the mitochondria, thereby quenching the calcein signal. Indeed, kinetic analysis should produce a slope that adequately reflects mPTP opening. The response to ionomycin can be partially blocked using CsA, a compound that has been reported to desensitize mPTP formation by binding to cyclophilin D[50]. Thus, under this experimental condition, calcein is not quenched after mPTP challenge, and the slope of the time-dependent calcein intensity should be nearly zero (**Fig 1**).

As oxidative stress is one of the best characterized homeostatic perturbations that promotes mPTP opening[51,52], the mitochondria of cells exposed to the prototypic pro-oxidant H_2O_2 underwent rapid depolarization. As described in the PROCEDURE section, the cells were stained with TMRM, a cell-permeant, cationic, red-orange fluorescent dye that is sensitive to $\Delta\psi m$. The time-lapse images were analyzed and converted to a plot as described above. In **Figure 2**, representative images of TMRM staining under basal, H_2O_2-stimulated, and residual polarization conditions and a representative trace are reported. TMRM fluorescence was stable for the first 5 min (basal conditions). Subsequently, challenge with 500 μM H_2O_2 induced a gradual decrease in the TMRM signal due to mPTP-opening-dependent depolarization. The slope of the trace directly correlates to mPTP opening. The slope of each trace derived from single cells can be used to compare different experimental conditions (i.e., vehicle versus CsA treatment). At the end of the experiment, FCCP, a mitochondrial electron-chain-uncoupling agent, was added to induce complete mitochondrial membrane depolarization. The residual TMRM staining intensity is due to non-mitochondrial membrane potential—for instance, cellular membrane potential—which should be excluded from analysis.

Traces obtained from the analysis are suitable indexes for interpreting when an experiment is not properly set up. **Supplementary Figure 1** shows two examples of the most common artifactual results; please also refer to the Troubleshooting guidelines.

Challenging cells with ionomycin leads to the deformation of mitochondrial filaments and transforms them into groups of spheroidal objects (**Fig 3**). The number of mitochondria obtained according to the instructions in this protocol is expected to markedly increase. This mitochondrial network rearrangement is inhibited by pretreatment with the mPTP-desensitizing agent CsA. If mitochondria sense some environmental stress (i.e., excess light illumination), then undesired fragmentation might be observed before the mPTP stimulation. In the case of unfortunate events such as that described, please refer to the Troubleshooting guidelines (**Supplementary Fig. 1**).

Note: Any Supplementary Information and Source Data files are available in the online version of the paper.

ACKNOWLEDGMENTS P.P. is grateful to Camilla degli Scrovegni for continuous support. This research was supported by the Italian Ministry of Education, University and Research (COFIN no. 20129JLHSY_002, FIRB no. RBAP11FXBC_002, and Futuro in Ricerca no. RBFR10EGVP_001), local funds from the University of Ferrara and the Italian Ministry of Health to P.P. and C.G., Telethon (GGP15219/B), the Italian Association for Cancer Research (IG-14442 and MFAG-13521 to P.P. and C.G.), and the Italian Cystic Fibrosis Research Foundation (19/2014) to P.P. M.R.W. was supported by the National Science Centre, Poland (grant 2014/15/B/NZ1/00490), grant W100/HFSC/2011, and HFSP grant RGP0027/2011.

AUTHOR CONTRIBUTIONS M.B., C.M., G.M., C.G., M.R.W., and P.P. contributed extensively to the writing of this paper. M.B., G.M., and C.M. performed the experiments, analyzed data, and generated visual guides.

COMPETING FINANCIAL INTERESTS The authors declare no competing financial interests.

1. Zoratti, M. & Szabo, I. The mitochondrial permeability transition. *Biochim. Biophys. Acta* **1241**, 139–176 (1995).

2. Kwong, J.Q. & Molkentin, J.D. Physiological and pathological roles of the mitochondrial permeability transition pore in the heart. *Cell Metab.* **21**, 206–214 (2015).
3. Bernardi, P. & Di Lisa, F. The mitochondrial permeability transition pore: molecular nature and role as a target in cardioprotection. *J. Mol. Cell. Cardiol.* **78**, 100–106 (2015).
4. Bonora, M. *et al.* Molecular mechanisms of cell death: central implication of ATP synthase in mitochondrial permeability transition. *Oncogene* **34**, 1475–1486 (2015).
5. Halestrap, A.P. The C ring of the F1Fo ATP synthase forms the mitochondrial permeability transition pore: a critical appraisal. *Front. Oncol.* **4**, 234 (2014).
6. Halestrap, A.P. & Richardson, A.P. The mitochondrial permeability transition: a current perspective on its identity and role in ischaemia/reperfusion injury. *J. Mol. Cell. Cardiol.* **78**, 129–141 (2015).
7. Morciano, G. *et al.* Molecular identity of the mitochondrial permeability transition pore and its role in ischemia-reperfusion injury. *J. Mol. Cell. Cardiol.* **78**, 142–153 (2015).
8. Bonora, M. *et al.* Role of the c subunit of the FO ATP synthase in mitochondrial permeability transition. *Cell Cycle* **12**, 674–683 (2013).
9. De Marchi, E., Bonora, M., Giorgi, C. & Pinton, P. The mitochondrial permeability transition pore is a dispensable element for mitochondrial calcium efflux. *Cell Calcium* **56**, 1–13 (2014).
10. Alavian, K.N. *et al.* An uncoupling channel within the c-subunit ring of the F1FO ATP synthase is the mitochondrial permeability transition pore. *Proc. Natl. Acad. Sci. USA* **111**, 10580–10585 (2014).
11. Azarashvili, T. *et al.* Potential role of subunit c of F0F1-ATPase and subunit c of storage body in the mitochondrial permeability transition. Effect of the phosphorylation status of subunit c on pore opening. *Cell Calcium* **55**, 69–77 (2014).
12. Crofts, A.R. & Chappell, J.B. Calcium ion accumulation and volume changes of isolated liver mitochondria. Reversal of calcium ion-induced swelling. *Biochem. J.* **95**, 387–392 (1965).
13. Chappell, J.B. & Crofts, A.R. Calcium ion accumulation and volume changes of isolated liver mitochondria. Calcium ion-induced swelling. *Biochem. J.* **95**, 378–386 (1965).
14. Hausenloy, D.J., Duchen, M.R. & Yellon, D.M. Inhibiting mitochondrial permeability transition pore opening at reperfusion protects against ischaemia-reperfusion injury. *Cardiovas. Res.* **60**, 617–625 (2003).
15. Wieckowski, M.R. & Wojtczak, L. Fatty acid-induced uncoupling of oxidative phosphorylation is partly due to opening of the mitochondrial permeability transition pore. *FEBS Lett.* **423**, 339–342 (1998).
16. Gautier, C.A. *et al.* Regulation of mitochondrial permeability transition pore by PINK1. *Mol. Neurodegener.* **7**, 22 (2012).
17. Crompton, M. The mitochondrial permeability transition pore and its role in cell death. *Biochem. J.* **341**, 233–249 (1999).
18. Wong, R., Steenbergen, C. & Murphy, E. Mitochondrial permeability transition pore and calcium handling. *Methods Mol. Biol.* **810**, 235–242 (2012).
19. Marcu, R., Neeley, C.K., Karamanlidis, G. & Hawkins, B.J. Multi-parameter measurement of the permeability transition pore opening in isolated mouse heart mitochondria. *J. Vis. Exp.* **67** (2012).
20. Varanyuwatana, P. & Halestrap, A.P. The roles of phosphate and the phosphate carrier in the mitochondrial permeability transition pore. *Mitochondrion* **12**, 120–125 (2012).
21. Piwocka, K. *et al.* A novel apoptosis-like pathway, independent of mitochondria and caspases, induced by curcumin in human lymphoblastoid T (Jurkat) cells. *Exp. Cell Res.* **249**, 299–307 (1999).
22. Griffiths, E.J. & Halestrap, A.P. Mitochondrial non-specific pores remain closed during cardiac ischaemia, but open upon reperfusion. *Biochem. J.* **307**, 93–98 (1995).
23. Gillessen, T., Grasshoff, C. & Szinicz, L. *Biomed. Pharmacother.* **56**, 186–193 (2002).
24. Hausenloy, D., Wynne, A., Duchen, M. & Yellon, D. Transient mitochondrial permeability transition pore opening mediates preconditioning-induced protection. *Circulation* **109**, 1714–1717 (2004).
25. Petronilli, V. *et al.* Transient and long-lasting openings of the mitochondrial permeability transition pore can be monitored directly in intact cells by changes in mitochondrial calcein fluorescence. *Biophys. J.* **76**, 725–734 (1999).
26. Woollacott, A.J. & Simpson, P.B. High throughput fluorescence assays for the measurement of mitochondrial activity in intact human neuroblastoma cells. *J. Biomol. Screen.* **6**, 413–420 (2001).
27. Petronilli, V. *et al.* Transient and long-lasting openings of the mitochondrial permeability transition pore can be monitored directly in intact cells by changes in mitochondrial calcein fluorescence. *Biophys. J.* **76**, 725–734 (1999).
28. Feldmann, G. *et al.* Opening of the mitochondrial permeability transition pore causes matrix expansion and outer membrane rupture in Fas-mediated hepatic apoptosis in mice. *Hepatology* **31**, 674–683 (2000).
29. Wakabayashi, T. Structural changes of mitochondria related to apoptosis: swelling and megamitochondria formation. *Acta Biochim. Pol.* **46**, 223–237 (1999).
30. Kaasik, A., Safiulina, D., Zharkovsky, A. & Veksler, V. Regulation of mitochondrial matrix volume. *Am. J. Phys.* **292**, C157–C163 (2007).
31. Song, W. *et al.* Assessing mitochondrial morphology and dynamics using fluorescence wide-field microscopy and 3D image processing. *Methods* **46**, 295–303 (2008).
32. Leonard, A.P. *et al.* Quantitative analysis of mitochondrial morphology and membrane potential in living cells using high-content imaging, machine learning, and morphological binning. *Biochim. Biophys. Acta* **1853**, 348–360 (2015).
33. Reis, Y. *et al.* Multi-parametric analysis and modeling of relationships between mitochondrial morphology and apoptosis. *PLoS One* **7**, e28694 (2012).
34. Nicholls, D.G. Simultaneous monitoring of ionophore- and inhibitor-mediated plasma and mitochondrial membrane potential changes in cultured neurons. *J. Biol. Chem.* **281**, 14864–14874 (2006).
35. Loew, L.M., Carrington, W., Tuft, R.A. & Fay, F.S. Physiological cytosolic Ca2+ transients evoke concurrent mitochondrial depolarizations. *Proc. Natl. Acad. Sci. USA* **91**, 12579–12583 (1994).
36. Haworth, R.A. & Hunter, D.R. The Ca2+-induced membrane transition in mitochondria. II. Nature of the Ca2+ trigger site. *Arch. Biochem. Biophys.* **195**, 460–467 (1979).
37. Takeyama, N., Matsuo, N. & Tanaka, T. Oxidative damage to mitochondria is mediated by the Ca(2+)-dependent inner-membrane permeability transition. *Biochem. J.* **294**, 719–725 (1993).
38. Kowaltowski, A.J., Castilho, R.F. & Vercesi, A.E. Mitochondrial permeability transition and oxidative stress. *FEBS Lett.* **495**, 12–15 (2001).
39. Petronilli, V. *et al.* The voltage sensor of the mitochondrial permeability transition pore is tuned by the oxidation-reduction state of vicinal thiols. Increase of the gating potential by oxidants and its reversal by reducing agents. *J. Biol. Chem.* **269**, 16638–16642 (1994).
40. Bravo, C., Chavez, E., Rodriguez, J.S. & Moreno-Sanchez, R. The mitochondrial membrane permeability transition induced by inorganic phosphate or inorganic arsenate. A comparative study. *Comp. Biochem. Physiol. B Biochem. Mol. Biol.* **117**, 93–99 (1997).
41. Kowaltowski, A.J., Castilho, R.F. & Vercesi, A.E. Opening of the mitochondrial permeability transition pore by uncoupling or inorganic phosphate in the presence of Ca2+ is dependent on mitochondrial-generated reactive oxygen species. *FEBS Lett.* **378**, 150–152 (1996).
42. Wieckowski, M.R., Brdiczka, D. & Wojtczak, L. Long-chain fatty acids promote opening of the reconstituted mitochondrial permeability transition pore. *FEBS Lett.* **484**, 61–64 (2000).
43. Beutner, G., Ruck, A., Riede, B., Welte, W. & Brdiczka, D. Complexes between kinases, mitochondrial porin and adenylate translocator in rat brain resemble the permeability transition pore. *FEBS Lett.* **396**, 189–195 (1996).
44. Pfeiffer, D.R., Gudz, T.I., Novgorodov, S.A. & Erdahl, W.L. The peptide mastoparan is a potent facilitator of the mitochondrial permeability transition. *J. Biol. Chem.* **270**, 4923–4932 (1995).
45. Li, J., Wang, J. & Zeng, Y. Peripheral benzodiazepine receptor ligand, PK11195 induces mitochondria cytochrome c release and dissipation of mitochondria potential via induction of mitochondria permeability transition. *Eur. J. Pharmacol.* **560**, 117–122 (2007).
46. Vianello, A. *et al.* The mitochondrial permeability transition pore (PTP)-an example of multiple molecular exaptation? *Biochim. Biophys. Acta* **1817**, 2072–2086 (2012).
47. Rizzuto, R., Brini, M., Pizzo, P., Murgia, M. & Pozzan, T. Chimeric green fluorescent protein as a tool for visualizing subcellular organelles in living cells. *Curr. Biol.* **5**, 635–642 (1995).
48. Schindelin, J. *et al.* Fiji: an open-source platform for biological-image analysis. *Nat. Methods* **9**, 676–682 (2012).
49. Di Virgilio, F., Fasolato, C. & Steinberg, T.H. Inhibitors of membrane transport system for organic anions block fura-2 excretion from PC12 and N2A cells. *Biochem. J.* **256**, 959–963 (1988).
50. Crompton, M., Ellinger, H. & Costi, A. Inhibition by cyclosporin A of a Ca2+-dependent pore in heart mitochondria activated by inorganic phosphate and oxidative stress. *Biochem. J.* **255**, 357–360 (1988).
51. Baines, C.P. *et al.* Loss of cyclophilin D reveals a critical role for mitochondrial permeability transition in cell death. *Nature* **434**, 658–662 (2005).

52. Kroemer, G., Galluzzi, L. & Brenner, C. Mitochondrial membrane permeabilization in cell death. *Physiol. Rev.* **87**, 99–163 (2007).
53. Goedhart, J. *et al.* Structure-guided evolution of cyan fluorescent proteins towards a quantum yield of 93%. *Nat. Commun.* **3**, 751 (2012).
54. Sarkar, A.R. *et al.* Red emissive two-photon probe for real-time imaging of mitochondria trafficking. *Anal. Chem.* **86**, 5638–5641 (2014).
55. Morozova, K.S. *et al.* MFar-red fluorescent protein excitable with red lasers for flow cytometry and superresolution STED nanoscopy. *Biophys. J.* **99**, L13–L15 (2010).
56. Dumas, J.F. *et al.* Effect of transient and permanent permeability transition pore opening on NAD(P)H localization in intact cells. *J. Biol. Chem.* **284**, 15117–15125 (2009).
57. Bejarano, I. *et al.* Role of calcium signals on hydrogen peroxide-induced apoptosis in human myeloid HL-60 Cells. *Int. J. Biomed. Sci.* **5**, 246–256 (2009).
58. Deniaud, A. *et al.* Endoplasmic reticulum stress induces calcium-dependent permeability transition, mitochondrial outer membrane permeabilization and apoptosis. *Oncogene* **27**, 285–299 (2008).
59. Gerasimenko, J.V. *et al.* Menadione-induced apoptosis: roles of cytosolic Ca(2+) elevations and the mitochondrial permeability transition pore. *J. Cell Sci.* **115**, 485–497 (2002).
60. Loor, G. *et al.* Menadione triggers cell death through ROS-dependent mechanisms involving PARP activation without requiring apoptosis. *Free Radic. Biol. Med.* **49**, 1925–1936 (2010).
61. Novgorodov, S.A. & Gudz, T.I. Ceramide and mitochondria in ischemic brain injury. *Int. J. Biochem. Mol. Biol.* **2**, 347–361 (2011).
62. Parra, V. *et al.* Changes in mitochondrial dynamics during ceramide-induced cardiomyocyte early apoptosis. *Cardiovasc. Res.* **77**, 387–397 (2008).
63. Perry, S.W., Norman, J.P., Barbieri, J., Brown, E.B. & Gelbard, H.A. Mitochondrial membrane potential probes and the proton gradient: a practical usage guide. *Biotechniques* **50**, 98–115 (2011).
64. Salvioli, S., Ardizzoni, A., Franceschi, C. & Cossarizza, A. JC-1, but not DiOC6(3) or rhodamine 123, is a reliable fluorescent probe to assess delta psi changes in intact cells: implications for studies on mitochondrial functionality during apoptosis. *FEBS Lett.* **411**, 77–82 (1997).
65. Ohno, R., Koie, K., Kamiya, T., Kawashima, K. & Ishiguro, J. [Treatment of pulmonary infections probably caused by fungi in patients with acute leukemia with chlotrimazole (author's transl.)]. *Rinsho Ketsueki* **17**, 876–883 (1976).